

**SPATIO-TEMPORAL APPRAISAL OF WATER-BORNE EROSION USING
OPTICAL REMOTE SENSING AND GIS IN THE UMZINTLAVA CATCHMENT
(T32E), EASTERN CAPE, SOUTH AFRICA**

By

KWANELE PHINZI

A dissertation submitted in fulfilment of the academic requirements for the degree of Master of Science in the School of Agricultural, Earth and Environmental Sciences, at the University of KwaZulu-Natal.

Durban

South Africa

August 2018

ABSTRACT

Globally, soil erosion by water is often reported as the worst form of land degradation owing to its adverse effects, cutting across the ecological and socio-economic spectrum. In general, soil erosion negatively affects the soil fertility, effectively rendering the soil unproductive. This poses a serious threat to food security especially in the developing world including South Africa where about 6 million households derive their income from agriculture, and yet more than 70% of the country's land is subject to erosion of varying intensities. The Eastern Cape in particular is often considered the most hard-hit province in South Africa due to meteorological and geomorphological factors. It is on this premise the present study is aimed at assessing the spatial and temporal patterns of water-borne erosion in the Umzintlava Catchment, Eastern Cape, using the Revised Universal Soil Loss Equation (RUSLE) model together with geospatial technologies, namely Geographic Information System (GIS) and remote sensing. Specific objectives were to: (1) review recent developments on the use of GIS and remote sensing technologies in assessing and deriving soil erosion factors as represented by RUSLE parameters, (2) assess soil erosion vulnerability of the Umzintlava Catchment using geospatial driven RUSLE model, and (3) assess the impact of landuse/landcover (LULC) change dynamics on soil erosion in the study area during the period 1989-2017.

To gain an understanding of recent developments including related successes and challenges on the use of geospatial technologies in deriving individual RUSLE parameters, extensive literature survey was conducted. An integrative methodology, spatially combining the RUSLE model with *Systeme Pour l'Obsevation de la Terre* (SPOT7) imagery within a digital GIS environment was used to generate relevant information on erosion vulnerability of the Umzintlava Catchment. The results indicated that the catchment suffered from unprecedented rates of soil loss during the study period recording the mean annual soil loss as high as $11\,752\text{ t ha}^{-1}\text{yr}^{-1}$. Topography as represented by the LS-factor was the most sensitive parameter to soil loss occurring in hillslopes, whereas in gully-dominated areas, soil type (K-factor) was the overriding factor. In an attempt to understand the impact of LULC change dynamics on soil erosion in the Umzintlava Catchment from the period 1989-2017 (28 years), multi-temporal Landsat data together with RUSLE was used. A post-classification change detection comparison showed that water bodies, agriculture, and grassland decreased by 0.038%, 1.796%, and 13.417%, respectively, whereas areas covered by forest, badlands, and

bare soil and built-up area increased by 3.733%, 1.778%, and 9.741% respectively, during the study period. The mean annual soil loss declined from 1027.36 t ha⁻¹yr⁻¹ in 1989 to 138.71 t ha⁻¹yr⁻¹ in 2017. Though soil loss decreased during the observed period, there were however apparent indications of consistent increase in soil loss intensity (risk), most notably, in the elevated parts of the catchment. The proportion of the catchment area with high (25 – 60 t ha⁻¹yr⁻¹) to extremely high (>150 t ha⁻¹yr⁻¹) soil loss risk increased from 0.006% in 1989 to 0.362% in 2017. Further analysis of soil loss results by different LULC classes revealed that some LULC classes, i.e. bare soil and built-up area, agriculture, grassland, and forest, experienced increased soil loss rates during the 28 years study period. Overall, the study concluded that the methodology integrating the RUSLE model with GIS and remote sensing is not only accurate and time-efficient in identifying erosion prone areas in both spatial and temporal terms, but is also a cost-effective alternative to traditional field-based methods. Although successful, few issues were encountered in this study. The estimated soil loss rates in Chapter 3 are above tolerable limits, whereas in Chapter 4, soil loss rates are within tolerable limits. The discrepancy in these results could be explained by the differences in the spatial resolution of SPOT (5m * 5m) and Landsat (30m * 30m) images used in chapters 3 and 4, respectively. Further research should therefore investigate the impact of spatial resolution on RUSLE-estimated soil loss in which case optical sensors including Landsat, Sentinel, and SPOT images may be compared.

Keywords: Water-borne erosion; Optical remote sensing; Geographic Information System (GIS); Revised Universal Soil Loss Equation (RUSLE); Land use/land cover (LULC) change; Umzintlava Catchment

PREFACE

The work described in this dissertation was carried out in the School of Agricultural, Earth and Environmental Sciences, University of KwaZulu-Natal, Durban, from July 2016 to August 2018, under the supervision of Dr. Njoya S. Ngetar.

This study represents original work by the author and has not otherwise been submitted in any form for any degree or diploma to any tertiary institution. Where use has been made of the work of others, it is duly acknowledged in the text.

Kwanele Phinzi Signed: 

Date: 28 November 2018

As the candidate's supervisor I have/have not approved this thesis/dissertation for submission.


Dr. Njoya S. Ngetar Signed: 

Date: 28 November 2018

DECLARATION 1 - PLAGIARISM

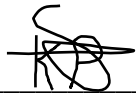
I, **Kwanele Phinzi**, declare that:

1. The research reported in this thesis, except where otherwise indicated, is my original research.
2. This thesis has not been submitted for any degree or examination at any other university.
3. This thesis does not contain other persons' data, pictures, graphs or other information, unless specifically acknowledged as being sourced from other persons.
4. This thesis does not contain other persons' writing, unless specifically acknowledged as being sourced from other researchers. Where other written sources have been quoted, then:
 - a. Their words have been re-written but the general information attributed to them has been referenced
 - b. Where their exact words have been used, then their writing has been placed in italics and inside quotation marks, and referenced.
5. This thesis does not contain text, graphics or tables copied and pasted from the Internet, unless specifically acknowledged, and the source being detailed in the thesis and in the References sections.

Signed:  _____

DECLARATION 2 - PUBLICATIONS AND MUNUSCRIPTS

1. **Phinzi, K.** and Ngetar, N.S. (In Revision). The assessment of water-borne erosion at catchment level using GIS-based RUSLE and remote sensing: A review. *International Soil and Water Conservation Research*.
2. **Phinzi, K.** and Ngetar, N.S. (In Review). Soil erosion risk assessment in the Umzintlava Catchment (T32E), Eastern Cape, South Africa, using geospatial-driven RUSLE model. *GIScience & Remote Sensing*.
3. **Phinzi, K.** and Ngetar, N.S. (In Review). The impact of land use/land cover change on soil erosion in the Umzintlava Catchment (T32E), Eastern Cape, South Africa. *Geoderma Regional*.

Signed:  _____

ACKNOWLEDGEMENT

This research project would not have been conducted, let alone finalised, without the support of others, including the following individuals and institutions to whom I am deeply indebted.

I would like to express my sincere gratitude to my supervisor, Dr. Njoya. It was through your diligent academic guidance, encouragement, and support that I today bear testimony to successful completion of this research project. It has always been an extreme and unconditional pleasure to work with you. Apart from your supervisory inputs, at a personal level, I will forever be grateful to you for so many things, not to forget your resolute effort including financial sacrifices to get me registered for my Honours Degree, a stepping stone towards this M.Sc. Degree.

Without strong and constant family support, it would have been extremely difficult or even impossible to get this project to this juncture. My mother, Thandiwe Phinzi, to say that I am grateful to you is an understatement. All I can say is that, by virtue of your existence and being my mother, I am blessed, and certainly trust that the Lord will continue to keep you alive.

I am deeply indebted to my brother, Dumisani and his wife, Thobeka, for not only warmly accommodating me, but for their outstanding moral support and guidance throughout my studies. *Bhuti*, many thanks for your kind assistance on the algebraic aspects of my work.

I appreciate all forms of support from my other siblings and friends in Eastern Cape. In particular, I wish to acknowledge with sincere gratitude, my brothers, Gedlii and Rich, and friends, Mboyana and Tamxo for their endless encouragement and support.

Many words of thank go to Mrs. Susan Sherriff for organising the logistics with respect to field data collection and other aspects of my work.

I cannot be more grateful to Dr. Lucky Nkomo and Mr. Sluleko Gwala, who during their busy schedule found it necessary to sacrifice their time and aid with field data collection which lasted about a week or so. It was not easy to get up early morning, navigating difficult terrain to various soil erosion sites. Your kind assistance is certainly not to be forgotten.

Special thanks go to Mr. Edward Powys for granting me unlimited access to and use of the soil laboratory. Thanks to Mr. Gbadebo Adeyinka for assisting with determining the physical and chemical properties of soil. I cannot thank enough Dr. Osadolor Ebhuoma for his helpful

suggestions regarding soil data analysis. Also, I wish to thank Khanyo and Mjaja for their important advice on SPSS-based statistical analysis.

I am particularly grateful to the National Research Foundation (NRF) for the financial support I received. Similarly, special thanks go to Professor Brij Maharaj for his generous financial contribution which covered part of the data collection costs.

The United States Geological Survey (USGS) is greatly acknowledged for availing remotely sensed data including Landsat images and SRTM DEM data for use at no cost. Thanks to the South African National Space Agency (SANSA) for providing free SPOT data. A word of thank is also extended to the South African Weather Services (SAWS) for providing rainfall data.

I wish to thank the University of KwaZulu-Natal, and in particular, the School of Agricultural, Earth and Environmental Sciences, for affording me this rare opportunity to read for my M.Sc. Degree with considerable financial relief, including 100% tuition fee remission. Thanks to all the academic, support, technical staff, and fellow students in the Department of Geography (Howard College Campus) for their assistance during the course of my studies.

I am very grateful to every institution and person (including those I may have erroneously omitted their names) who contributed to my work in one way or the other.

Above all, I thank the Lord for his unfailing love and wonderful deeds for me which I cannot even begin to express in words.

Kwanele Phinzi

TABLE OF CONTENTS

ABSTRACT	i
PREFACE	iii
DECLARATION 1 - PLAGIARISM	iv
DECLARATION 2 - PUBLICATIONS AND MUNUSCRIPTS	v
ACKNOWLEDGEMENT	vi
LIST OF FIGURES	xii
LIST OF TABLES	xiii
CHAPTER 1	1
GENERAL INTRODUCTION	1
1.1. Soil erosion in context	2
1.2. Understanding soil erosion by water.....	3
1.2.1. <i>Detachment</i>	3
1.2.2. <i>Transportation</i>	4
1.2.3. <i>Deposition</i>	4
1.3. Assessment of water-borne erosion	4
1.4. Aim	5
1.5. Objectives	5
1.6. Description of study area	5
1.6.1. <i>Climate</i>	7
1.6.2. <i>Topography</i>	7
1.6.3. <i>Vegetation</i>	7
1.6.4. <i>Soils</i>	8
1.7. Thesis outline	8
CHAPTER 2	10
LITERATURE REVIEW	10
Abstract	11
2.1. Introduction.....	11

2.2. An overview of the RUSLE model for erosion assessment.....	13
2.3. Derivation of RUSLE parameters using GIS and remote sensing.....	14
2.3.1. <i>Rainfall (R) factor</i>	18
2.3.2. <i>Erodibility (K) factor</i>	24
2.3.3. <i>Topographic (LS) factor</i>	30
2.3.4. <i>Cover management (C-factor)</i>	34
2.3.5. <i>Support Practice (P) factor</i>	40
2.4. Summary and conclusions	41
CHAPTER 3	44
SOIL EROSION RISK ASSESSMENT	44
Abstract.....	45
3.1. Introduction.....	45
3.2. Materials and methods	47
3.2.1. <i>Study area</i>	47
3.2.2. <i>Data and pre-processing</i>	47
3.2.3. <i>Image classification and error assessment</i>	49
3.3. Determination of RUSLE parameters	50
3.3.1. <i>Rainfall erosivity (R-factor)</i>	51
3.3.2. <i>Soil erodibility (K-factor)</i>	52
3.3.3. <i>Slope length and steepness (LS-factor)</i>	53
3.3.4. <i>Cover and management factor (C-factor)</i>	54
3.3.5. <i>Support practice factor (P-factor)</i>	54
3.4. Statistical analysis	54
3.5. Results.....	55
3.5.1. <i>LULC and soil erosion features mapping</i>	55
3.5.2. <i>Soil erosion factors</i>	57
3.5.3. <i>Soil loss rates and its relation to RUSLE parameters</i>	62

3.6. Discussion	66
3.7. Conclusion	70
CHAPTER 4.....	72
LAND USE/LAND COVER CHANGE AND SOIL EROSION	72
Abstract.....	73
4.1. Introduction.....	73
4.2. Materials and methods	75
4.2.1. <i>Study area</i>	75
4.2.2. <i>Datasets</i>	75
4.2.3. <i>Image pre-processing</i>	77
4.2.4. <i>Classification and accuracy assessment</i>	77
4.2.5. <i>Calculation of RUSLE parameters</i>	78
4.3. Results.....	80
4.3.1. <i>LULC classification</i>	80
4.3.2. <i>Accuracy assessment</i>	83
4.3.3. <i>Temporal trends of soil loss and rainfall</i>	83
4.3.4. <i>LULC change, cover management, and soil loss trends</i>	89
4.4. Discussion	93
4.5. Conclusion	97
CHAPTER 5	99
SYNTHESIS AND RECOMMENDATIONS.....	99
5.1. Introduction.....	100
5.2. Objective 1: Recent developments in the integrated use of GIS and remote sensing for assessing and deriving RUSLE parameters	100
5.3. Objective 2: Soil erosion vulnerability assessment	102
5.4. Objective 3: LULC change and soil erosion.....	103
5.5. Limitations	104

5.6. Conclusions.....	105
5.7. Recommendations and directions for future research.....	106
5.7.1. <i>Recommendations</i>	106
5.7.2. <i>Directions for future research</i>	106
REFERENCES.....	108
APPENDICES	131
Appendix A: Elevation of the study area.....	131
Appendix B: Major vegetation types in the Umzintlava Catchment.	132
Appendix C: Spatial distribution of six major soil types in the Umzintlava Catchment...	133
Appendix D: Physical properties of soil used to calculate soil erodibility.....	134
Appendix E: Spatial distribution of random points that were used to extract values from soil loss map and individual RUSLE parameters for statistical analysis.....	136

LIST OF FIGURES

Figure 1.1 Location of study area.	6
Figure 2.1 Proportion of studies conducted worldwide that used different sensors in estimating RUSLE parameters.....	18
Figure 3.1 Methodology flow chart for this study.	48
Figure 3.2 (a) LULC types, (b) soil erosion distribution, and (c) field photos of gully erosion observed in the study area.....	56
Figure 3.3 R-factor (a), K-factor (b), and LS-factor (c).....	58
Figure 3.4 NDVI (a), C-factor (b), and P-factor (c).....	59
Figure 3.5 Spatial distribution map of soil loss for the Umzintlava Catchment. The graph shows the mean annual soil loss rates by different wards with a $\pm 5\%$ standard error indicated by the sign (I) for each ward.	64
Figure 3.6 Soil erosion risk map for the study area. (Note: this map combines both NDVI-derived soil erosion and RUSLE-estimated soil loss).....	65
Figure 3.7 Relationship between soil loss and RUSLE parameters: (a) LS-factor, (b) P-factor, (c) C-factor, (d) K-factor, and (e) R-factor.	68
Figure 4.1 LULC for different years: (a) 1989, (b) 2001, and (c) 2017.....	81
Figure 4.2 LULC aerial coverage: (a) 1989, (b) 2001, and (c) 2017.....	82
Figure 4.3 Mean annual soil loss: (a) 1989, (b) 2001, and (c) 2017.....	87
Figure 4.4 Mean annual rainfall (1989 – 2016) from three meteorological stations adjacent to Umzintlava Catchment with a $\pm 5\%$ standard error indicated by the sign (I) for each year. ...	88
Figure 4.5 Overall LULC change with corresponding change in the mean annual soil loss over the last 28 years (1989 – 2017).....	90
Figure 4.6 Field photos of soil erosion observed in the study area: (a) gully erosion next to the road, (b) classical gully system, and (c) initiation of rill erosion.....	91

LIST OF TABLES

Table 2.1 Characteristics of available optical remote sensing data for erosion assessment at catchment scales.....	16
Table 2.2 Empirical relationships commonly used to estimate the R-factor ($\text{MJ mm ha}^{-1}\text{h}^{-1}\text{yr}^{-1}$).....	20
Table 2.3 Overview of satellite-borne precipitation products and their main characteristics.	21
Table 2.4 Equations that are commonly used to calculate the K-factor ($\text{ton h MJ}^{-1}\text{mm}^{-1}$).	27
Table 2.5 Methods commonly used to relate various soil attributes to remote sensing spectra.	28
Table 2.6 Most commonly used equations for deriving the slope length (L) and steepness factors (S) collectively called LS-factor.	32
Table 2.7 Spectral Indices-based C-factor assessment methods.	37
Table 3.1 NDVI classification thresholds for various LULC classes.	50
Table 3.2 NDVI classification thresholds for soil erosion and non-erosion features.	50
Table 3.3 Distribution of soil samples on major soil types (After ARC-ISCW, 2006).	53
Table 3.4 Confusion matrix of NDVI-derived LULC map.....	56
Table 3.5 Confusion matrix of NDVI-derived soil erosion map.....	57
Table 3.6 Mean annual rainfall erosivity in relation to altitude and mean annual rainfall over the period of 44 years (1972-2016).....	62
Table 3.7 Mean values of physio-chemical properties of soil with corresponding K values.	61
Table 3.8 LULC classes and their respective mean NDVI, and C-factor values.....	62
Table 3.9 Pearson's correlations for spatial autocorrelation between RUSLE parameters and soil loss.....	67
Table 4.1 Landsat images and their characteristics.....	76
Table 4.2 LULC classes and their respective NDVI classification thresholds.	77
Table 4.3 Empirical equations used to derive RUSLE parameters in this study.	79
Table 4.4 Confusion matrix for 1989 LULC.....	85
Table 4.5 Confusion matrix for 2001 LULC.....	85
Table 4.6 Confusion matrix for 2017 LULC.....	86
Table 4.7 Annual soil loss rates with corresponding severity classes and area covered in each year.....	88
Table 4.8 Mean C values and average annual soil loss ($\text{t ha}^{-1}\text{yr}^{-1}$) by LULC class for different years.	92

CHAPTER 1

GENERAL INTRODUCTION

1.1. Soil erosion in context

Increasingly, soil erosion is internationally recognised as one of the most critical forms of land degradation adversely affecting the productivity of terrestrial ecosystems including land (Lal and Stewart, 1990; Pimentel and Kounang, 1998; Pimentel, 2006). In general, it is the most fertile topsoil that is eroded, resulting in loss of arable land (Huete, 2004). Over the past 40 years or so, almost one-third (30%) of the world's productive land has been lost to the consequences of soil erosion (Lal., 2003; Yang et al., 2003; Jahun et al., 2015). A threat to land productivity is a threat to agricultural productivity. Currently, about 80% of the world's agricultural land suffers moderate to severe erosion, whilst the remainder experiences slight erosion (Pimentel, 1993; Lal, 1994). Consequently, it is estimated that about 1 billion people worldwide are currently at risk of soil erosion whereas over 250 million are directly affected (Adger et al., 2001). Due to these devastating effects, soil erosion still remains a source of serious concern not only in the developing world but also in the developed world, where persistent and often successful soil conservation efforts have been made (Carter, 1977).

The developing world however, unlike its developed counterparts, which are relatively industrialised and technologically advanced, suffers the most, primarily because of its reliance on agriculture. An example is Africa, where agriculture plays a pivotal role in job creation, contributing to economic growth. According to the New Partnership for Africa's Development (NEPAD, 2013), nearly half (48%) of the African population relies on agriculture, yet the continent is said to have the highest proportion of eroded agricultural land (Scherr and Yadav, 1997). It is reported that the continent records an annual average yield losses of about 8.2% from past erosion (Ashiagbor et al., 2013). If this trend continues unabated, yield reductions by 2020 may exceed 16% (Lal, 1995), potentially undermining food security in many countries across the continent. South Africa for instance, is one country in the continent where about 6 million households derive their income from agriculture (Department of Agriculture - DoA, 2007).

Unfortunately, more than 70% of South Africa's land is affected by soil erosion of varying intensities (Garland et al., 2000), costing the country about R12 billion per year (Hoffman and Ashwell, 2001). The Eastern Cape is often considered the most hard-hit province in South Africa due to meteorological and geomorphological factors. In this province, soil erosion negatively affects not only land as a natural resource and part of the terrestrial ecosystem but also its availability for sustainable livelihood. The latter is particularly true in most rural areas of the province where most households primarily rely on subsistence

agriculture for their livelihoods (Phinzi and Ngetar, 2017). Although national food security may not be in jeopardy, household food security is (De Villiers et al., 2003). This background provides the impetus to assess the spatial and temporal patterns of soil erosion in affected areas. The assessment of soil erosion however, requires an understanding of erosion processes and related factors (Renard et al., 2011) because spatial and temporal patterns of soil erosion are a direct product of complex interactions of such erosion processes and factors (Mitasova et al., 2013).

1.2. Understanding soil erosion by water

It is difficult if not impossible to provide a satisfactory definition of soil erosion considering the multiplicity of processes and factors involved in erosion which all vary in both spatial and temporal terms. Perhaps, it is for this reason many definitions of soil erosion exist (e.g. Meyer, 1975; Boardman et al., 1990; Ritchie, 2000; Huete, 2004; Morgan, 2005; Kinnel, 2010). Although there is no universal definition of soil erosion, there is however a general consensus amongst scholars that soil erosion is a three-fold process, comprising of detachment, transportation, and deposition phases (Foster and Meyer, 1972; Merritt et al., 2003). For the purpose of this study, the definition provided by Meyer and Wischmeier (1969) is adopted since it captures all three erosion phases (i.e. detachment, transportation, and deposition) which are critical when assessing soil erosion. Meyer and Wischmeier (1969) define soil erosion by water as the process involving the detachment, transportation, and deposition of soil particles due to erosive forces of raindrops and runoff. To fully appreciate soil erosion, the underlying processes related to detachment, transportation, and deposition ought to be understood.

1.2.1. Detachment

Defined as the removal or entrainment of soil particles either by rainfall or runoff, detachment marks the beginning of soil erosion (Ghadiri, 2004) and occurs when the shear stress exceeds the cohesive strength of soil particles (Merritt et al., 2003). Rainfall initiates erosion as soon as the falling raindrops hit the soil surface, detaching soil particles and causing them to splash into the air, hence the name splash erosion (Parlak and Parlak, 2010). The capacity of rainfall to detach soil particles is a function of raindrop impact size, kinetic energy, duration, drop velocity, soil properties, and slope steepness (Meyer and Wischmeier, 1969; Cruse et al., 2000; Ran et al., 2012). Once detached or at least left in a detachable state (Lal, 2001), such soil particles can easily be transported with the aid of overland flow.

1.2.2. Transportation

Transportation of soil particles by overland flow occurs in two forms, *viz.* sheet and rill erosion. When overland flow results in the uniform removal of soil particles from the entire slope, the resulting erosion form is called sheet erosion. Sheet erosion is sometimes used interchangeable with interrill erosion, but in general, the latter accounts for both splash and sheet erosion (Wei et al., 2009). In other words, interrill erosion results from the rainfall that detaches (splash erosion) soil particles from the soil surface and transports them in a thin sheet (Jayawardena and Bhuiyan, 1999). Interrill erosion is termed so because it occurs on the lands between the rills (Morgan, 2005). Rill erosion is caused by small but concentrated overland flows (Mitasova et al., 2013), which are characterised by V-shaped channels of less than 30cm deep within which soil particles are transported as suspended load (Nill et al., 1996). Overtime, rills may evolve into deep and large channels created by overland flow through headwall migration (Mitasova et al., 2013; Luffman et al., 2015), resulting in gully erosion. Gully erosion can also develop from subsurface erosion (also called piping). Upon the collapse of a pipe roof for instance; gully erosion may be initiated (Beckehdahl and De Villiers, 2000).

1.2.3. Deposition

A third phase of erosion, deposition, may occur at any point depending on the capacity of the erosive agent, in this case water, to carry soil particles. As Morgan (2005) notes, when sufficient energy is no longer available to transport the particles, deposition takes place. In general, the carrying capacity of the overland flow is reduced by decrease in velocity (Lal, 2001). Deposition can be caused by anything that slows or reduces runoff and causes sediment to deposit (Renard et al., 2011). Among other things, an increase in surface roughness caused by management change (e.g. a strip of dense vegetation, or decrease in slope steepness) can lead to deposition of sediments (Renard et al., 2011).

1.3. Assessment of water-borne erosion

The assessment of soil erosion caused by water has been traditionally confined to man-made erosion plots or small sub-catchments using empirical models such as the Universal Soil Loss Equation (USLE) (Wischmeier and Smith (1978), or Revised USLE (RUSLE) (Renard et al., 1991; Renard et al., 1997). Although considerable successes have been achieved with these models, the results of small-plot studies are difficult to extrapolate to the catchment level, due to the necessity of sampling temporal and spatial variability (Huete, 2004; Li et al., 2011), which can be both costly and time-consuming. However, the availability of geospatial

technologies related to Geographic Information System (GIS) and remote sensing have made the soil erosion assessment using the RUSLE model more comprehensive and robust (Wang et al., 2003), curtailing exorbitant fieldwork expenditures (Peng et al., 2003). A plethora of research is available on the use of these technologies in conjunction with RUSLE (Jain and Das, 2010; Mhangara et al., 2012; Alkharabsheh et al., 2013; Ostovari et al., 2017).

In South Africa however, literature survey reveals that substantial research has yet to be done on the integration of RUSLE and remote sensing within a digital GIS environment to understand spatial and temporal patterns of soil erosion in relation to land use/land cover (LULC) change dynamics at catchment level. In data poor countries like South Africa, optical remote sensing including freely available Landsat and *Systeme Pour l'Obsevation de la Terre* (SPOT) data, may be the only feasible and cost-effective means that can be relied on if effective management and monitoring of soil resources are to be achieved at catchment level. It is for the latter reason that the present study intends to assess soil erosion using readily available optical remotely sensed data in conjunction with RUSLE.

1.4. Aim

Based on the above observations (Section 1.3), the main aim of this study was to assess the spatial and temporal patterns of water-borne erosion in the Umzintlava Catchment, Eastern Cape, using the RUSLE model in conjunction with geospatial technologies related to GIS and remote sensing.

1.5. Objectives

The specific objectives of this study were:

- 1) To review recent developments on the use of GIS and remote sensing technologies in assessing and deriving soil erosion factors as represented by RUSLE parameters.
- 2) To assess soil erosion risk in the Umzintlava Catchment using a geospatial driven RUSLE model.
- 3) To assess the impact of land use/land cover (LULC) change on soil erosion in the Umzintlava Catchment during the period 1989 – 2017.

1.6. Description of study area

The study was conducted in the Umzintlava Catchment (T32E). Occupying about 382km², the catchment is located in the Eastern Cape, one of the most severely eroded provinces in South Africa (Figure 1.1). Geographically, the catchment extends between latitudes 30°36'55"

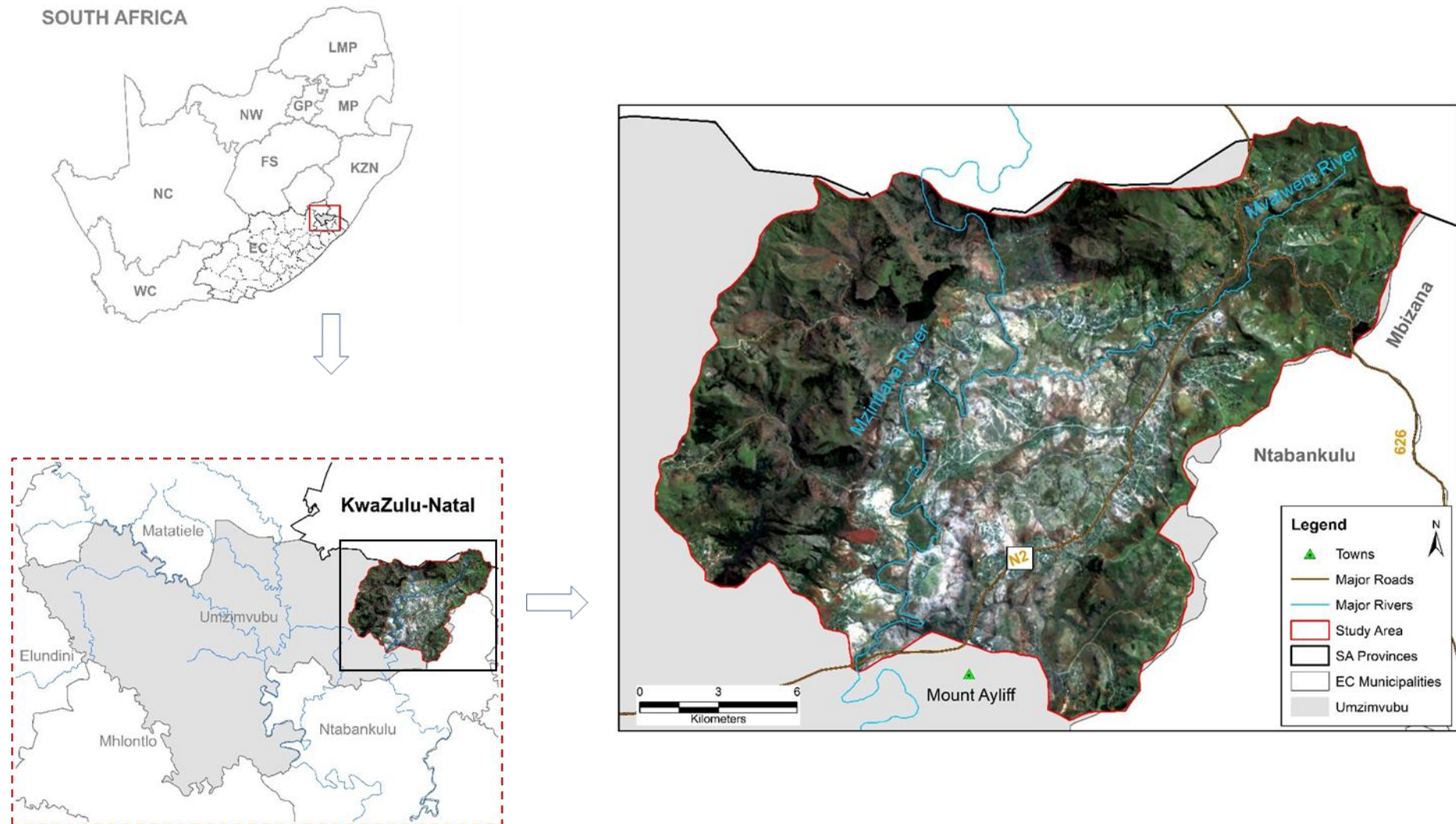


Figure 1.1 Location of study area. The true colour composite image was generated using Landsat-8 bands 2 (Blue), 3 (Green), and 4 (Red) (Data source: United States Geological Survey and the School of Agricultural, Earth and Environmental Science, University of KwaZulu-Natal, Howard College, Durban, South Africa).

¹ Note: The abbreviations SA and EC in the legend stand for South Africa and Eastern Cape, respectively.

S and 30°49'28" S to longitudes 29°32'34" E and 29°14'26" E. It is located on the western section of Umzimvubu Local Municipality, bordered by KwaZulu-Natal on the north and north-west, and by Ntabankulu and Mbizana Local municipalities on the south and south-west. The major rivers draining the catchment are Umzintlava River, followed by Mvalweni River and its tributaries. Like in most rural areas of South Africa, the majority of inhabitants in the Umzintlava Catchment are involved in agriculture in the form of livestock and crop farming at subsistence level.

1.6.1. Climate

The climate of the study area has been described by Boardman et al. (2003) and falls under that of Umzimvubu Municipality which can be classified as semi-arid with warm and rainy summer months (e.g. November to January) as well as dry and cold winter months (e.g. May to July) with occasional snowfalls. The average minimum temperatures range from 7 °C to 10 °C in winter and 18 °C to 30 °C in summer with the annual rainfall of 671mm. Convictional thunderstorms, tornados, and floods are generally experienced during summer (Boardman et al., 2003).

1.6.2. Topography

The catchment is characterised by hills and mountains (Integrated Development Plan-IDP, 2013), with the latter dominating the south-eastern, eastern, and northern parts of the catchment (Appendix A). In terms of elevation, mountains vary from 1490m to 2015m above sea level. With an altitude of approximately 890m to 900m above sea level, low lying areas are found on the central parts of the catchment.

1.6.3. Vegetation

Forest, Thicket, and Grassland biomes characterise the study area, with latter occupying a significant portion of the area. Three major vegetation types as per Acocks's (1988) classification are found within the Umzintlava Catchment. These include the Temperate and Transitional Forest and Scrub Types (Highland Sourveld and Dohne Sourveld) which are widely distributed across high lying areas, the False Grassveld Types (Southern Tall Grassveld), as well as the Karoo and Karroid Types (Vally Bushveld) which typically occur in areas of low elevation (Appendix B).

1.6.4. Soils

The study area is covered by six broad soil types (Appendix C), namely, Fa, Ac, Aa, Ab, Ea, and Ib soils, as classified by Agricultural Research Council – Institute for Soil, Climate, and Water (ARC-ISCW, 2006). Associated with rocky and shallow lithosols (Council for Geoscience report, 2012), the Fa land type dominates with more than 65% coverage of the total surface area (e.g. 382 km²) of the Umzintlava Catchment. The Ib land type which is characterised by rock outcrops covers the least aerial extent of the catchment. In general, most of the soils found within the study area are predominantly red-yellow apedal freely drained soils providing lands with great potential for cropping owing to the high levels of iron and other minerals in such soils (IDP, 2013).

1.7. Thesis outline

This thesis consists of five chapters beginning with the introductory chapter (Chapter 1) and ending with the concluding chapter (Chapter 5). In between these chapters, are Chapters 2, 3, and 4 presented as a series of individual journal articles addressing the first, second, and third objectives of the study, respectively. These three chapters have been written as manuscripts, submitted for publication in the Department of Higher Education and Training (DHET) accredited peer-reviewed journals. Although each chapter has been written as a separate research manuscript which can be read independently from the thesis, each chapter is linked to the main aim of the study. For this reason, there are some replications and overlaps in the ‘introduction’ and ‘method’ sections of individual chapters. To avoid duplication of references, a single reference list for the entire thesis was compiled. A brief overview of each chapter is provided below.

Chapter 1 has presented a general introduction to the thesis, outlining the research aim and objectives including the description of study area.

Chapter 2 provides an overview of recent developments on the use of GIS and remote sensing technologies in deriving individual RUSLE factors, placing an emphasis on related successes and challenges. The chapter also highlights gaps in the literature.

Chapter 3 focuses on the erosion risk assessment in the study area, using the RUSLE model coupled with GIS and remote sensing. In this chapter, quantitative and qualitative information on

areas susceptible to soil erosion within the catchment is provided. RUSLE-derived soil loss and remote sensing-classified soil erosion map are spatially integrated in a digital GIS environment. Also, the relationship between soil loss and each RUSLE parameter is statistically explored.

Chapter 4 explores the relationship between LULC change and soil erosion from 1989-2017. Multispectral Landsat data, available free of charge, are utilised to study LULC changes from 1989 to 2017. The temporal and spatial patterns of soil erosion as influenced by LULC change dynamics are analysed.

Chapter 5 presents a synthesis of different chapters, summarising findings, contributions, and providing concluding remarks. Directions for future research are also outlined in this chapter.

CHAPTER 2

LITERATURE REVIEW

This chapter is based on:

Phinzi, K. and Ngetar, N.S. (In Revision). The assessment of water-borne erosion at catchment level using GIS-based RUSLE and remote sensing: A review. *International Soil and Water Conservation Research*.

Abstract

Soil erosion is a direct product of the complex interactions between natural and anthropogenic factors. Such factors vary over space and time, making the assessment of soil erosion even more difficult. Empirical models such as the Revised Universal Soil Loss Equation (RUSLE) provides a rather simple and yet comprehensive framework for assessing soil erosion and its causative factors. RUSLE considers rainfall (R), topography (LS), soil erodibility (K), cover management (C), and support practice (P) as important factors affecting soil erosion. In the past few years, RUSLE has benefited tremendously from advances in geospatial technologies like Geographic Information System (GIS) and remote sensing. In this paper, an overview of recent developments on the use of these geospatial technologies in deriving individual RUSLE factors is provided, placing an emphasis on related successes and challenges. This review is expected to improve the understanding of the role played by such technologies in deriving RUSLE parameters despite existing challenges. Future research, however, must pay special attention to error assessment of remote sensing-derived RUSLE parameters.

Keywords: Soil erosion; Revised Universal Soil Loss Equation (RUSLE) parameters; Geographic Information System (GIS); Remote sensing

2.1. Introduction

Soil erosion by water is often reported as the worst form of land degradation with serious environmental and socio-economic ramifications (Oldeman et al., 1991; Fu et al., 2006; Rahman et al., 2009; Aiello et al., 2015). Throughout the world, the struggle to combat soil erosion and other forms of land degradation has drawn the attention of decision-makers, land managers and politicians (Röder and Hill, 2009). This is reflected in numerous global initiatives including but not restricted to Global Land Assessment of Degradation (GLASOD), United Nations Convention to Combat Desertification (UNCCD), as well as the United Nations Environment Programme (UNEP) (Röder and Hill, 2009). Due to this worldwide concern, the invaluable role increasingly played by erosion models in estimating soil loss at catchment levels cannot be overemphasized. Modelling soil erosion provides both quantitative and qualitative estimation of the phenomenon under various conditions (Aiello et al., 2015). In addition to estimating spatial and temporal patterns of soil loss, erosion models serve as a guide to policy formulation and

implementation of effective strategies on the conservation of soil and water resources at catchment levels (Smith, 1999; Prasannakumar et al., 2012; Farhan et al., 2013).

Several models have been developed around the world for the assessment of water-borne erosion (Lal, 2001), ranging from physical (Beasley et al., 1980; Laflen et al., 1991; Yu et al., 1997), conceptual (Johanson et al., 1980; Viney and Sivalapan, 1999), and empirical (Wischmeier and Smith, 1978; Mitsova et al., 1996; Renard et al., 1997) models. Empirical models are generally the simplest (Merritt et al., 2003), with comparative ease of application and less computational requirements (Eisazadeh et al., 2012); hence the most preferred and widely used models worldwide. The assessment of soil erosion using empirical-based models has long been an active research topic (Aiello et al., 2015). The so-called Universal Soil Loss Equation (USLE) initially introduced in the mid-1960s (Wischmeier and Smith, 1965) and improved in late 1970s (Wischmeier and Smith, 1978), is possibly the most widely applied and accepted erosion empirical model worldwide. Over the past few decades, USLE has undergone significant modifications resulting to improved versions such as the Modified USLE (MUSLE) developed by Williams and Berndt (1977), Soil Loss Estimation Model for Southern Africa (SLEMSA) developed by Elwell (1977), and Revised USLE (RUSLE) proposed by Renard et al. (1991) and Renard et al. (1997). Amongst these models, RUSLE has proven to be the most frequently used computer-based model (Alexakis et al., 2013) which provides a clear perspective for understanding the interaction of erosion and its causative factors (Xiao et al., 2015).

As a computer-based model, RUSLE has tremendously benefited from the burgeoning computer processing power, and even more so from the advances in Geographic Information System (GIS) and remote sensing technologies. Although important challenges still remain despite these technological advances (Boardman, 2006), previous studies have shown that such geospatial technologies make the determination of soil erosion and its spatial distribution attainable at limited costs and with reasonable accuracies (Wang et al., 2003). Recently, a growing number of studies using the RUSLE model took advantage of these technologies more than before (Rodriguez and Suarez, 2012; de Carvalho et al., 2014; Panagos et al., 2015, Lazzari et al., 2015; Noori et al., 2016; Tamene et al., 2017). However, little effort has been directed towards understanding the role of GIS and remote sensing in estimating the RUSLE parameters, providing a rationale for this paper to review the role of these geospatial technologies, outlining

recent developments and challenges. In the next section, a brief overview of erosion modelling using the RUSLE procedure is provided. The second section reviews the utility of GIS and remote sensing in estimating individual RUSLE factors including associated developments and challenges. The final section presents summary and concluding remarks.

2.2. An overview of the RUSLE model for erosion assessment

Soil erosion results from a synergy of natural and anthropogenic factors. Accordingly, erosion assessment requires the specific knowledge of such factors (Aiello et al., 2015). Using traditional methods relating to field measurements, though detailed and accurate at plot scales, these can be difficult or even inappropriate to employ at catchment levels given that they require considerable amount of time, money, and effort. RUSLE provides an ideal framework for assessing soil erosion and its factors. Specifically, RUSLE considers rainfall (R), topography (LS), soil erodibility (K), cover management (C), and support practice (P) as important factors affecting soil erosion. Like its predecessor (USLE), RUSLE maintains the same empirical principles and fundamental structure (Renard et al., 1994; Farhan et al., 2013). The models can both be mathematically expressed as (Renard et al., 2011):

$$A = R \times K \times LS \times C \times P \quad [1]$$

Where A is the mean annual soil loss rate ($\text{t ha}^{-1}\text{yr}^{-1}$)², R is the rainfall erosivity ($\text{MJ mm.m}^{-2}\text{h}^{-1}$)³, K is the soil erodibility factor ($\text{t ha J}^{-1}\text{mm}^{-1}$)⁴, LS is slope length and slope steepness factor (dimensionless), C is the cover and management factor (dimensionless), and P is the support practice factor (dimensionless).

Various setbacks surrounding USLE model have been identified and rigorously discussed in the literature (i.e. Renard et al., 1994; Hann et al., 1996; Smith, 1999; Lin et al., 2002; Kinnell, 2005) and will therefore not be treated here. The introduction of RUSLE was a direct attempt to address USLE limitations. Some of the most prominent modifications of RUSLE include, among others (see Renard et al., 1991; Eisazadeh et al., 2012; Mitasova et al., 2013):

- Correction of the classical USLE factor- R to account for rainfall on ponded water.

² t (tons), ha (hectare), and yr (year)

³ MJ (megajoule), mm (millimetre), m (metre), and h (hour)

⁴ J (joule)

- Derivation of topographic parameters from digital elevation model (DEM).
- Introduction of new equations based on the ratio of rill to interrill erosion that accommodate complex aspects of the LS-factor.

Given the same structure and basic empirical principles as the classical USLE model, RUSLE suffers the same limitations as its predecessor. Listed below are some of the limitations associated with RUSLE as found in Tran et al. (2002), Merritt et al. (2003) and Kinnell (2005):

- RUSLE only accounts for soil loss resulting from sheet/interrill and rill erosion, and does not consider gully erosion.
- The model does not directly represent sediment yield from the catchment.
- In the RUSLE expression, there is no explicit consideration of runoff (an important factor of erosion); instead, runoff is incorporated within the R-factor.
- RUSLE was originally developed to estimate the annual soil loss based on a single storm and its application for individual storm events leads to large errors.

In spite of these major drawbacks, the use of the RUSLE model increases almost on a day by day basis (Noori et al., 2016), because the model still represents a good compromise between easy applicability and accuracy of the derived soil loss estimates (Risse et al., 1993). Such proliferation in the use of RUSLE can also, to a large degree, be attributed to the advances in GIS and remote sensing technologies. When combined with GIS and remote sensing, RUSLE has proven to be an important tool for soil conservation planning in different areas around the world including Brazil (Lu et al., 2004), South Africa (Mhangara et al., 2012), India (Kumar and Kushwaha, 2013), Jordan (Alkharabsheh et al., 2013), Ethiopia (Tadesse et al., 2017), Italy (Napoli et al., 2017) and many other countries. While several reviews have covered the application of space-borne remote sensing in water erosion assessment and monitoring (e.g. Vrieling, 2006; Sepuru and Dube, 2017; Seutloali et al., 2018), no specific attempt has been made to review the use of GIS and remote sensing in deriving RUSLE parameters until now.

2.3. Derivation of RUSLE parameters using GIS and remote sensing

Interest in the use of GIS and remotely sensed data to derive RUSLE parameters is growing. The former is defined as any computer based set of procedures used to store and manipulate geographically referenced data (Aronoff, 1989). As per this definition, in RUSLE modelling,

GIS is commonly used for data analysis, management and visualization of the results, in addition to combining RUSLE factors within a single digital environment. On the other hand, remote sensing, which is defined as the science and art of acquiring information about material objects from measurements made at a distance and without coming into physical contact with the objects (Johannsen and Barney, 1981), serves as a main data source from which RUSLE parameters can be directly or indirectly estimated. This article focuses on satellite remote sensing as opposed to airborne (e.g. aerial imagery, Lidar, and airborne radar data) and proximal (e.g. spectroradiometer) remote sensing. Satellite remote sensing data are available from a wide variety of sensors covering the optical (Table 2.1) and microwave (Table 2.3 and Table 2.7) regions of the electromagnetic spectrum.

First launched in 1972, Landsat provides the oldest archive of images from different sensors ranging from Landsat Multispectral Scanner (MSS) to Landsat Operational Land Imager (OLI) and Thermal Infrared Sensor (TIRS). With a spatial resolution of 30 m, Landsat remains one of the most commonly used satellite images in erosion modelling (Figure 2.1). Other low or medium spatial resolution sensors include Advanced Spaceborne Thermal Emission and Reflection (ASTER), Sentinel, Linear Imaging Self-scanning Sensor (LISS), and *Systeme Pour l'Observation de Terre* SPOT. As illustrated in Table 2.1, the acquisition costs for most of these images is generally low or even completely free for some. High spatial resolution sensors such as IKONOS, GeoEye, and QuickBird are also available for assessing erosion factors. However, high acquisition costs often limit their usage (Napierallski et al., 2013) for erosion assessment over large areas. Illustrated in Figure 2.1, is the percentage (%) proportion of RUSLE-based studies conducted worldwide using the sensors mentioned in the preceding paragraph for assessing individual RUSLE parameters such as K-factor, LS-factor, C-factor, and P-factor. Though the climate factor (R-factor) can be retrieved from other parts of the electromagnetic spectrum, for example, the microwave region (discussed later in this article), there is apparently no optical remote sensing application in literature for assessing the rainfall characteristics (Vrieling, 2006). Hence, the R-factor has not been considered in Figure 2.1. As portrayed in Figure 2.1, though conducted at catchment scales, the majority of RUSLE studies use medium spatial resolution sensors to assess the cover management (C) factor. Landsat for instance, has been the most frequently used sensor worldwide for estimating the C-factor while ASTER data

Table 2.1 Characteristics of available optical remote sensing data for erosion assessment at catchment scales

Satellites (operational period)	Sensor*	Spatial resolution	Spectral resolution	Use in soil erosion assessment	Cost
Landsat 1, 2 and 3 (1972 – 1983)	MSS	80 m	4	Vegetation cover, soil erosion, and land use/land cover (LULC) mapping. Evaluation of soil properties. Most suited for large catchment areas.	Free
Landsat 4 and 5 (1982 – 1999)	TM	30 m and 120 m	6		
Landsat 7 (1999 – present)	ETM+	30 m	8		
Landsat 8 (2013 – present)	OLI and TIRS	30 m and 100 m	11		
IRS-1A and 1B (1988 – 1991)	LISS-1, and 2	72.5 m, 36.25 m	4	Vegetation cover, soil erosion, and LULC mapping. Mapping of soil attributes. Suitable for large catchment areas.	Free/low
IRS-1C and 1D (1995 – 1997)	LISS-3 and PAN		1-3		
Terra (1999 – present)	ASTER	15 m, 30 m and 90 m	14	Topographic features (e.g. slope steepness and length) extraction. Suitable for medium and large catchment applications.	Free
Santinel-1A and 2A (2014 – present)		10 m, 20 m and 60 m	13	Vegetation cover, soil erosion, and LULC mapping in small to large catchment areas. Suited for spectral characterization of soil properties.	Free
SPOT 1, 2 and 3 (1986 – 1993)	HRV	10 m, 20 m	1	Vegetation, soil erosion, and LULC mapping at small, medium, and large catchments. Extraction of topographic parameters.	Free/low
SPOT 4 and 5 (1998 – present)	HRVIR and	10 m, 20 m	1- 4		
SPOT 6 and 7 (2012 – present)	HRG and NAOMI	6 m	4		

Table 2.1 (Continued)

Satellites (operational period)	Sensor*	Spatial resolution	Spectral resolution	Use in soil erosion assessment	Cost
IKONOS (1999 – present)	PAN, MS	1 m, 4 m	5	Vegetation, soil erosion, and LULC mapping at fine resolution scales (e.g. sub-catchment and small catchment areas). Also allows for topographic features characterization at similar scales.	High
QuickBird (2001 – present)	PAN, MS	0.61 m, 2.4 m	5	Allows for vegetation, LULC mapping and detection of small erosion features. Topographic feature extraction (stereoscopic images). Most suited for sub-catchment to very small catchment applications.	High
GeoEye (2008 – present)	HRG	0.41 m, 1.65 m	5	Detailed vegetation, soil erosion, and LULC mapping. Topographic features extraction and characterization. Most suited for sub-catchment to very small catchment applications.	High
WorldView (2007 – present)	PAN, MS	0.46 m, 2 m	8	Detailed vegetation, soil erosion, and LULC mapping. Topographic feature extraction and quantification of soil attributes. Suited for sub-catchment to very small catchment applications.	High

*MSS (Multi Spectral Scanner); TM (Thematic Mapper); ETM+ (Enhanced Thematic Mapper plus); OLI (Operational Land Imager); TIRS (Thermal Infrared Sensor); LISS (Linear Imaging Self-scanning Sensor); ASTER (Advanced Spaceborne Thermal Emission and Reflection); HRV (High Resolution Visible); HRVIR (High Resolution Visible Infrared); HRG (High Resolution Geometry); NAOMI (New AstroSat Optical Modular Instrument); PAN (Panchromatic); MS (Multispectral).

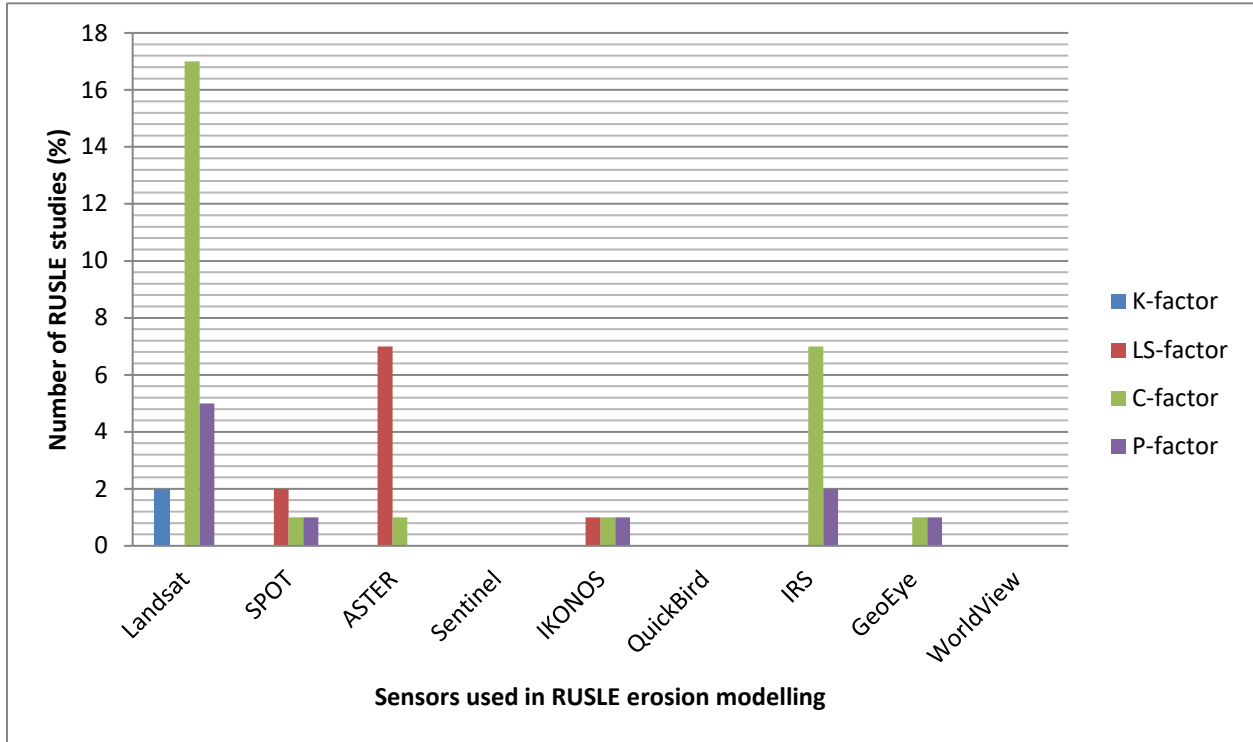


Figure 2.1 Proportion of studies conducted worldwide that used different sensors in estimating RUSLE parameters. *Note: This Figure was generated by the authors of this article from different search engines including Google Scholar and Science Direct, using key words like erosion modelling, RUSLE parameter derivation, GIS, and remote sensing.*

has been commonly used for deriving the LS-factor. A more detailed review of the application of these sensors in estimating individual RUSLE parameters is presented in subsequent sections.

2.3.1. Rainfall (R) factor

Rainfall is a prerequisite for any water-borne erosion to take place. Rainfall amount and intensity are considered the most important rainfall attributes (Foster et al., 2003). The higher the amount, and intensity of a given rainfall event, the greater is the propensity for erosion to occur. The relationship between these rainfall characteristics and soil detachment has been explored in the literature (Ma et al., 2014), revealing a strong correlation between them (Angulo-Martínez and Beguería, 2009). Thus, the R-factor is a function of the rainfall amount and intensity. Various equations are available for deriving the R-factor (Table 2.2).

Commonly obtained from meteorological gauge stations, rainfall data is one key input parameter in all the equations presented in Table 2.2. Such rainfall data is then interpolated within a GIS environment to create a continuous surface of rainfall distribution and variability. While rainfall measurements by traditional rain gauge stations provide relatively accurate estimates (Collison et al., 2008), representativeness of a sparse and irregular gauge network is a major problem (Kidd et al., 2012), particularly in remote locations (Li et al., 2012). The spatio-temporal characteristics of remote sensing together with its ability to acquire data from inaccessible locations are considered to be of primary advantage in environmental studies (Sepal et al., 2016), and can potentially be an alternative to in-situ-based rainfall measurements. During the last few decades, satellites instruments have been specifically designed for precipitation monitoring (Prevent, 2010). The most well-known satellite instruments for monitoring precipitation are summarized in Table 2.3.

In many parts of the world, the lack of high temporal resolution rainfall intensity data has been one key impediment to successful application of the RUSLE model in erosion assessment (Loureiro and Coutinho, 2001; Bonilla and Vidal, 2011; Wang et al., 2016). With the availability of space-based precipitation instruments such as HydroEstimator and MPE (Multi-sensor Precipitation Estimate), it is now possible to obtain rainfall intensity data with a temporal resolution as high as 15 minutes. The TRMM-TMPA (Tropical Rainfall Measurement Mission-Multi-satellite Precipitation Analysis) offers multiple resolution rainfall data including 3 hourly intensity (3B42, 3B42 real time), and monthly data (3B43). The use of these and other satellite-products (Table 2.3) in rainfall erosivity assessment is explored in more detail below.

Based on 11 years (1998-2008) TMPA data, Vrieling et al. (2010) calculated average annual erosivity for Africa using two erosivity methods, with one method based on 3-hourly intensity data and the other based on monthly precipitation data. The authors concluded that the 3-hourly TMPA data could not sufficiently represent high-intensity erosive events while on the contrary; monthly satellite-based TMPA data provided good spatial estimates of average annual erosivity. In calculating the R-factor as the product of the maximum 180-min rainfall intensity and the rainfall energy, Zhu et al. (2011) used the TMPA 3B42 data together with interpolated rain-gauge data. According to their results, the TMPA dataset showed a strong correlation with the interpolated rain-gauge data. The authors concluded that the TMPA data can represent the impact

Table 2.2 Empirical relationships commonly used to estimate the R-factor (MJ mm ha⁻¹h⁻¹yr⁻¹)

Equation*	Reference
$R = \frac{1}{n} \sum_{j=1}^n \left(\sum_{k=1}^m (E)_k (I_{30})_k \right)$ <p>Where E is the kinetic energy ($mJha^{-1}$), I_{30} is the maximum 30 minutes rainfall intensity ($cm h^{-1}$), j is an index of the number of years used to produce the average, k is an index of the number of storms in each year, n represents the number of years used to obtain the average R, m is the number of storms in each year.</p>	Wischmeier and Smith (1959); Renard <i>et al.</i> (1997)
$R = \sum_{i=1}^{12} 1.735 \times 10^{(1.5 \log \frac{p_i^2}{p} - 0.8188)}$ <p>Where p_i represents the total monthly precipitation (mm), and p is the mean annual precipitation (mm).</p>	Wischmeier and Smith (1978)
$R = \frac{2.5P^2}{100(0.073P + 0.73)}$ <p>Where P is the annual precipitation (mm)</p>	Bols (1978)
$MFI = \frac{\sum_{i=1}^{12} p_i^2}{\sum_{i=1}^{12} p}$ <p>Where MFI is the Modified Fournier Index (mm), p_i is the monthly precipitation (mm), and p is the mean annual precipitation (mm). This index approximates the R-factor reasonable well (Arnoldus, 1980), and has been used as an input parameter in empirical equations deriving the R-factor</p>	Arnoldus (1977, 1980)
$R = aP\sqrt{P_{md}}(b + cL)$ <p>Where P is the annual precipitation (cm), P_{md} is the annual maximum daily precipitation (cm), L is site longitude (°), and a, b, and c are site-specific coefficients.</p>	Diodato and Bellocchi (2010)
$E = \sum_{i=1}^n \left(\left(29.8 - \frac{127.5}{k \tan \theta_i} \right) \times q_i \right) (J/m^2)$ <p>Where E is the total kinetic energy, q_i is the quantity of rain (mm) in increment, i, k is the constant equivalent to 4.675 for Zimbabwe, and θ is the angle for each increment.</p>	Stocking and Elwell (1976)

*Note: cm (centimetre), mm (millimetre), MJ (megajoule), J (joule), ha (hectares), h (hour), yr (year), m (metre).

Table 2.3 Overview of satellite-borne precipitation products and their main characteristics

Satellite product*	Operational period	Temporal resolution	Spatial resolution	Spatial domain	Acquisition cost	Reference
CFSR	1979 - present	1 h	0.5° x 0.5°	Global	Free	Saha et al. (2010)
CMAP	1979 – 2009	5 days	2.5° x 2.5°	Global (90°N-90°S, 0°-36°E)	Free	Xie and Arkin (1997)
CMORPH	2002 – present	30 min	0.07° x 0.07°	Global (60°N-60°S, 180°W-180°E)	Free	Joyce et al. (2004)
CPC-RFE2.0	2001 – present	1 day	0.10° x 0.10°	Global (70°E-110°E, 5°N-35°N)	Free	Xie et al. (2002)
GPCP 1DD	1997 – 2008	1 day	1.0° x 1.0°	Global (40°N-40°S)	Free	Huffman et al. (2001)
GPCP-V2	1979 – 2008	1 month	2.5° x 2.5°	Global	Free	Adler et al. (2003)
GSMaP	2003 – 2006	1 h	0.10° x 0.10°	Global (60°N-60°S)	Free	Kubota et al. (2007)
HydroEstimator	2006 – present	15 min	4 km x 4 km	Global (60°N-60°S)	Free	Vincente et al. (1998)
MPE	2004 – present	15 min	3 km x 3 km	Global (57°N-57°S)	Free	Heinemann et al. (2002)
MWCOMB	2002 – present	3 h	0.25° x 0.25°	Global (60°N-60°S)	Free	Joyce et al. (2004)
NRL-Blended	2003 – present	3 h	0.25° x 0.25°	Global (60°N-60°S)	Free	Turk and Miller (2005)
PERSIANN	2000 – present	1 h	0.25° x 0.25°	Global (50°N-50°S, 180°W-180°E)	Free	Hsu et al. (1997)
TAMSAT	1983 – present	10 days	3 km x 3 km	Africa	Free	Grimes et al. (1999)
TRMM TMPA 3B42	1998 – present	3 h	0.25° x 0.25°	Global (50°N-50°S)	Free	Adler et al. (2000)

Table 2.3 (Continued)

Satellite product*	Operational period	Temporal resolution	Spatial resolution	Spatial domain	Acquisition cost	Reference
TRMM-TMPA 3B42-RT	2000 – present	3 h	0.25° x 0.25°	Global (50°N-50°S)	Free	Adler et al. (2000)
TRMM-TMPA 3B43	1998 – present	1 month	0.25° x 0.25°	Global (50°N-50°S)	Free	Adler et al. (2000)

*CFSR (Climate Forecast System Reanalysis), CMAP (merged Analysis of Precipitation), CMORPH (Climate Prediction Centre MORPHing), CPC-RFE (Climate Prediction Centre-RainFall Estimation), GPCP 1DD (Global Precipitation Climatology Project 1 Degree Daily), GPCP-V2 (Global Precipitation Climatology Project-version 2), GSMap (Global Satellite Mapping of Precipitation), MPE (Multi-sensor Precipitation Estimate), MWCMB (simple average of the microwave-based estimates used in creating the CMORPH), NRL-Blended (Naval Research Laboratory-Blended), PERSIANN (Precipitation Estimation from Remotely Sensed Information using Artificial Neural Network), TAMSAT (Temporal Applications of Meteorology using SATellite), and Tropical Rainfall Measurement Mission (TRMM) TMPA (Multi-satellite Precipitation Analysis), TMPA-RT (TMPA-Real Time).

of rainfall on erosion more accurately because such data are based on rainfall intensity. In an attempt to improve rainfall erosivity estimates across China, Teng et al. (2017) merged the TRMM data and rain-gauge data. The merged dataset achieved desirable accuracy in terms of the rainfall erosivity estimates in comparison to using rain-gauge and TRMM data alone. It is apparent from these studies that the TRMM data has been, so far, the only satellite-borne precipitation product used to derive the R-factor. This may be due to its relatively high spatial and temporal resolution precipitation estimates compared to other space-borne precipitation products (Li et al., 2013; Huffman et al., 2017). Additionally, the TRMM uniquely provides both the rainfall intensity and monthly rainfall estimates (Huffman et al., 2017), making it possible to investigate the spatial and temporal variability of rainfall erosivity.

While the spatial and temporal resolutions of TRMM data have proven sufficient, the short period of data records (e.g. since 1998 – present) greatly limits their use in RUSLE erosivity calculation. Rainfall data spanning a period of at least 22 years is required for the calculation of the RUSLE R-factor, as recommended by Renard et al. (2011). One way to solve this problem of limited TRMM data archive has been to combine the TRMM data with other satellite-borne precipitation products such as the long-term (since 1979-present) GPCP data (AghaKouchak and Nakhjiri, 2012). Apart from the TRMM data, the use of many other space-based precipitation products in deriving the RUSLE R-factor has not yet been reported in the literature. Instead, comparisons have been made between ground-based rainfall estimates and satellite-derived rainfall estimates (e.g. Shen et al., 2010; AghaKouchak et al., 2011; Getirana et al., 2011). Thus, the feasibility of these satellite products remains to be evaluated from the point of view of soil erosion modelling in general and R-factor derivation in particular. Despite this predicament, these satellite products especially those readily available could offer unprecedented benefits to areas with relatively few meteorological stations (Wang et al., 2017). A good case in point is the study by Worqlul et al. (2014) who tested the use of three satellite products (TRMM, MPEG, and CFSR) for augmenting gauge-based data in providing improved spatial estimates of rainfall. Their results indicated that the MPEG and CFSR satellites provided the most accurate rainfall estimates.

Although the possibility of estimating global and near-real time rainfall from satellite-borne rainfall measurements is extremely attractive for erosion modelling (Kidd and Huffman, 2011),

satellite instruments still represent a significant challenge as these do not allow for direct measurements of rainfall rates. Quantitative determination of rainfall from various space-borne sensors is a challenging undertaking, requiring sophisticated algorithms (Levizzani et al., 2001). Such complex algorithms may under/overestimate precipitation in some regions, given that different satellites are used at different latitudes, leading to some spatial heterogeneity (Pendergrass et al., 2016). Huffman et al. (2017) notes that TRMM precipitation radar algorithm likely underestimates precipitation in regions of intense convection over land and higher latitudes. In the United States, AghaKouchak et al. (2011) evaluated four satellite-derived precipitation products *viz.* CMORPH, PERSIANN, TMPA-RT, and TMPA-V6 and found that no single satellite product can be considered ideal for detecting extreme rainfall events and that such precipitation products tend to miss a significant volume of rainfall. Contrary to the above study, Shen et al. (2010) found that MWCORB, CMORPH, PERSIANN, NRL, TMPA-RT and TMPA-V6 products represent the overall spatial distribution and temporal variations of precipitation reasonably well in China. Given the variability of observations from these studies, it is apparent that different satellite-based precipitation products have their own pros and cons at different spatio-temporal scales (Qin et al., 2014; Yang et al., 2016). For this reason, it is not wise to select any satellite product for use in one region on the basis of its performance in another region.

2.3.2. Erodibility (*K*) factor

Different soils exhibit different degrees of susceptibility to water-borne erosion. By definition, soil erodibility (*K*-factor) refers to the inherent susceptibility of soil to erosion by rain water and runoff (Thomas et al., 2017). Soil erodibility is affected by a wide variety of physical and chemical properties of soil. The RUSLE model considers the physical properties such as the primary particle size distribution, organic matter, soil structure, and permeability as the most important factors influencing the erodibility of a soil. These soil properties are quantitatively determined in a laboratory using conventional methods such as the pipette for particle size distribution and dry combustion or Walkley-Black methods for soil organic matter content determination (Yufeng et al., 2011). The *K* values are then calculated for each soil type using any of the soil erodibility equations presented in Table 2.4. Alternatively, *K* values can be determined from the soil erodibility nomograph (Wischmeier and Smith, 1978) or obtained from literature for certain locations (Renard et al., 2011). While laboratory-based methods are still

commonly used, these are not only expensive and time-consuming but may also cause environmental problems through generating chemical residues (Nanni and Demattê, 2006; Demattê et al., 2007). Even more concerning, is the issue of inaccuracy associated with these methods. Yufeng et al. (2011) note that the extrapolation of soil properties from a limited number of locations where they are known, to much greater locations where they are not known introduces errors. Such errors are often ignored (Jamshidi et al., 2014), compromising the reliability of the RUSLE model in guiding conservation efforts.

Geostatistical methods available within the GIS environment have been found useful for simulating the RUSLE erodibility parameter (Goovaerts, 1997, Wang et al., 2001; Parysow et al., 2003; Panagopoulos and Antunes, 2008), whilst simultaneously providing spatial uncertainty and error estimates of simulated soil erodibility values (Jamshidi et al., 2014). One advantage of geostatistical methods over traditional approaches is the ability to establish the spatial variability and dependency among soil properties and erodibility index. A special tool in geostatistics known as semivariogram allows for evaluation of such spatial variability and dependency. Gyamfi et al. (2016) assessed soil erodibility using the kriging-based semivariogram model and the spatial dependence of soil parameters such as sand, silt, clay, bulk density and organic matter content was established based on the nugget/silt ratio. Baskan et al. (2009) used the Sequential Gaussian Simulation (SGS) geostatistical method for mapping soil erodibility factor of the RUSLE model and a reliable erodibility map was produced. Jamshidi et al. (2014) also confirmed in their study that the SGS approach generated reliable estimates of soil erodibility in most areas.

Though reasonable results can be obtained with geostatistical methods as evident in the above studies, such methods tend to rely on laboratory-determined soil samples which could be laborious and time-consuming. Furthermore, unless coupled with remotely sensed data, the application of geostatistical methods over large catchments is not an alternative either. Few studies have rarely combined remote sensing with geostatistics (Wang et al., 2003). Remote sensing still presents a much cheaper, faster, and fairly accurate method for quantitative characterization of soil attributes (Yufeng et al., 2011), and is environmentally friendly unlike laboratory-based methods. There are two possible ways in which the information relating to soil properties can be retrieved from remotely sensed data (Grunwald et al., 2015). The first is the

direct method whereby soil attributes are extracted directly from remote sensing images of bare soil. The second method is indirect in which case soil characteristics are inferred indirectly by sensing biotic (vegetation) properties. The former is the most commonly used method as shown in the next paragraph.

There have been successes in retrieving soil properties from remote sensing data (Vidhya et al., 2015) using various statistical and geostatistical models (Table 2.5). Wang et al. (2003) combined geostatistical techniques related to collocated co-kriging and joint sequential co-simulation with Landsat TM band 7 to generate the spatial variability of the RUSLE K-factor. A study by Dematte et al. (2007) determined a number of physical and chemical attributes of soil from Landsat7 ETM+ based on a multiple-linear regression (MLR) model. The results indicated that soil properties can be predicted in similar landscapes using both remote sensing and MLR. Forkuor et al. (2017) investigated the use of RapidEye and Landsat data to map the spatial distribution of soil properties based on four statistical models, including MLR, random forest regression (RFR), support vector machine (SVM), as well as stochastic gradient boosting (SGB). As is evident in these studies, remotely sensed data has undoubtedly led to better understanding of complex soil characteristics (Nanni and Demattê, 2006) and at the centre of that, is the use of statistical models which predict soil attributes from or relate to spectral reflectance. An important challenge, however, is that a statistical model developed for relating specific soil properties to spectral reflectance in one geographic region may not be able to measure the same soil properties in another region (Yufeng et al., 2011), due to different environmental conditions.

Soil colour is perhaps one readily observable soil property from which other soil properties such as organic matter can be inferred and mapped through remote sensing. For instance, though not in all cases, dark-coloured soils commonly indicate the presence of humus, hence high organic matter content whereas lighter soils typically suggest low organic matter content. Generally, soil reflectance is a direct product of the interactions of several factors, *viz.* particle size, soil structure, water content (Demattê et al., 2007), as well as different types and amount of rock-forming minerals (Breul and Gourves, 2006). For this reason, quantifying organic matter through soil colour reflectance can be extremely challenging (Hill and Schutt, 2000). Acquired in many

Table 2.4 Equations that are commonly used to calculate the K-factor ($\text{ton h MJ}^{-1}\text{mm}^{-1}$)

Equation	Reference
$K = \left[\frac{2.1 \times 10^{-4}(12 - OM)M^{1.14} + 3.25(S - 2) + 2.5(P - 3)}{7.59} \times 100 \right]$ <p>Where <i>OM</i> is soil organic matter content, <i>M</i> is product of the primary particle size fractions (%silt + %very fine sand) \times (100 - %clay), <i>S</i> is soil structure code, <i>P</i> is permeability class.</p>	Wischmeier and Smith (1978)
$K = 311.63 - 4.48 \times (SG\% + S\%) + 613.4 + 6.45 \times EC$ <p>Where <i>SG</i> is the coarse sand content (%), <i>S</i> is the sand content (%), and <i>EC</i> is the electrical conductivity.</p>	Merzouk (1985)
$K = (0.2 + 0.3e^{[-0.0256SAN(1-\frac{SIL}{100})]}) \times (\frac{SIL}{CLA+SIL})^{0.3} \times [1 - \frac{0.25C}{C+e^{(3.72-2.95C)}}] \times [1 - \frac{0.7SN_1}{SN_1+e^{(22.9SN_1-5.51)}}]$ <p>Where <i>SAN</i> is the sand content (%), <i>SIL</i> is the silt content (%), <i>CLA</i> is the clay content (%), <i>C</i> is the soil organic content (%), and $SN_1 = 1 - SAN/100$.</p>	Sharply and Williams (1990)
$K = 0.0034 + 0.0387 \exp\left[-\frac{1}{2} \frac{(\log_{10}(D_g) + 1.533)^2}{0.7671}\right]$ $D_g = \exp\left(0.1 \times \sum_{i=1}^n f_i 1n m_i\right)$ <p>Where D_g is the geometric mean diameter of the soil particles (mm), f_i is the weight percentage of the particle size fraction (%), m_i is the arithmetic mean of the particle size limits (mm), and <i>n</i> is the number of particle size fractions.</p>	Römken et al. (1997)
$K = 0.0293(0.65 - D_g + 0.24D_g^2) \exp\left\{-0.0021 \frac{OM}{Cl} - 0.00037\left(\frac{OM}{Cl}\right)^2 - 4.02Cl^2 + 1.72Cl^2\right\}$ $D_g = \sum_i f_i 1n(\sqrt{d_i d_{i-1}})$ <p>Where D_g is the Naperian logarithm of the geometric mean of the particle size distribution, <i>OM</i> is the organic matter content (%), <i>Cl</i> is the clay fraction (%), f_i is the mass fraction in the corresponding particle size class (%), <i>n</i> is the number of particle size fractions, d_i is the maximum diameter of the <i>i</i>th class (mm), and d_{i-1} is the minimum diameter (mm).</p>	Torri et al. (1997)

Table 2.5 Methods commonly used to relate various soil attributes to remote sensing spectra

Study	Location	Soil attributes*	Methods*	Remotely sensed data	Reference
Use of high resolution remote sensing data for generating site-specific soil management plan	India	Sand, silt, clay, OM, and N	MLR	IKONOS	Ray et al. (2004)
Quantification of tropical soil attributes from ETM+/Landsat-7 data	Brazil	Sand, silt, clay, OM, SB, CEC, AS, BS, K, SC, Ca, Al, P, pH, Mg, H	MLR	Landsat-7 ETM+	Demattê et al. (2007)
Spatial prediction of soil properties using EBLUP with the Matérn covariance function	Australia	Zn, pH, and clay	KEXD, cokriging, regression kriging, and REM-EBLUP	Landsat-5 TM	Minasny and McBratney (2007)
Prediction of soil texture distribution using VNIR-SWIR reflectance spectroscopy	Italy	Sand, silt, and clay	CR and PLSR	VNIR-SWIR Reflectance spectroscopy	Curcio et al. (2013)
Spatial prediction of soil surface texture in a semiarid region using random forest and multiple linear regressions	Brazil	Sand, silt, and clay	MLR and RFR	Landsat-5 TM	Da Silva et al. (2016)
High resolution mapping of soil properties using remote sensing variables in south-western Burkina Faso: a comparison of machine learning and multiple linear regression models	Burkina Faso	Sand, silt, clay, CEC, SOC, and N	MLR, RFR, SVM, and SGB	RapidEye, Landsat-8 OLI, and ASTER	Forkuor et al. (2017)

*OM (organic matter); N (nitrogen); CEC (cations exchange capacity); AS (aluminum saturation); BS (base saturation); K (kalium); SC (sum of cations); Ca (calcium); Al (aluminum); P (potassium); pH (potential of hydrogen); Mg (magnesium); H (hydrogen); Zn (zinc); SOC (soil organic carbon). MLR (multiple linear regression); KEXD (kriging with external drift); REM-EBLUP (residual maximum likelihood-empirical best linear unbiased predictor); CR (continuum removal); PLSR (partial least squares regression); RFR (random forest regression); SVM (support vector machine); SGB (stochastic gradient boosting)

narrow-wavelength bands, hyperspectral images are capable of quantifying many soil attributes (Jamshid and Abbas, 2002), although these may not be affordable in many parts of the world.

At medium or coarse resolution scales, optical sensors with improved spectral resolution (available at no cost) like Landsat OLI and Sentinel may permit better spectral discernment amongst different soil colours. However, their coarse spatial resolutions and spectral confusion between different soils may undermine the success of this type of mapping. This challenge has often been resolved through the use of spectral unmixing approaches, such as linear spectral unmixing, a process by which a proportion of several land cover classes is determined within a single pixel (Vidhya et al., 2015). Spectral unmixing has also been used to retrieve soil properties from remote sensing data. For instance, using three endmembers related to medium sand, fine sand, and water content, Lakshmi et al. (2015) successfully performed spectral unmixing on Landsat ETM+ and IKONOS images. Nonetheless, when the same soil type is highly spectrally variable, there is still much uncertainty, even with the use of spectral unmixing. Further investigations are therefore needed to deal with such uncertainty. Such investigations may focus but not be restricted to the use of spectral indices and image band ratios. Already, the potential use of the latter in generating textural indices has been demonstrated. For instance, Minasny and Mcbratney (2007) successfully derived the clay index from Landsat TM band 5/band 7 ratio. This ratio effectively generates a clear spectral contrast between land and water because of the absorption of soil in band 7 and high reflectance in band 5, highlighting the distribution of clay in the area under study. With the aid of spectral indices such as Hue Index (HI), and Coloration Index (CI), high spatial resolution optical sensors particularly, IKONOS, Quick-Bird, and Rapid-Eye have a potential for mapping spatial variation of soil colour at fine spatial resolution scales despite their possession of low spectral resolutions.

In instances where vegetation inhibits direct remote sensing mapping of soils, indirect mapping methods may be an alternative. Since vegetation is, to a large extent influenced by physical and chemical properties of a particular soil type; its spectral reflectance can be used to classify different types of soils. In this case, an assumption is made that different soil types produce different vegetation cover. The accuracy of such indirect method relies on the existence of a direct relationship between natural vegetation and soil types in the area under study (Vrieling, 2006). Very few studies have investigated the relationship between natural vegetation and soil

types (Rankin et al., 2007). It may be therefore necessary to establish whether a link between vegetation and soil types exists in the study area prior to mapping. When a strong relationship between the two is present, the spatial variability of erodibility will probably be better represented through remote sensing than when assigning erodibility values to a soil classification (Vrieling, 2006). Additionally, the use of remote sensing to characterize or map the chemical and physical properties of soil could further improve the spatial distribution and variability of the RUSLE erodibility factor.

2.3.3. Topographic (LS) factor

Slope length (L) and slope steepness (S) are the most important topographic attributes influencing soil susceptibility to erosion (Datta and Schack-Kirchner, 2010), and are accounted for by the LS-factor in the RUSLE model (Prasannakumar et al., 2012). Normally, areas with steep slopes tend to be more susceptible to erosion than flat or gentle sloping areas. Likewise, longer slope facilitates erosion, thus soil erosion increases with increasing slope length and vice-versa. This shows the sensitivity of topographic parameters to soil loss, hence, accurate derivation of this factor is deemed necessary. The slope steepness alone is said to be highly sensitive to soil loss that a small error could result in erroneous estimation of the overall soil loss (Renard et al., 2011).

Like all current spatial erosion models, RUSLE requires a digital elevation model (DEM) as an input parameter in order to quantitatively represent the continuous variation of topographic features across the landscape. Though a wide variety of sources exist including ground surveys, stereo photogrammetry, and laser scanning (Hutchinson and Gallant, 2000; Datta and Schack-Kirchner, 2010), DEMs have traditionally been derived from topographical maps. This normally involves interpolating vectorised contour lines extracted from regional topographical maps (Breetzke et al., 2013; de Carvalho et al., 2014). DEMs with a spatial resolution as high as 5 m can be generated using 1:10 000 scale topographical maps (Wang et al., 2016). However, contours are not ideal for interpolating DEM as their densities tend to vary with slope gradient (Mashimbye et al., 2014). Hence, the reliability of interpolated DEMs becomes questionable particularly in gentle sloping areas where contours are often horizontally spaced far apart. To overcome this challenge, contours are often used in conjunction with elevation points such as spot heights distributed across gentle sloping areas (van Niekerk, 2014). Nonetheless, if not

properly executed, merging these two elevation datasets (i.e. lines and points) may itself be a source of error given that it requires some degree of processing and interpolation to produce a DEM (Fisher and Tate, 2006). Presented in Table 2.6 are some of the most commonly used equations to derive the LS-factor from a DEM. Remote sensing has matured as an alternative data source to provide topographic related information.

Many satellite-borne DEM products now exist including Cartosat-1, ASTER GDEM, GMTED2010 (Global Multi-resolution Terrain Elevation Data 2010), Shuttle Radar Topography Mission (SRTM), GEODATA and GTOPO30. Amongst these DEMs, the ASTER Global DEM (GDEM) and SRTM products are the most widely used DEMs in erosion modelling possible because they provide datasets covering almost the entire earth's surface at no cost (Hirt et al., 2010). Available at 90 m and 30 m spatial resolutions, the ASTER Global DEM (GDEM) datasets are obtained by stereoscopic techniques (Toutin and Gray, 2000) whereas the SRTM DEM products are obtained by radar interferometry at 90 m and 30 m spatial resolutions (Moura-Bueno et al., 2016). Although satellite-based DEMs are readily available, researchers also have an option of extracting DEMs from the stereoscopic pair of the concerned satellite imagery. For example, the ASTER near-infrared band 3 and the back looking band form a stereo pair that allows the generation of a DEM (De Vente et al., 2009).

Attempts have been made to derive the LS-factor from space-based DEM products. For example, Gashaw et al. (2016) derived the slope length and slope steepness values from the ASTER GDEM at 30 m spatial resolution. Likewise, a study by Bahrawi et al. (2016) computed RUSLE topographic related parameters from ASTER-derived DEM product. Though successfully computed the LS-factor from satellite-based products, a shortcoming with these studies and many other RUSLE-related studies is that they generally do not take into consideration the accuracy of the DEM products they use. Furthermore, it is not always articulated in these studies as to why a particular DEM product is selected or preferred for deriving the LS-factor. Often, many erosion studies (e.g. Devatha et al., 2015; Noori et al., 2016; Tadesse et al., 2017) incorporate space-based DEMs into RUSLE as a given parameter without testing their suitability for terrain modelling at the desired scale of the study (Datta and Schack-Kirchner, 2010). Yet, satellite-derived DEMs, like all other digital spatial data, are subject to errors or anomalies

Table 2.6 Most commonly used equations for deriving the slope length (L) and steepness factors (S) collectively called LS-factor

Equation	Reference
$LS = \left(\frac{\ell}{72.6}\right) m(65.41 \sin^2 \beta + 4.56 \sin \beta + 0.065)$	Wischmeier and Smith (1978)
<p>Where ℓ is the cumulative slope length in metres, β is the downhill slope angle, m is a slope contingent variable, 0.5 if the slope angle is greater than 2.86°, 0.4 on slopes of 1.72° to 2.86°, 0.3 on slopes of 0.57° to 1.72°, and 0.2 on slopes less than 0.57°.</p>	
$LS = (Flow\ accumulation \times \frac{Cell\ size}{22.13})^{0.4} \times \left(\frac{\sin\ Slope}{0.0896}\right)^{1.3}$	Moore and Burch (1986)
<p>Where <i>Flow accumulation</i> represents the contribution of an area accumulated upslope for a given cell, <i>Cell size</i> is the size of the grid cell, and the <i>sin Slope</i> is the slope degree value in sin.</p>	
$LS = \left(\frac{Flow\ accumulation \times Grid\ size}{22.1}\right)^{0.4} \times \left(\frac{\sin(slope) \times 0.1745}{0.09}\right)^{1.4}$	Mitasova et al. (1996)
<p>Where <i>Flow accumulation</i> is a raster of accumulated flow to each cell, <i>Grid size</i> is the length of a cell side, and <i>sin (Slope)</i> is the slope degree value in sin.</p>	
$LS = \frac{X}{22.1} m(0.065 + 0.045S + 0.0065S^2)$	Bizuwerk et al. (2008)
<p>Where X is the slope length (m), S is the slope gradient (%), and m is a slope contingent variable.</p>	

(Athmania and Achour, 2014), such as voids, residual cloud patterns and stripe effects resulting from instrument errors or from the processing and generation of DEM from a stereo pair image (Fisher and Tate, 2006; Hirt et al., 2010). Knowledge of these errors and their propagation into the resultant LS-factor is important if meaningful information is to be obtained. Before attempting to extract the LS-factor from any space-borne DEM product, it is advisable to validate the accuracy and understand the potential and limitations of using a particular product for a specific area (Athmania and Achour, 2014).

Another important consideration when generating the LS-factor is the spatial resolution of a DEM. Spatial resolution has a strong bearing on the accuracy of the extracted topographical attributes (Li, 1992; Datta and Schack-Kirchner, 2010; Hirt et al., 2010; Mashimbye et al., 2014). Bhattarai and Dutta (2007) compared the influence of two SRTM DEM resolutions, a native 90 m resolution and 30 m resampled resolution, on the LS-factor. The authors observed that the results obtained from the 30 m DEM were much better than those derived from the 90 m DEM. This is to be expected because the 30 m resolution DEM is closer to the 22.4 m slope length used in the calculation of the LS-factor (Oliveira et al., 2013). Various studies have compared the SRTM to ASTER DEMs with a spatial resolution of 30 m (e.g. Athmania and Achour, 2014; Mashimbye et al., 2014; van Niekerk, 2014), many of which have consistently observed SRTM DEM to be superior to ASTER DEM. An example is De vente et al. (2009) whose study found that SRTM DEM provided more accurate estimates of slope gradient and upslope drainage area than ASTER DEM.

Although the SRTM DEM has been observed to have a relatively high accuracy compared to the ASTER GDEM, these two datasets generally do not have the spatial resolution necessary to pick up the small concentrated flow channels commonly found at the bottom of a RUSLE hillslope where substantial deposition may occur (Renard et al., 2011). Consequently, these elevation datasets are likely to negatively impact on the RUSLE topographic derivations due to the larger horizontal distances applied in their calculations (Polidori et al., 2014). Good quality DEMs with much higher spatial resolution can be extracted from stereo satellite imagery such as SPOT, GeoEye, QuickBird, IKONOS, and IRS amongst others. However, in view of the high costs associated with the acquisition of these images, other alternatives have been explored, including fusing coarse resolution ASTER or SRTM data with high spatial resolution elevation lines and

points. Van Niekerk (2014) generated a high spatial resolution (5 m) from fusing the 30 m SRTM data with 5 m contours and spot heights. The study revealed that DEM quality can be significantly improved (especially in relatively flat areas) when these three datasets are combined.

2.3.4. Cover management (C-factor)

The C-factor is one important erosion factor that can most easily be influenced by humans to reduce erosion (McCool et al., 1995). Defined as the ratio of soil loss under specific cropping conditions to soil loss occurring in bare soil (Wischmeier and Smith, 1978; Alkharabsheh et al., 2013), the C-factor reflects the effect of cropping and other management practices on erosion rates (Uddin et al., 2016).

The information for this factor has historically been derived from field experiments. Five sub-factors are considered for calculating the RUSLE C-factor (Renard et al., 1997). These include (i) prior land use; (ii) soil cover by plant canopy; (iii) soil cover by crop residues; (iv) soil surface roughness; and (v) soil moisture. Further discussion on these sub-factors including equations describing them can be found in Renard et al. (1997). The evaluation of each sub-factor is difficult because of the many possible combinations, and the time spent with data acquisition and analysis (Gabriels et al., 2003; Schonbrodt et al., 2010; Dutta, 2016).

Remote sensing-based techniques like land use/land cover (LULC) classification (Millward and Mersey, 1999, Reusing et al., 2000), spectral indices (Meusburger et al., 2010; Puente et al., 2011; Vijith et al., 2017), and linear spectral unmixing (Asner and Heidebrecht, 2002; De Asis and Omasa, 2007) are now preferred over conventional techniques owing to their low costs, rapid and relative accurate data analysis (Durigon et al., 2014). Upon deriving LULC classes through remotely sensed imagery, corresponding C-factor values obtained from USLE guide tables (Wischmeier and Smith, 1978) or from the literature are assigned. Various image classification methods exist and can be broadly grouped into supervised and unsupervised classification. In Ethiopia, Gelagay and Minale (2016) performed unsupervised image classification on Landsat TM and produced thematic land cover maps of Koga watershed to which corresponding C-factor values were assigned. Using the same classification method, Li et al. (2010) mapped the C-factor values of the Liao watershed from the Landsat ETM+. All these

studies assume that the same land cover types have the same C-factor values across the entire study area (Panagos et al., 2015).

The success of this approach however, depends amongst other things, on the classification accuracy of remotely sensed images, and the selection of suitable C-factor values for individual land cover classes (Panagos et al., 2015). Significant to classification accuracy, is the use of fine spatial resolution images especially in small catchments. On the contrary, the majority of RUSLE studies use coarse resolution images (e.g. Landsat, ASTER) for land cover classification and the details relating to the accuracy of the classified maps are often not revealed by such studies. An apparent limitation with this method is that, the same land cover class may have different C-factor estimates due to spatial variation in vegetation density within cover classes over large geographic locations (Wang et al., 2002; Lu et al., 2004). Also, different land uses with same vegetation coverage result in different C-factors (Panagos et al., 2014).

Increasingly, of particular interest to many researchers, has been the use of spectral indices (Zongming et al., 2010; Puente et al., 2011; Fathizad et al., 2014; Kamaludin et al., 2013; Rahaman et al., 2015; Noori et al., 2016; Phinzi and Ngetar, 2017; Ostovari et al., 2017; Vijith et al., 2017; Tamene et al., 2017) to assess the fraction of vegetation and its influence on C-factor values. These include amongst others, the Normalized Difference Vegetation Index (NDVI), Soil Adjusted Vegetation Index (SAVI), Soil and Atmospherically Resistance Index (SARVI), Modified Soil Adjusted Vegetation Index (MSAVI), Normalized Different Tillage Index (NDTI), Ratio Vegetation Index (RVI), Normalized Difference Senescent Vegetation Index (NDSVI), and Green Vegetation Index (GVI). One advantage of using spectral indices is related to their ability to enhance the spectral contribution of green vegetation in images while minimizing contributions from bare soil, atmosphere and illumination angle (Meusburger et al., 2010).

Several empirical relations or equations have been established to relate vegetation indices values to C-factor values (Table 2.7). These equations have been employed in many catchments studies around the world. Uddin et al. (2016) extracted the C-factor values directly from Landsat TM and ETM+ based NDVI images using De Jong's (1994) regression equation (Equation 2.2). Using the same equation, Patil and Sharma (2013) successfully generated the C-factor map from an NDVI map. In their assessment of soil erosion in Kenya, Moses (2017) and Okorafor et al.

(2017) derived the RUSLE C-factor from NDVI based on the empirical relations (Equation 2.3) of Van der Knijff et al. (1999; 2000). Parveen and Kumar (2012) also generated a C-factor map from Landsat TM-derived NDVI using Equation 2.3. Despite the general acceptance and wide use of these methods, low correlations between NDVI and the C-factor have been reported for some regions (Tweddles et al., 2000; De Asis and Omasa, 2007; Smith et al., 2007). A possible explanation for this, is that these methods do not take into account the variation of climatic conditions for calculating the C-factor. For example, Dutta (2016) observes that under tropical climate conditions, the C-factor obtained through these methods (e.g. De Jong, 1994; Van der Knijff et al., 1999, 2000) tends to be low for the same vegetation cover. Due to these setbacks, Durigon et al. (2014) proposed an equation (Equation 2.4) based on NDVI rescaling. When compared to Van der Knijff et al. (1999; 2000) method, Durigon et al. (2014) found that the rescaled NDVI method was the most adequate for determining the C-factor. As can be observed from Table 2.7, many other vegetation index-based methods are available for assessing the C-factor (Qi et al., 1994; Valor and Caselles, 1996; Gutman and Ignatov, 1998; Johnson et al., 2002; Bingfeng et al., 2004; Li et al., 2010).

Despite these successes, spectral indices like NDVI do not satisfactorily represent non-photosynthetic vegetation such as dry or dead vegetation (De Jong, 1994), yet dry vegetation has a considerable impact on the C-factor as well (Puente et al., 2011). The increasing effect of the spatial variability of bare soil background albedo (Harris and Asner, 2003), may further aggravates this problem. In response to this limitation, some researchers have explored the possibilities of using a combination of methods (Puente et al., 2011). For example, Tamene et al. (2017) used different enhancement and transformation techniques like the Principal Component Analysis (PCA), NDVI, and SAVI to aid the spectral separability of land cover types. Vijith et al. (2017) evaluated the effectiveness and suitability of cover management factors generated through different techniques including LULC-based arbitrary value, NDVI, and MSAVI-based methods. Likewise, Zhongming et al. (2010) used NDVI, MSAVI, NDTI, and NDSVI. Puente et al. (2011) applied thirty vegetation indices in order to establish the relation between them and C-factor field samples. While these spectral indices have their own shortcomings, the use of multiple indices is recommended in mapping the C-factor because of the combined ability which has a potential to pinpoint areas where vegetation cover offers low protection (Vijith et al., 2017). Other alternatives have been suggested including pixel spectral unmixing and geostatisti

Table 2.7 Spectral Indices-based C-factor assessment methods

Equation ^a	Comment	Reference
$C = 0.431 - 0.805 \times NDVI$ <p>Where C represents the C-factor.</p>	[2.2] This method assumes a linear relationship between NDVI and RUSLE C-factor. However, this assumption only holds true for photosynthetic and not senescent vegetation.	De Jong (1994)
$C = \exp\left(-a \frac{NDVI}{(\beta - NDVI)}\right)$ <p>Where a and β parameters determine the shape of the NDVI curve.</p>	[2.3] The parameters, a and β give better results in terms of relating NDVI to C-values for certain locations than assuming a linear relationship.	Van der Knijff et al. (1999; 2000)
$C_r = \left(\frac{-NDVI + 1}{2}\right)$ <p>Where C_r is the denominated rescaled C-factor.</p>	[2.4] More realistic C-values can be obtained with this method especially for tropical regions.	Durigon et al. (2014)
$P_V = \frac{\left(1 - i/i_g\right)}{\left(1 - i/i_g\right) - k \left(1 - i/i_v\right)}$ $k = (\rho_{2v} - \rho_{1v}) / (\rho_{2g} - \rho_{1g})$ <p>Where P_V is the proportion of vegetation cover, i is NDVI pixels, i_g is pure soil NDVI pixels, i_v is pure vegetation NDVI pixels. ρ_{2v} is NIR and ρ_{1v} is Red reflectance for pure vegetation pixels, whereas ρ_{2g} is NIR and ρ_{1g} is Red for pure soil pixels.</p>	[2.5] The method provide best estimation of the proportion of vegetation by separating soil pixels from vegetation pixels. This is particularly important in reducing the effects of soil background albedo at different moisture content levels.	Valor and Caselles (1996); Mallick et al. (2014)

Table 2.7 (Continued)

Equation	Comment	Reference
$f = \frac{NDVI - NDVI_{min}}{NDVI_{max} - NDVI_{min}}$ <p>Where f represents vegetation cover, $NDVI_{max}$ is best vegetation cover, and $NDVI_{min}$ is worst vegetation cover in the study area.</p>	[2.6] The method effectively distinguishes between areas of strong vegetation cover and poorly vegetated areas.	Li et al. (2010)
$fc = \frac{(NDVI - NDVI_{soil})}{(NDVI_{veg} - NDVI_{soil})}$ <p>Where fc is the vegetation fraction, $NDVI_{soil}$ is NDVI of a pure soil pixel, and $NDVI_{veg}$ is NDVI of a pure vegetation pixel.</p>	[2.7] This method relies on the assumption that a pixel consists of two components, viz. soil and vegetation. Hence, the parameters, $NDVI_{veg}$ and $NDVI_{soil}$ accounts for the influences of vegetation and soil types, respectively.	Bingfang et al. (2004)
$FVC = \frac{VI_i - VI_s}{VI_v - VI_s}$ <p>Where FVC is the fractional vegetation cover, VI_i is the VI of pixel i, VI_s is the bare soil or dead vegetation pixels, and VI_v is the fully-vegetated pixels</p>	[2.8] In this method, it is assumed that senescent (dead or dry) vegetation is spectrally-similar to bare soil. The method also assumes that bare soil and vegetation pixels are invariant throughout the image.	Johnson et al. (2012); Gutman and Ignatov (1998)
$C_{MSAVI} = \frac{(2 \times NIR + 1 - \sqrt{2 \times (NIR + 1)^2 - 8 \times (NIR - R)})}{2}$ <p>Where C_{MSAVI} represents the C-factor, NIR is the near-infrared reflectance, and R is the visible red reflectance.</p>	[2.9] As a modified version of NDVI, MSAVI accounts for some of the pertinent factors affecting its predecessor such soil background albedo. Theoretically, MSAVI is better than NDVI.	Qi et al. (1994); Vijith et al. (2017)

cal analysis (Wang et al., 2002; Gertner et al., 2002; Asner and Heidebrecht, 2002; Meusberger et al., 2010; Li et al., 2015; Jia et al., 2017) as discussed below.

Pixel spectral unmixing has already been discussed in Section 2.3.2. In vegetation analysis, it is used to extract vegetation coverage with linear or non-linear mixture model (Li et al., 2015). Linear spectral mixture model is the most widely used (Bu, 1993; De Asis and Omasa, 2007) because of its ability to detect both photosynthetic and non-photosynthetic (dry and dead) vegetation cover (Meusberger et al., 2010). Unlike spectral indices, linear spectral unmixing is not affected by the soil background albedo (Lin et al., 2017). In an effort to map bare soil, healthy and unhealthy vegetation cover, Asner and Heidebrecht (2002) employed the spectral unmixing approach to hyperspectral and multispectral data. Meusberger et al. (2010) assessed the applicability of NDVI, linear spectral unmixing, and mixture-tuned matched filtering method (MTMF) in estimating vegetation abundance. Their results indicated that the linear spectral unmixing outperformed other methods and successfully identified erosion features and areas vulnerable to erosion. Recently, Jia et al. (2017) evaluated three types of vegetation cover estimation models using Landsat 7 ETM+ data. According to their validation results, the spectral mixture analysis model achieved the best estimation accuracy.

While spectral unmixing has proved superior to other C-factor estimation methods, Jones et al. (2009) note that this method cannot be used when vegetation completely covers the surface, or when the data is affected by multiple scattering. Furthermore, the selection of image endmembers often requires the availability of pixels comprised purely of each dominant cover type (Asner and Heidebrecht, 2002), thus a critical challenge in the spectral mixture model is how to determine the endmembers and their corresponding spectral responses, given the complexity of land surface (Jia et al., 2017). In addition to these challenges, spectral endmembers collected in one area may not be applicable to another area, depending on the spatial and temporal variability of vegetation, soils, rocks and other features (Asner and Heidebrecht, 2002).

Another suggested method has been the use of geostatistical related analysis together with field data for both improving (Wang et al., 2002) and estimating the C-factor, in which case remote sensing is used as an ancillary data. Gartner et al. (2011) employed this method to map the C-factor from a joint co-simulation using multiple primary variables related to canopy cover, ground cover, and vegetation height. Often, the suggestion of each approach

discussed in this section is based on the relative advantages of that method. In general, each approach has its own pros and cons, hence there is no one single method that can satisfy all the requirements. Some previous studies including that of Jia et al. (2017) have tested different models and a combination strategy of individual models was proposed to improve the vegetation cover accuracy. The study by Tadele et al. (2017) also demonstrated that ground truth data, high spatial resolution Google Earth images, combined with GIS and remote sensing provide major advantages for not only deriving C-factor values but also conducting the subsequent accuracy assessment.

2.3.5. Support Practice (P) factor

In general, the P-factor is related to the C-factor in that they are both meant to reflect the positive impact of management practices in minimizing soil erosion (Toy et al., 1999; Renard et al., 2011). However, the P-factor is distinguishable from the C-factor as it indicates the impact of management through the control of runoff, with specific reference on how the management practices (e.g. contour tillage, strip cropping, and terraces) reduces and alters the pattern, direction and speed of that runoff (Renard and Foster, 1983; Renard et al., 1997; Renard et al., 2011). Information on the P-factor can be derived in many ways as discussed in the next paragraph.

Similar to C-factor, the most commonly used approach to obtain the P-factor information is through field observation and visual image interpretation. Historically, the latter has been dominated by the use of aerial photographs as these provide a high level of spatial detail for assessing agricultural management practices (Lord and McLean, 1969; Iyer, 1974; Morgan et al., 2010). Though not yet reported in the literature, ArcGIS Online aerial photographs and Google Earth images also offer sufficient spatial resolution for visual assessment of the P-factor. Nevertheless, estimating the P-factor through visual image interpretation is tedious and lacks objectivity. An alternative therefore, has been to assign the P-factor values obtained from the literature to satellite derived LULC maps (Pelletier and Griffin, 1985; Lee, 2004). Prasannakumar et al. (2012) derived the P-factor map from a remote sensing-based LULC map. Kumar and Kushwaha (2013) classified IKONOS and IRS Resourcesat-1 LISS-IV and assigned P-values into relevant conservation practices present in their study area. In their study, Gelagay and Minale (2016) assigned the P-values suggested by Wischmeier and Smith (1978) to Landsat-derived LULC map based on the corresponding slope class in each LULC type.

However, similar to the setback related to the use of satellite imagery to determine the C-factor, satellite images with adequate spatial resolution to detect conservation practices (contour ridge and terrace etc.) are not freely available. In this regard, readily available satellite imagery such as Landsat are commonly used (Uddin et al., 2016) despite their coarse spatial resolution. The use of coarse spatial resolution imagery is a cause for concern particularly in per-pixel classification (Cracknell, 1998), where mixed pixels are often categorized as one class. Subpixel-oriented classification methods such as linear spectral mixture analysis (see Section 2.3.4) offers a more appropriate and accurate estimation of LULC than per-pixel approaches (Lu and Weng, 2007). Empirical equations assist in estimating the P-factor though their predictive ability may be limited to those regions for which they were developed (De Vente and Poesen, 2005). However, despite the related strengths, a critical limitation with subpixel classification is the difficulty in selecting representative endmembers (see Section 2.3.4) and assessing accuracy (Lu and Weng, 2007). The P-factor information can also be directly extracted from the slope map (%) (Wener, 1981). The accuracy of such information however depends on the quality and spatial resolution of the DEM used to derive the slope map.

Often, as in the case of the C-factor, various methods are combined in order to optimally estimate the P-factor. Wang et al. (2016) determined the P-factor values based on aerial images, ground data, and the land use/land cover (LULC) map derived from satellite image (Pleiades-1A). In South Africa, Mhangara et al. (2012) obtained information related to the P-factor through field observations using a Global Positioning System (GPS) in conjunction with protected areas maps.

2.4. Summary and conclusions

This review has shown how GIS and remote sensing technologies aid in estimating the RUSLE parameters including rainfall erosivity (R-factor), topography (LS-factor), erodibility (K-factor), cover and management (C-factor), and support practice (P-factor). GIS is mainly used for computation of individual RUSLE parameters while satellite remote sensing forms an increasingly important data source for all the RUSLE parameters. The contribution of remote sensing towards the assessment or estimation of individual RUSLE parameters varies considerably as summarized below.

- R-factor – attempts have been made to derive the R-factor from satellite-borne precipitation data, though such have been restricted to TRMM-TMPA data. The use

of many other space-based precipitation products such as CFSR, CMAP, GSMaP, HydroEstimator, MPE, NRL-Blended, and PERSIANN in estimating the R-factor has not been reported in the literature. Instead, comparisons have been made between ground-based rainfall estimates and satellite-derived rainfall estimates. Although in situ-based measurements are still precise and more representative of the precipitation events than satellite-borne rainfall measurements, satellite products can complement ground based measurements in remote areas where gauge stations are extremely limited or non-existence. Prior to their use however, such satellite products must be assessed for suitability of use and validated against in situ-based measurements within the area of interest.

- K-factor – the RUSLE model considers the physical properties such as the primary particle size distribution, organic matter, soil structure, and permeability as the most important factors influencing the erodibility of a soil. The combination of remote sensing and GIS has proven helpful in determining soil erosion properties. Some soil properties can be determined from remote sensing spectra using statistical analysis while others are inferred from other properties such as soil colour. The use of remote sensing to map the soil chemical properties, which are not currently accounted for in the RUSLE K-factor equation, could improve soil erodibility estimates. In terms of analysis, multiple regression, geostatistics, and spectral mixture analysis are the most commonly used approaches to extract information from remote sensing images. Though the determination of soil erodibility factors has been successful using geostatistics and remote sensing, it is still a challenge to satisfactorily quantify relevant soil properties from remotely sensed data for input in the RUSLE erodibility equation.
- LS-factor - various space-borne DEMs allow for direct calculation of the LS-factor. Amongst these, the ASTER and SRTM DEMs have been the most widely applied products, probably because they are freely available to the research community and provide near-global coverage. Of great concern, however, is that these DEM products are incorporated in soil erosion studies as a given parameter without testing their suitability for terrain modelling at the desired scale of the study. Yet, these products are subject to systematic errors such as voids in case of the SRTM and residual cloud patterns in case of ASTER GDEM. Given that soil loss is very sensitive to topographic parameters, it is essential to assess the accuracy of DEMs in general,

prior to any further analysis. The combination of elevation points or contour lines with satellite-derived DEMs could improve the accuracy of topographic derivatives.

- C-factor and P-factor – remote sensing classified LULC maps, and spectral indices including NDVI and related indices are now preferred over conventional techniques owing to their objectivity, low costs, and relative accurate data analysis. Regression equations and statistical analysis are used to relate the C values to spectral indices. Landsat data has been the most frequently used sensor for deriving LULC maps and spectral indices from which the C-factor information is obtained. Linear spectral unmixing has been commonly used to separate photosynthetic vegetation from senescent vegetation. Similarly, the P-factor information is obtained from LULC maps in conjunction with field observation. However, in many RUSLE studies the information relating to accuracy of the classified LULC maps is not often revealed. Although remote sensing is preferred over traditional methods, there appears no satisfactory remote sensing methodology for estimating C-factor and P-factors. So far, comparison and testing of different remote sensing-oriented methods based on a given study purpose, scale, and data availability have been the panacea to obtaining reasonable C-factor results.

Overall, although important challenges still remain, this paper has shown that the benefits of using freely available geospatial technologies in erosion modelling far outweigh the associated setbacks mentioned in this paper. This is reflected by the continuous increase of studies that incorporate remote sensing and GIS in RUSLE erosion modelling. Different remote sensing products and techniques have been presented and their pros and cons with respect to the derivation of individual RUSLE factors have been discussed. The present paper is expected to improve the understanding of the role of geospatial technologies in deriving individual RUSLE parameters despite existing challenges. Future research, however, must pay special attention to error assessment of remote sensing-derived RUSLE parameters.

CHAPTER 3

SOIL EROSION RISK ASSESSMENT

This chapter is based on:

Phinzi, K. and Ngetar, N.S. (In Review). Soil erosion risk assessment in the Umzintlava Catchment (T32E), Eastern Cape, South Africa, using a geospatial-driven RUSLE model. *GIScience & Remote Sensing*.

Abstract

Designing and implementing relevant soil and water conservation measures at the catchment level depend largely on the identification of soil erosion prone areas with sufficient detail and reasonable accuracy. The aim of this study was to assess soil erosion risk in the Umzintlava Catchment by exploring the relationship between soil loss and erosion factors as represented by different Revised Universal Soil Loss Equation (RUSLE) parameters. To achieve this aim, an integrated methodology was adopted, including the RUSLE model, remote sensing and Geographic Information System (GIS). Elevation data, monthly rainfall data, *Systeme Pour l'Obsevation de la Terre* (SPOT7) imagery, and soil data were analyzed using the RUSLE model, remote sensing or GIS to derive erosion factors, which were used to determine soil loss in the study area. The results indicate that the catchment suffered from unprecedented rates of soil loss, recording a high mean annual soil loss of 11 752 t ha t ha⁻¹yr⁻¹. Statistically, the slope length and steepness (LS-factor) was the most important factor causing erosion ($p < 0.001$ and $r^2 = 0.954$), suggesting that areas with steep slopes are the most vulnerable to hillslope erosion. This is corroborated by results of remotely sensed classified imagery, indicating that not only areas with steep slopes are vulnerable to erosion but also gently sloping areas suffer from erosion, mostly gully erosion. The spatial overlay of RUSLE-derived soil loss results and remote sensing-classified soil erosion results provided reasonable representation of soil erosion in the study area. The accuracy of these results highlights the strong potential and the role of remote sensing and GIS technologies in providing high quality information on soil erosion at least costs, which in turn assist in determining appropriate soil erosion control and management practices.

Keywords: Soil erosion risk; Umzintlava catchment; geospatial technologies; revised universal soil loss equation (RUSLE)

3.1. Introduction

Worldwide, soil erosion is regarded as one of the most important contributors to environmental and socio-economic problems (Fu et al., 2006; Rahman et al., 2009; Aiello et al., 2015). Literature on the effects of soil erosion is vast (Oldeman et al., 1991; Singer and Warkentin, 1996; Lal, 2001; Morgan, 2005; Pimentel, 2006; Van Oost et al., 2007). In general, soil erosion negatively affects soil fertility and soil productivity. Over the last four decades, almost one-third (30%) of the world's productive land has been lost to the consequences of soil erosion at a rate of more than 10 million hectares per year (Pimentel et al., 1995; Lal, 2003; Yang et al., 2003; Jahun et al., 2015). The declining soil fertility due to

soil erosion is a contributing factor to food insecurity in many rural parts of the world, particularly the developing world including South Africa, where subsistence agriculture is widely practiced. If food security is to be realized, especially at the household level in such rural areas like in South Africa, then soil erosion must be thoroughly contained and managed. Mandatory in this endeavor, is the availability of qualitative and quantitative information on the spatial distribution of soil erosion risk.

The identification of soil erosion prone areas with sufficient detail and accuracy is now deemed a prerequisite for designing and implementing relevant soil and water conservation measures at the catchment level (Lane et al., 2000; Shi et al., 2004; Prasannakumar et al., 2012). A variety of models on the spatial distribution of soil erosion exists and many have been summarized in Merritt et al. (2003). Among these, the Universal Soil Loss Equation (USLE) proposed by Wischmeier and Smith (1978) and revised by Renard et al. (1997) is the most commonly used model worldwide. Although the revised USLE (RUSLE) has its own shortcomings, it is currently at the core of soil erosion assessment throughout the world, because it still represents a reasonable compromise between accuracy and ease of application (Risse et al., 1993).

RUSLE was originally designed to assess soil loss from rill and interill erosion on agricultural fields (Wischmeier and Smith, 1978; Renard et al., 1997; Karydas et al., 2009), and does not account for soil loss from gully erosion (Poesen et al., 2003). Yet, gullies represent an important source of sediment entering the stream because of their high delivery ratios especially when well connected to streams (Wasson et al., 1996). For this reason, many investigators including among others Onyando et al. (2004), Lim et al. (2005), Duraes, de Mello, and Beskow (2016), and Tamene et al. (2017), have coupled RUSLE with sediment delivery models in an attempt to determine aggregate soil loss from catchment areas. Besides assisting in quantitative estimates of soil loss, sediment yield calculation may also provide useful information pertaining to the spatial representation of ephemeral and classical gully erosion processes. Sadly, the paucity of validation data often makes sediment yield assessment rather difficult to achieve (De Vente and Poesen, 2005).

Progress in the application of geospatial tools, particularly Geographic Information System (GIS) and remote sensing has improved the efficiency and cost-effectiveness in soil erosion assessment using the RUSLE model than it has historically been the case. However, despite the continuous use of these geospatial tools in RUSLE erosion assessment at catchment level

(Noori et al., 2016); relatively few studies have attempted to combine RUSLE-estimated soil loss with remote sensing-classified soil erosion results to analyze the spatial pattern of this problem. This study is an attempt to integrate the RUSLE model and soil erosion features extracted from remotely sensed imagery in a GIS environment to analyze soil erosion risk at the catchment level using the case of the Umzintlava Catchment in South Africa. The objectives are (1) to assess soil erosion vulnerability of the Umzintlava Catchment, and (2) to explore the relationship, if any, between soil loss and different erosion factors as represented by RUSLE parameters.

3.2. Materials and methods

3.2.1. Study area

The study area is confined to a small catchment (T32E) drained by the Umzintlava River and its tributaries. The catchment is predominantly rural with the majority of its inhabitants involved in subsistence agriculture. Extending from 30°36'55" S and 29°32'34" E to 30°49'28" S and 29°14'26" E, the catchment covers an approximate surface area of 382km² and occupies the eastern section of Umzimvubu Local Municipality. A highly uneven topography with an elevation of approximately 890m for low lying areas and 2015m for elevated areas characterises the catchment. Three major vegetation types are found in the study area with the Highland Sourveld and Dohne Sourveld widely distributed across the elevated areas while the Southern Tall Grassveld, as well as the Valley Bushveld typically occupy areas of low elevation (Acocks, 1988). The climate of the study area falls under that of Umzimvubu Municipality and can be classified as semi-arid with warm and rainy summer months (November to January) as well as dry and cold winter months (May to July) (Boardman et al., 2003). The average minimum temperatures range from 7 °C to 10 °C in winter and 18 °C to 30 °C in summer with the annual rainfall of 671mm. The study area is covered by six broad soil types, namely: Fa, Ac, Aa, Ab, Ea, and Ib soils (Table 3.1 and Appendix B). Subsequent sections detail the methodology employed in this study. Figure 3.1 provides a summary of such methodology in the form of a flow chart diagram.

3.2.2. Data and pre-processing

The *Systeme Pour l'Obsevation de la Terre* (SPOT7) image with 12168 columns and 12060 rows was obtained from the South African National Space Agency (SANSA) free of charge. Acquired on 16 April 2016 at 07:41:11 AM, the image consists of four multispectral bands (Blue, Green, Red, and Infrared) with a spatial resolution of 5.5m, and a panchromatic band

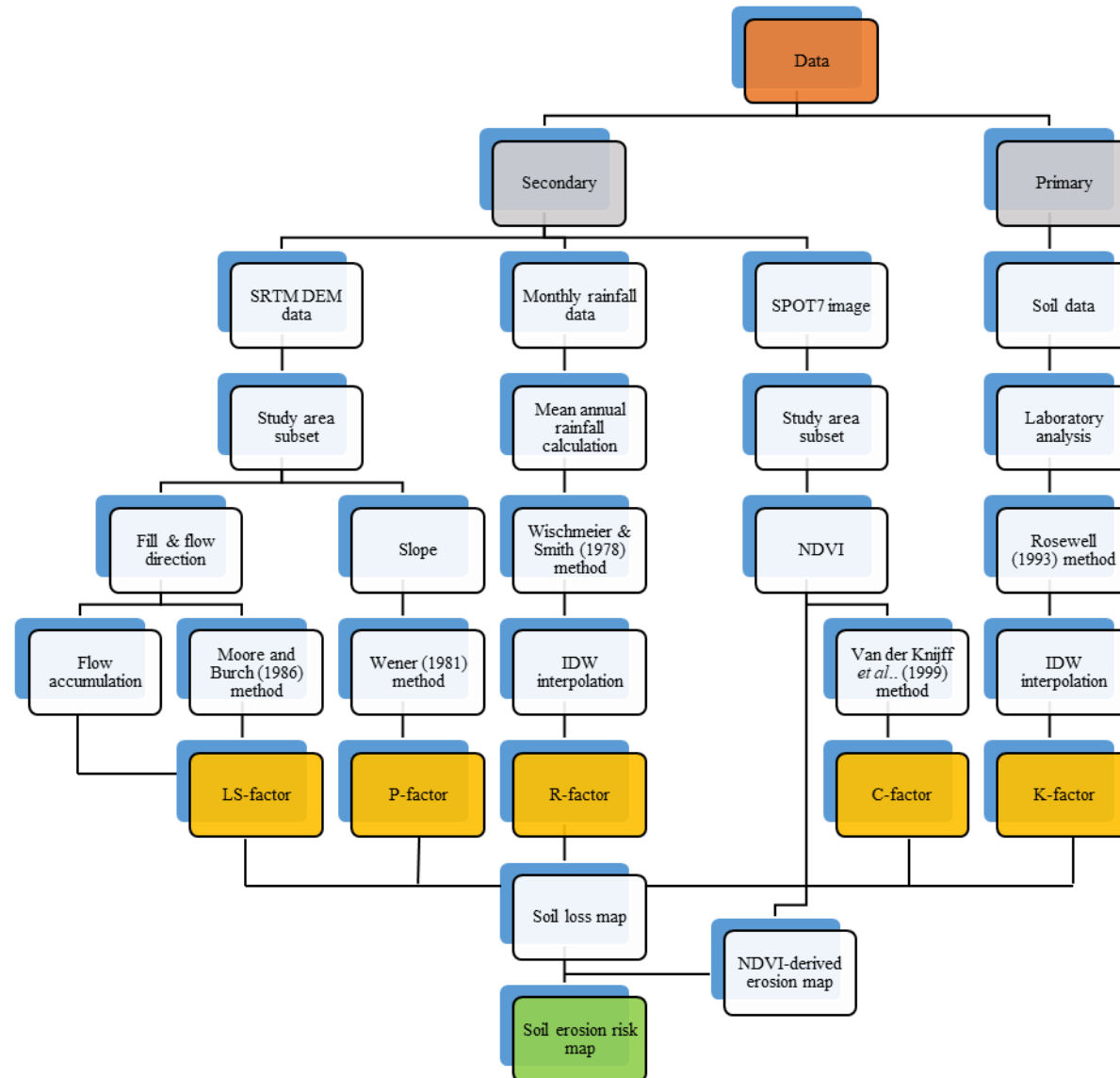


Figure 3.1 Methodology flow chart for this study.

with a spatial resolution of 1.5m. The SPOT7 image product was already orthorectified by the suppliers, hence no further geometric corrections were necessary. Only radiometric normalisation was conducted, using the ‘Apparent Reflectance’ function located within the Image Analysis module in ArcGIS 10.4 to convert the SPOT image digital numbers (DNs) to top of atmosphere reflectance.

Other data used in this study include rainfall data, digital elevation model (DEM), and soil data. The monthly rainfall data spanning a period of 46 years (1970-2016) was obtained from the South African Weather Services (SAWS). A 1-arc second (approximately 30m) Shuttle Radar Topography Mission (SRTM) Void Filled DEM was downloaded from the United States Geological Survey (USGS) at no cost. Twenty four soil samples representing major soil types in the study area were collected from the top soil (between 0 and 30cm). Given that the data are obtained from multiple sources, efforts were made to improve the spatial accuracy by co-registering all the spatial data to a common coordinate system, comprising the Universal Traverse Mercator (UTM) projection, zone 35 South and World Geodetic System 1984 (WGS84) datum.

3.2.3. Image classification and error assessment

The Normalised Difference Vegetation Index (NDVI) was developed in the 1970s by Rouse et al. (1974), and since then has become a useful tool for feature extraction from remotely sensed data (e.g. Bhandari et al., 2012; Phinzi and Ngetar, 2017). One advantage of using spectral vegetation indices like NDVI is their ability to highlight spatial objects in an image while minimizing atmospheric and illumination angle effects (Meusburger et al., 2010). In the present study, NDVI (Equation 3.1) derived from SPOT7 was used to extract information on both land use/land cover (LULC) and soil erosion features with the help of different NDVI classification thresholds (Tables 3.1 and 3.2, respectively). These thresholds were determined on a trial and error basis in ArcMap 10.4 using Map Algebra. The rationale for selecting the best thresholds was based on the overall and kappa statistics results of the derived LULC and soil erosion features (Phinzi and Ngetar, 2017).

$$NDVI = \frac{NIR - Red}{NIR + Red} \quad [3.1]$$

Where *NIR* is the near-infrared (Band 4) reflectance, and *Red* is the visible red (Band 3) reflectance. NDVI was generated in ERDAS IMAGINE 2016 software using an in-built NDVI module. NDVI-classified LULC and soil erosion results were subjected to error

assessment through the confusion matrix. For LULC, 180 randomly selected points were generated in ArcMap 10.4 using the ‘Create Accuracy Assessment Points’ tool within which the ‘Equalized Stratified Random’ option was selected as a sampling strategy to ensure that each LULC class was assigned the same number of points, *viz.* 30 points per class. Using the same procedure, 60 random points (30 points per class) were generated to assess the soil erosion results.

Table 3.1 NDVI classification thresholds for various LULC classes

LULC	Description	NDVI threshold
Water Bodies	Rivers, dams, and lakes	$0 \leq$
Built-up Areas	Residential areas including roads, and other impervious surface features	$0 - 0.10$
Barren Land	Areas with no vegetation cover such as bare soil, exposed rocks and sand	$0.11 - 0.28$
Agricultural Land	Uncultivated agricultural areas with minimal or sparse vegetation cover.	$0.29 - 0.33$
Rangeland	Grassland areas including shrub lands.	$0.34 - 0.44$
Forest	Photosynthetic, and dense vegetation cover such as trees.	$0.45 - > 0.70$

Table 3.2 NDVI classification thresholds for soil erosion and non-erosion features

Feature	Description	NDVI threshold
Erosion	Gully (i.e. ephemeral and permanent), and stream erosion features.	$0.03 - 0.20$
Non-erosion	Any feature other than erosion feature.	$0 \leq, < 0.03, \text{ and } > 0.20$

The SPOT7 panchromatic band with a high spatial resolution, together with Google Earth (Phinzi and Ngetar, 2017; Tadele et al., 2017) were used for ground truth after which randomly selected points were updated for both LULC and soil erosion results using the ‘Update Accuracy Assessment Points’ tool. Thereafter, the ‘Compute Confusion Matrix’ tool was used to generate error matrices.

3.3. Determination of RUSLE parameters

The RUSLE model estimates annual soil loss based on five input parameters (Wischmeier and Smith, 1978; Renard et al., 1997) using the equation:

$$A = R \times K \times LS \times C \times P \quad [3.2]$$

Where A represents the mean annual soil loss rate ($\text{t ha}^{-1}\text{yr}^{-1}$), R is the rainfall erosivity ($\text{MJ mm. ha}^{-1}\text{h}^{-1}\text{yr}^{-1}$), K is the soil erodibility factor ($\text{t J}^{-1}\text{mm}^{-1}$), LS is slope length and slope steepness factor (dimensionless), C is the cover and management factor (dimensionless); and P is the support practice factor (dimensionless). All the RUSLE parameters were determined and integrated within the ArcMap 10.4 environment following a grid-based approach (Thomas et al., 2017). A standard output cell value of 5m was used in the computation of each parameter so as to ensure consistency and accuracy. The methods used to determine each parameter are briefly described in the subsections that follow.

3.3.1. Rainfall erosivity (R-factor)

Rainfall is one important natural factor influencing water-borne erosion. Rainfall-runoff erosivity (R) refers to the ability of raindrops and overland flow to cause soil erosion (Morgan, 2005). Traditionally, the RUSLE R-factor is calculated based on the product of rainfall kinetic energy (E) and the maximum 30 minute rainfall intensity (I_{30}) (Wischmeier and Smith, 1978). An important setback with this method however, is the difficulty to reflect continuous records of rainfall data (Wang et al., 2016). In addition, the method requires high resolution pluviograph data of at least 20 years (Renard et al., 1997) which is difficult to obtain for many parts of the world (Bonilla and Vidal, 2011), including the study area. An alternative to overcome this constraint has been to establish a relationship between readily available daily, monthly, or annual rainfall data and rainfall erosivity (Da Silva, 2004; Fu et al., 2006; Salako, 2010). Using Wischmeier and Smith's (1978) empirical equation, the monthly rainfall data (1972-2016) from three meteorological stations adjacent to Umzintlava Catchment were used to calculate the R-factor [3.3]:

$$R = \sum_{i=1}^{12} 1.735 \times 10^{(1.5 \log \frac{p_i^2}{p} - 0.8188)} \quad [3.3]$$

Where R represents the rainfall erosivity (R-factor) ($\text{MJ mm. ha}^{-1}\text{h}^{-1}\text{yr}^{-1}$), p_i represents the total monthly precipitation (mm), and p is the mean annual precipitation (mm). Upon obtaining the R values for each station, the Inverse Distance Weighted (IDW) interpolation technique available in ArcMap 10.4 was employed to compute the spatial variability of the R-factor throughout the catchment.

⁵ Note: These abbreviations have been described in Chapter 2, Section 2.2.

3.3.2. Soil erodibility (*K*-factor)

Some soils are much more susceptible to erosion than others due to inherent soil properties (Renard and Foster, 1983). Thus, soil erodibility (*K*-factor) represents the degree to which a particular soil is resistant or susceptible to detachment by rainfall in the form of splash and runoff due to overland flow. A commonly used and accepted method for deriving the *K*-factor values is the soil erodibility nomograph (Wischmeier et al., 1971). Algebraic expressions that approximate the monographic-derived *K*-values are available (e.g. Wischmeier and Smith, 1978; Foster et al., 1981; Rosewell, 1993). In this study, Rosewell's (1993) numeric expression which provides the *K*-factor estimates in international system of units (SI units) was used as given by equations [3.4] and [3.5]. Compared to other RUSLE erodibility equations, this equation is relatively simple and recent, hence preferred in this study.

$$K = 2.77 \times 10^{-7}(12 - OM)M^{1.14} + 4.28 \times 10^{-3}(s - 2) + 3.29 \times 10^{-3}(p - 3) \quad [3.4]$$

$$M = [(Sil + vFSa) \times (100 - Cla)] \quad [3.5]$$

Where *K* is the soil erodibility factor ($t\ h\ MJ^{-1}mm^{-1}$), *OM* is the soil organic matter content (%), *Sil* is the silt fraction (%), *vFSa* is the very fine sand fraction (%), *Cl* is the clay fraction (%), *S* is a soil structure code, and *P* is a permeability class (Appendix D). Twenty-four soil samples representative of six major soil types found within the study area were collected from the first 30cm of the topsoil (A horizon) (Table 3.3). In each soil type, the sampling locations were selected on the basis of soil colour and land use. The Garmin-eTrex 10 handheld Global Positioning System (GPS) receiver was used to capture the sampling locations. Prior to preparation, the soil samples were air-dried at ambient temperature of 21 °C – 23 °C as recommended by the U.S. Environmental Protection Agency-EPA (2008).

Following standard laboratory procedures outlined in Rowell (1994), the above-mentioned physical and chemical properties of soil such as the cations exchange capacity (CEC), and soil pH were determined. Since the RUSLE erodibility (*K*-factor) expression only considers physical properties, CEC and soil pH were indirectly incorporated as ancillary data in order to enhance soil erodibility estimation. According to Wang et al. (2016), soil chemical and physical properties work cumulatively to determine soil erodibility.

Table 3.3 Distribution of soil samples on major soil types (After ARC-ISCW, 2006)

Soil type*	Description	Area (km ²)	Samples
Aa	Freely drained, red and yellow apedal soils with humic topsoils comprise >40% of the land Type.	34	1
Ab	Freely drained, red and yellow, dystrophic/mesotrophic, apedal soils comprise >40% of the land type (yellow soils <10%).	16	2
Ac	Freely drained, red and yellow, dystrophic/mesotrophic, apedal soils comprise >40% of the land type (red and yellow soils each >10%).	55	5
Ea	Black or red clays comprise >50% of land type.	13	3
Fa	Shallow soils (Mispah and Glenrosa forms) predominate; little or no lime in landscape.	254	12
Ib	Rock outcrops comprise >60% of land type.	10	1

*Note: Contained in this column are the broad soil pattern codes representing the dominant grouping of soil forms as suggested by ARC-ISCW (2006).

3.3.3. Slope length and steepness (LS-factor)

The slope length and slope steepness (LS-factor) represent the overall contribution of topography to soil loss (Tanyaş et al., 2015). *Ceteris Paribas*, areas with steep and lengthy slopes tend to suffer more erosion than flat or gentle sloping areas (Morgan, 2005). A 30m SRTM Void Filled DEM product downloaded from the USGS website was used to compute the LS-factor. Prior to its use, the DEM was hydrologically corrected using the “Sink” tool located within the hydrology toolset of ArcMap 10.4. Various well-established methods exist for deriving the LS-factor from a DEM (e.g. McCool et al., 1989; Moore and Wilson, 1992; Desmet and Govers, 1996). For this study, the LS-factor was directly computed from the 30m DEM based on Moore and Burch (1986):

$$LS = \left(\frac{A}{22.13}\right)^m \times \left(\frac{\sin\beta}{0.0896}\right)^n \quad A = (\text{Flow accumulation} \times \text{Cell value}) \quad [3.6]$$

Where LS is the slope length and slope steepness (dimensionless), A is the upslope contributing area per unit cell (m), m (0.4) is a variable slope length exponent, n (1.3) is a slope steepness exponent. By substituting equation [3.6], the LS-factor becomes [3.7]:

$$LS = \{power(((\text{"FlowAcc"}*30)/22.13),0.4)*power((\sin(\text{"Slope"} * 0.01745)/0.0896),1.3)\} \quad [3.7]$$

3.3.4. Cover and management factor (C-factor)

Ranging from 0 to 1, the C-factor relates to the ratio of soil loss under specific cropping conditions to soil loss occurring in bare soil (Wischmeier and Smith, 1978). If the land use completely prevents erosion, then the C-factor becomes 0; if there is no land use that acts as a protection against erosion, then the C-factor becomes 1 and for the rest of the conditions, it is lower than 1 (Tanyaş et al., 2015). In this study, the NDVI map [Equation 3.1] was used to derive the C-factor values as given by equation [8] (Van der Knijff et al., 1999, 2000). The calculation of this factor was done in ArcMap 10.4 using Raster Calculator.

$$C = \exp\left(-a\frac{NDVI}{(\beta-NDVI)}\right) \quad [3.8]$$

Where C represents the cover and management factor (dimensionless), a and β are the parameters that determine the shape of the NDVI curve. In the present work, the values of 2 and 1 were applied for a and β parameters respectively, since such values are said to produce reasonable results (Van der Knijff et al., 2000; Gitas et al., 2009; Kouli et al., 2009; Heung et al., 2013; Bhat et al., 2017).

3.3.5. Support practice factor (P-factor)

The support practice (P) factor indicates the impact of management through the control of runoff, with specific reference to how the management reduces and alters the pattern, direction and speed of that runoff (Renard and Foster, 1983; Renard et al., 2011). It represents the ratio of soil loss after a specific conservation practice to the corresponding soil loss after upward and downward cultivation (Renard et al., 1997). The P-factor values lie in the range of 0 – 1, with 0 representing areas with strong protective measures whereas 1 represents the areas with no support practice (Wang et al., 2016). In this study, the P-factor information was extracted from the slope layer using Wener's (1981) algebraic formula [3.9]. The calculations were carried out in Raster Calculator of ArcMap 10.4.

$$P = 0.2 + 0.03 \times S \quad [3.9]$$

Where P is the support practice factor (dimensionless), and S is the slope (%). Wener's (1981) equation was preferred because of its fairly objectivity and simplicity.

3.4. Statistical analysis

A total of 45 randomly created sample points across the entire study area (Appendix E), were used to extract the mean annual soil loss values from the soil loss map as well as the R, K,

LS, C, and P values from respective GIS-derived RUSLE parameters. These were accomplished using the “Extract Values by Points” tool available in ArcMap 10.4 software. These random sample points were later used in the correlation analysis between soil loss and each RUSLE parameter. The Statistical Package for the Social Sciences (SPSS) version 25 software was used for statistical analysis.

Prior to any further statistical analysis, sample points representing soil loss and RUSLE parameter values were subjected to a One-Sample Kolmogorov-Smirnov (1-Sample K-S) normal distribution test. Given that the data for some variables were not normally distributed, the data for all variables were transformed to normalise them. Thereafter, a parametric correlation analysis, i.e. Pearson’s correlation, was used to quantitatively assess the relationship between soil loss and RUSLE parameters. Not only does it correlates RUSLE parameters to soil loss, the Pearson’s correlation also conveniently allows for the examination of the relationship amongst the parameters themselves. Further to this correlation analysis, scatter plots with different lines of best fit such as linear, quadratic, and cubic fit were applied to the results to visualise the nature of the relationship between soil loss and RUSLE parameters. Amongst these lines of best fit, the cubic line best described the relationship, hence it was chosen in this study.

3.5. Results

3.5.1. LULC and soil erosion features mapping

Figure 3.2a illustrates the spatial distribution of six major LULC types identified in this study. These include water bodies, built-up areas, barren land, agricultural land, rangeland, and forest. A significant portion of the study area is covered by Barren Land (34.79%) closely followed by Rangeland (34.31%). Given the apparent limitation of the RUSLE model to account for soil loss from gully erosion, an attempt was made in the present study to extract gully erosion including rill erosion features. The spatial distribution of these erosion features is presented in Figure 3.2b, while Figure 3.3c shows photographs of some gully erosion features observed in the study area during field observation. Erosion features, particularly gullies, mostly occur in the central part of the catchment (Figure 3.2b) where the LULC is predominantly barren land and agricultural land (Figure 3.2a) in relatively low elevations.

Accuracy assessments of NDVI-classified LULC results (Figure 3.2a) and soil erosion results (Figure 3.2b) is provided in the confusion matrices (Tables 3.4 and 3.5, respectively). While

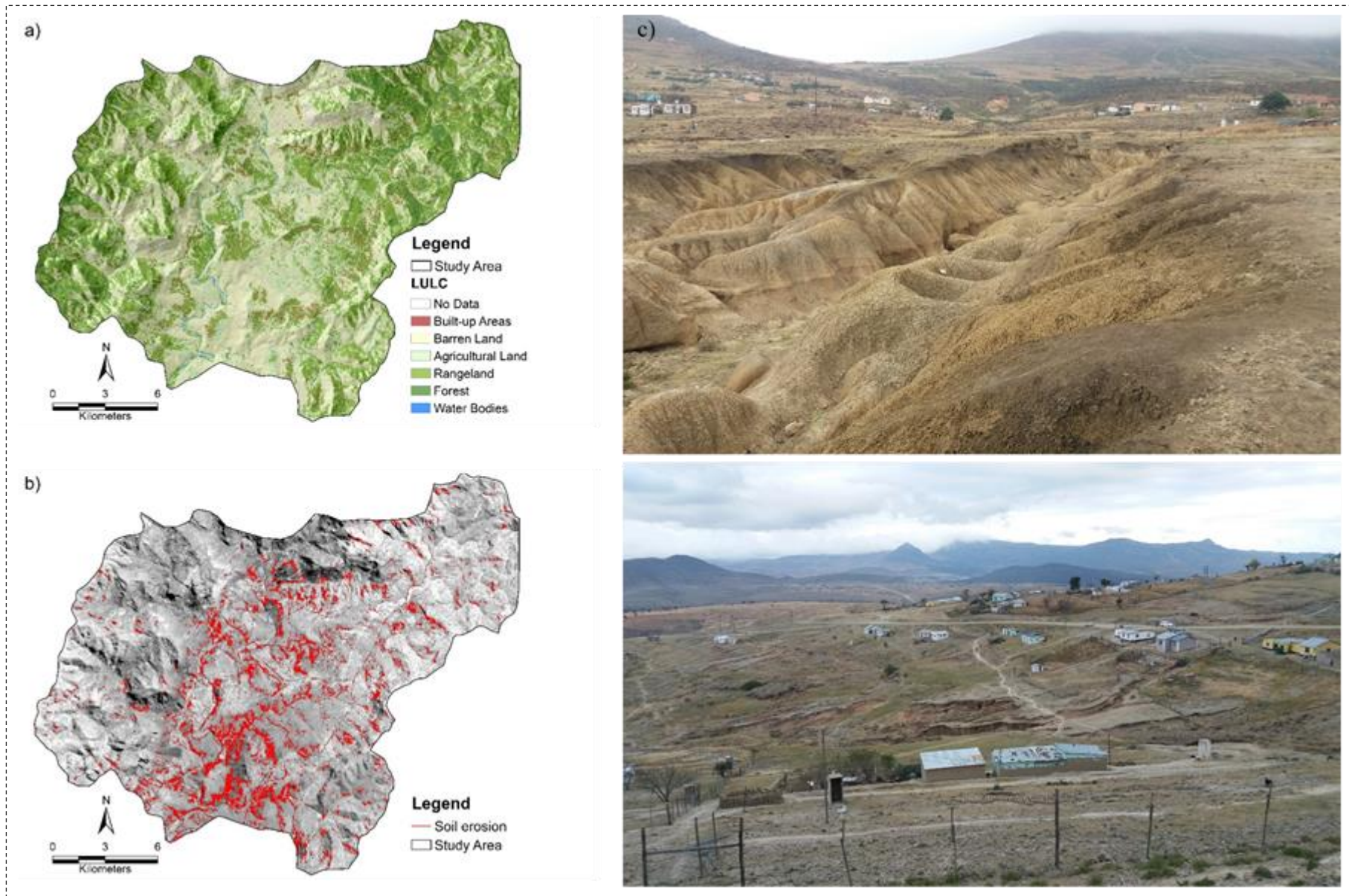


Figure 3.2 (a) LULC types, (b) soil erosion distribution, and (c) field photos of gully erosion observed in the study area.

several indices on accuracy assessments are provided in the confusion matrix, the overall accuracy together with kappa coefficient are considered the most important indices in judging the performance of the classification method under consideration (Lillesand and Kiefer, 2000), in this case, the NDVI threshold technique. Tables 3.4 shows that the LULC results achieved an overall accuracy of 0.75 (75%) and a kappa coefficient of 0.79 (79%), whereas Table 3.5 shows that soil erosion classification results recorded an overall accuracy and kappa coefficient of 0.73 (73%) and 0.87 (87%), respectively.

Table 3.4 Confusion matrix of NDVI-derived LULC results

Class Value*	C1	C2	C3	C4	C5	C6	Total	UA	Kappa	OA
C1	28	2	0	0	0	0	30	93%	-	-
C2	7	6	15	0	2	0	30	20%	-	-
C3	0	1	27	2	0	0	30	90%	-	-
C4	0	0	2	27	1	0	30	90%	-	-
C5	0	0	0	2	28	0	30	93%	-	-
C6	0	0	0	0	3	27	30	90%	-	-
Total	35	9	44	31	34	27	180	-	-	-
PA	80%	67%	61%	87%	82%	100%	-	-	-	-
Kappa	-	-	-	-	-	-	-	-	0.75	-
OA	-	-	-	-	-	-	-	-	-	79%

*C1 = Water Bodies, C2 = Built-up Areas, C3 = Barren Land, C4 = Agricultural Land, C5 = Rangeland, C6 = Forest, UA = User's Accuracy, PA = Producer's Accuracy, and OA = Overall Accuracy.

Table 3.5 Confusion matrix of NDVI-derived soil erosion results

Feature	Non-erosion	Soil erosion	Total	UA	Kappa	OA
Non-erosion	29	1	30	97%	-	-
Soil erosion	7	23	30	77%	-	-
Total	36	24	60	-	-	-
PA	81%	96%	-	-	-	-
Kappa	-	-	-	-	0.73	-
OA	-	-	-	-	-	87%

3.5.2. Soil erosion factors

Figures 3.3 shows the spatial distribution of the (a) R-factor, (b) K-factor, and (c) LS-factor while Figure 3.4 presents (a) NDVI, (b) C-factor, and (c) P-factor in the study area. Quantitative information on the R-factor, K-factor, and C-factor is presented in Tables 3.6, 3.7, and 3.8, respectively. The R-factor for the 1972-2016 period ranges from 814 to 1060 MJ mm. ha⁻¹h⁻¹yr⁻¹ with the latter mostly distributed across the south-western parts

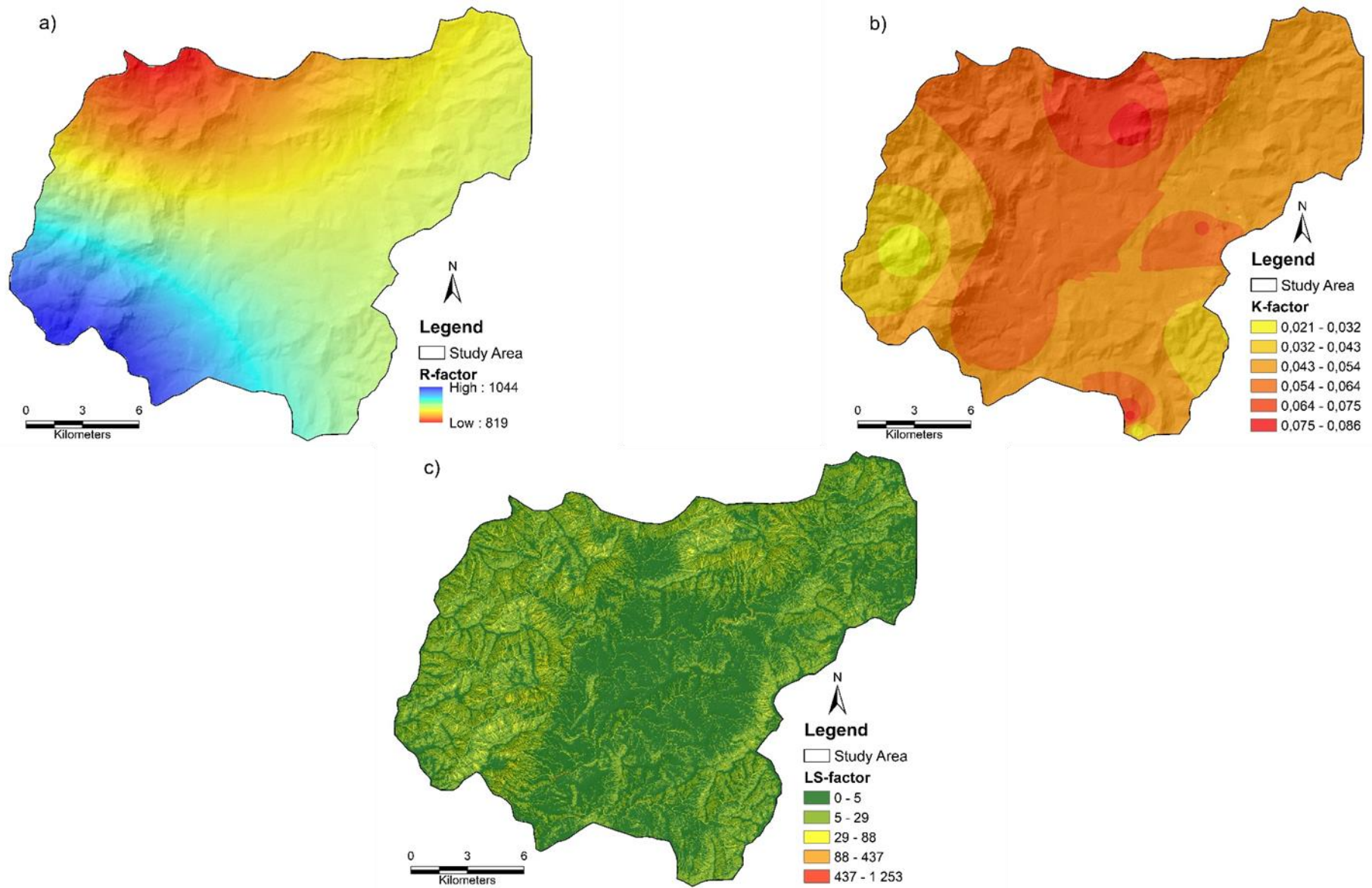


Figure 3.3 (a) R-factor, (b) K-factor, and (c) LS-factor.

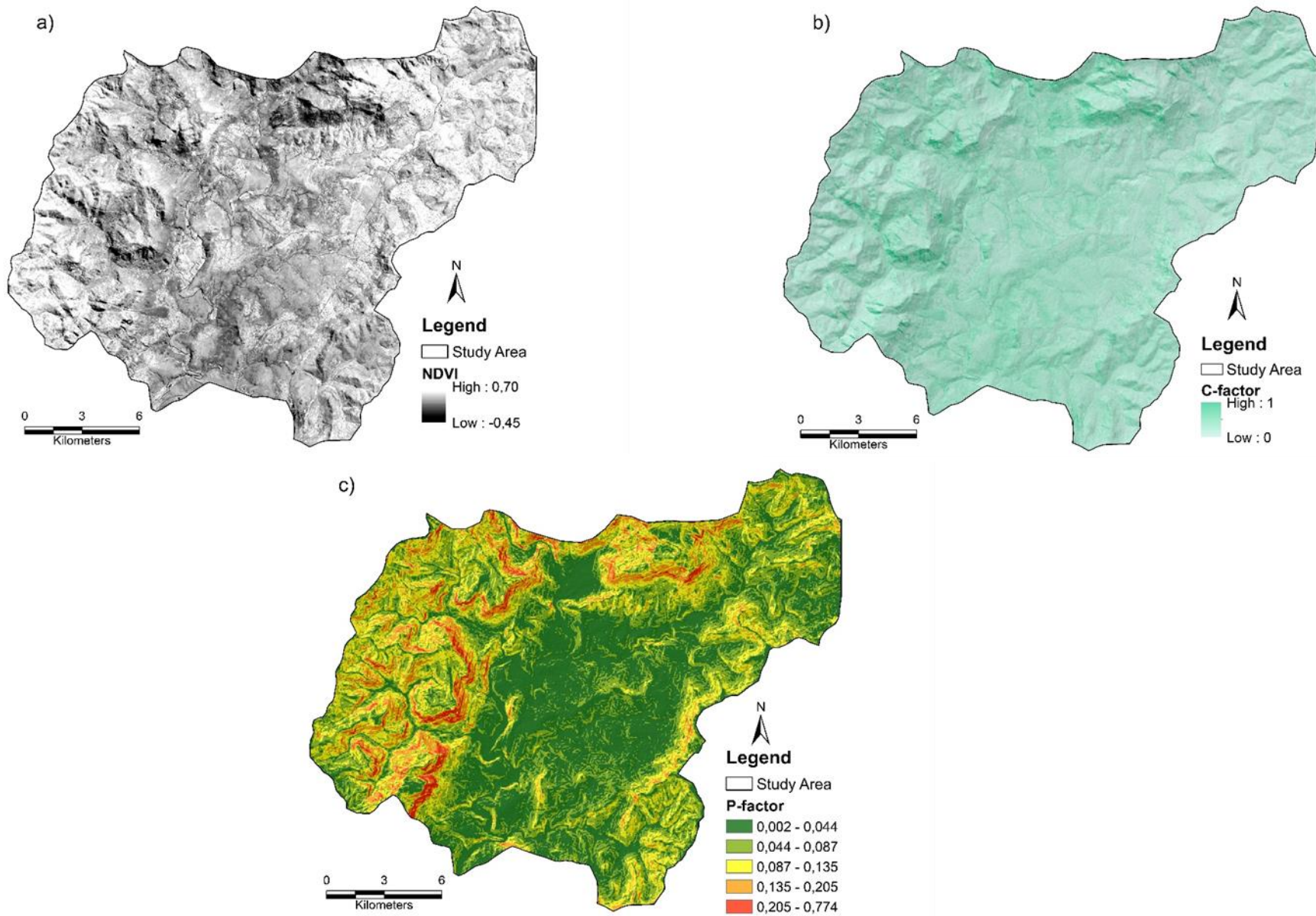


Figure 3.4 (a) NDVI, (b) C-factor, and (c) P-factor.

whereas low R values are found in the northern section of the catchment (Figure 3.3a). Of the three meteorological stations, the Hillendale station recorded the least average annual rainfall erosivity ($814 \text{ MJ mm. ha}^{-1}\text{h}^{-1}\text{yr}^{-1}$), relating to the lowest average annual rainfall (804 mm) from 1972-2016 (Table 3.6). On the contrary, the Fort Donald station located at highest altitude (1440 m) with a relatively high average annual rainfall amount (946 mm), produced low rainfall erosivity of $913 \text{ MJ mm. ha}^{-1}\text{h}^{-1}\text{yr}^{-1}$, reflecting a rather weak relationship between average rainfall amount and rainfall erosivity at this station. With an average annual rainfall of 898 mm and an altitude of 1138 m, the Insizwa station recorded the highest average erosivity of $1060 \text{ MJ mm. ha}^{-1}\text{h}^{-1}\text{yr}^{-1}$.

Table 3.6 Mean annual rainfall erosivity in relation to altitude and mean annual rainfall over the period of 44 years (1972-2016)

Station name	Latitude	Longitude	Altitude (m)	Annual rainfall (mm)	Mean R-factor ($\text{MJ mm. ha}^{-1}\text{h}^{-1}\text{yr}^{-1}$)
Hillendale	30.6181	29.3178	1402	804	814
Fort Donald	30.7916	29.5215	1440	946	913
Insizwa	30.8202	29.2609	1138	898	1060

Soil erodibility (K-factor) values lie in the range of $0.021 - 0.086 \text{ t h MJ}^{-1}\text{mm}^{-1}$ for the study area (Figure 3.3b). Low K values ($0.021 - 0.043 \text{ t h MJ}^{-1}\text{mm}^{-1}$) are found in the western parts whereas high values, ranging from $0.054 - 0.086 \text{ t h MJ}^{-1}\text{mm}^{-1}$ mostly cover the northern, central, and some southern and south-eastern parts of the study area. Using the zonal statistics tool available in ArcMap 10.4 software, mean values of various physio-chemical soil attributes including K-factor were extracted to different soil types in the study area (Table 3.7). The extraction of these mean values revealed that the mean soil erodibility values range from $0.048 - 0.066 \text{ t h MJ}^{-1}\text{mm}^{-1}$.

Of all soil types presented in Table 3.7, the Ea soil type occupying about 3.6% of the total surface area of the catchment is the most potentially highly erodible soil type with the mean K-factor of $0.066 \text{ t h MJ}^{-1}\text{mm}^{-1}$ (Schulze, 2007; Parwada and Van Tol, 2017). This soil type also recorded the highest cations exchange capacity (CEC), viz. $20.2 \text{ cmol}_c/\text{kg}$. A high CEC contributes to soil erodibility since it indicates the presence of certain dispersive clay minerals (Gerber and Harmse, 1987; Rienks et al., 2000). Besides a high CEC value for the Ea soil type, high soil pH (8.6) (Wishchmeier and Mannering, 1969) and particle size distribution including high sand content (87.1%), and low soil organic matter (SOM) content (5.6%) (Wang et al., 2016), and clay content (7.6%) (Wishchmeier and Mannering, 1969) may have

Table 3.7 Mean values of physio-chemical properties of soil with corresponding K values

Soil type	Area (%)	Sand (%)	Silt (%)	Clay (%)	SOM* (%)	pH*	CEC* cmol_c/kg	K-factor (t h MJ⁻¹mm⁻¹)
Ac	14.4	81.2	7.5	11.3	6.1	7.6	7.8	0.048
Ib	2.6	78.3	8.3	13.4	6.4	7.9	12.8	0.048
Aa	8.9	75.9	10.5	13.6	6.3	7.5	11.2	0.051
Ab	4.2	74.9	11.1	14.0	6.0	7.6	10.6	0.053
Fa	66.5	79.2	8.7	12.1	5.7	7.8	10.7	0.054
Ea	3.4	87.1	5.3	7.6	5.6	8.6	20.2	0.066

*SOM = soil organic matter, pH = potential of hydrogen, and CEC = cations exchange capacity.

contributed to high soil erodibility of this soil type. These relationships however were not always consistent for all soil types in the study area. For instance, the Fa soil type which covers more than 65% of the catchment recorded a CEC of 10.7 cmol_c/kg and pH of 7.8 with a mean K-factor of 0.054 t h MJ⁻¹mm⁻¹ compared to the Ib soil type covering about 2.6% of the catchment which recorded the least mean K-factor (0.048 t h MJ⁻¹mm⁻¹) but higher CEC (12.8 cmol_c/kg) and pH (7.9). The other soil types including Ac, Aa, and Ab have mean K values of ≤ 0.053. The pH which ranges from 7.5 – 8.6 and SOM which ranges from 5.6 – 6.4 varied the least amongst all soil types. The results further showed that the pH and SOM covary for most soil types (Table 3.7). For example, high pH values were associated with low SOM values for most soil types, and therefore high soil erodibility.

The LS-factor (Figure 3.3c) varies from 0 to 1253 with a significant portion, especially in the central part of the study area varying from 0 – 29. High LS-factor values of 437 to 1252 occupy steep sloping lands (Mhangara et al., 2012), particularly the north-western, northern, and north-eastern parts of the catchment (Figure 3.3c).

The NDVI generally ranges from -1 to 1, and distinguishes between vegetated and non-vegetated areas (Rouse et al., 1974). In this study, NDVI values range from -0.45 to 0.70 with negative values representing non-vegetative features such as water and shadows, whereas positive values represent features like built-up areas, rangeland, barren land, and forest (Figure 3.4a). The highest value, 0.70 corresponds to dense and photosynthetic vegetation cover.

Figure 3.4 (b) and (c) respectively shows the spatial distribution of the C-factor varying from 0.21 to 0.84 and the P-factor values ranging from 0.002 to 0.774 across the study area. Low C values which represent strong vegetation cover are generally found in elevated areas covered by forests, most notable the western, south-western, northern as well as the eastern parts of

the study area (Figure 3.4b). High C values occur in some central parts of the study area where barren land and built-up areas are found. High C values can also be observed in mountainous areas in the western and northern parts of the study area. In these mountainous areas, high C values are associated with shadows and water bodies occurring in mountain valleys. Lower P values (0.002 – 0.044) are generally found in the central parts whilst high values (0.205 – 0.774) are found in the south-western, western and northern parts of the study area (Figure 3.4c).

The mean NDVI, C, and P values for individual LULC classes are reported in Table 3.8. Low C values are found in vegetated areas with forest recording the lowest mean C value of 0.21, followed by rangeland and agricultural land with mean C values of 0.33 and 0.42, respectively. The lowest mean P value, 0.066, can be observed in agricultural land (Table 3.8). This may be due to the effects of support practices such as contouring that are currently in place (Laker, 2004; Renard et al., 2011). As expected, high P values of 0.118 and 0.075 are found in built-up areas and barren land, respectively (Table 3.8).

Table 3.8 LULC classes and their respective mean NDVI, C-factor and P-factor values

LULC	Mean NDVI	Mean C value	Mean P value
Water Bodies	-0.12	0	0
Agricultural Land	0.30	0.42	0.066
Rangeland	0.36	0.33	0.068
Forest	0.44	0.21	0.069
Barren Land	0.22	0.57	0.075
Built-up Areas	0.08	0.84	0.118

3.5.3. Soil loss rates and its relation to RUSLE parameters

The average annual soil loss in the Umzintlava Catchment is 11 752 t ha⁻¹yr⁻¹. Figure 3.5 shows that a considerable proportion covering approximately 90.19% of the catchment area experiences very low soil loss rates *viz.* 0 – 5 t ha⁻¹yr⁻¹. The areas falling within this soil loss category (0 – 5 t ha⁻¹yr⁻¹) are found at lower altitudes characterised by gentle sloping to nearly flat surfaces. About 8.86% and 0.79% portions of the catchment are respectively subject to low (5 – 12 t ha⁻¹yr⁻¹) and moderate (12 – 25 t ha⁻¹yr⁻¹) soil erosion rates. The remainder of the catchment, namely, 0.95% experiences, high (25 – 60 t ha⁻¹yr⁻¹), very high (60 – 150 t ha⁻¹yr⁻¹), and extremely high (> 150 t ha⁻¹yr⁻¹) rates of soil loss. Figure 3.5 (graph insert) further reports annual average soil loss rates on a ward by ward basis, with ward 6 experiencing the least soil loss rate, namely 5.48 t ha⁻¹yr⁻¹ while ward 5 records the

highest mean soil loss ($28.68 \text{ t ha}^{-1}\text{yr}^{-1}$), closely followed by Ward 2 with $28.32 \text{ t ha}^{-1}\text{yr}^{-1}$. The rates of soil loss in the last two Wards exceed the reported provincial soil loss rate of $25 \text{ t ha}^{-1}\text{yr}^{-1}$ (Le Roux et al., 2008). The soil erosion risk map (Figure 3.6) is an overlay of the RUSLE soil loss estimates (Figure 3.5) and the NDVI-extracted soil erosion features (Figure 3.2b). This soil erosion risk map (Figure 3.6) shows that the entire catchment suffers from or is vulnerable to soil erosion with elevated areas being more vulnerable to hillslope erosion due to relatively steep slopes. Gently sloping areas in the study area have suffered severe gully erosion for reasons discussed in the next section.

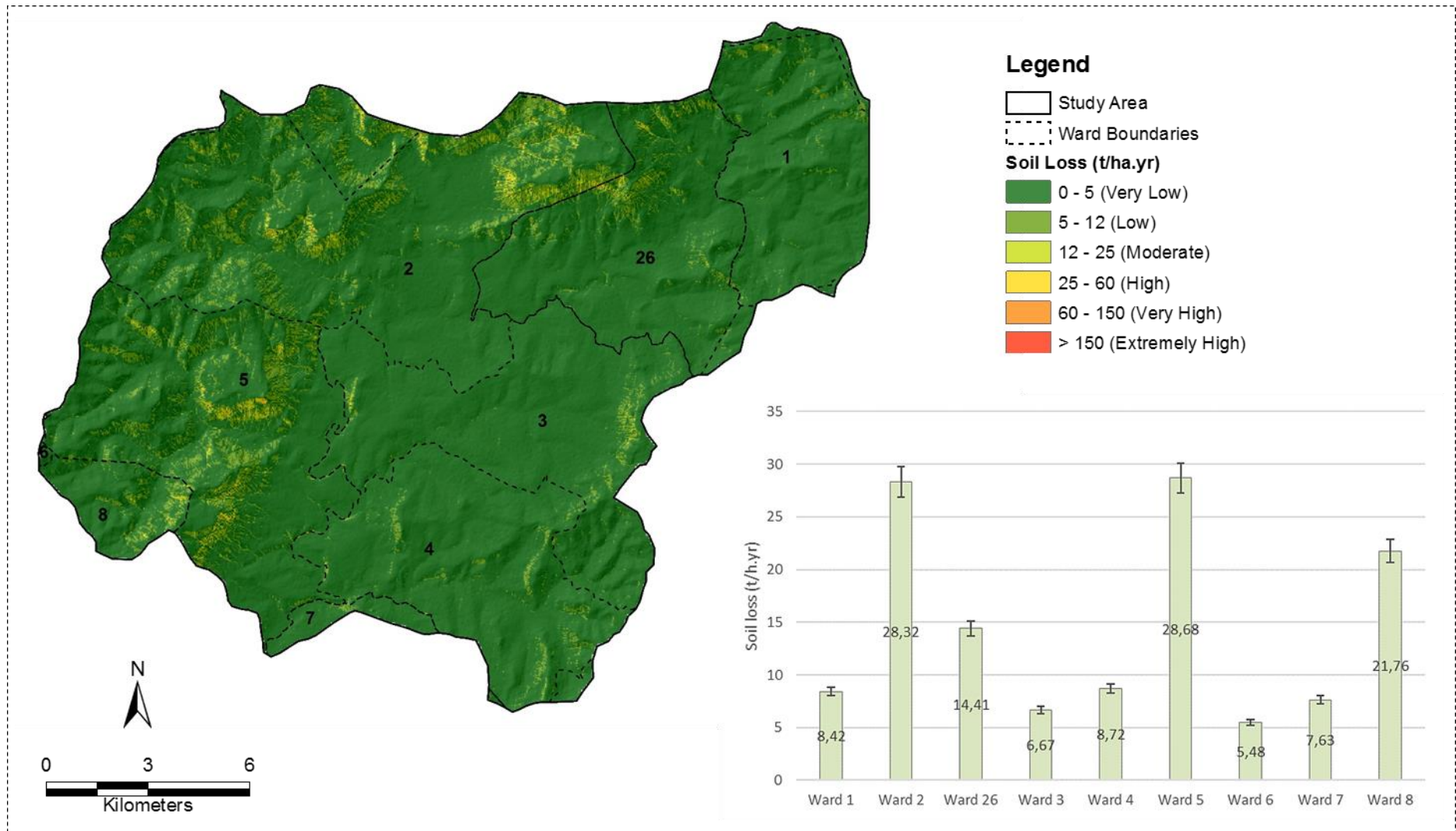


Figure 3.5 Spatial distribution map of soil loss for the Umzintlava Catchment. The graph shows the mean annual soil loss rates by different wards with a $\pm 5\%$ standard error indicated by the sign (I) for each ward.

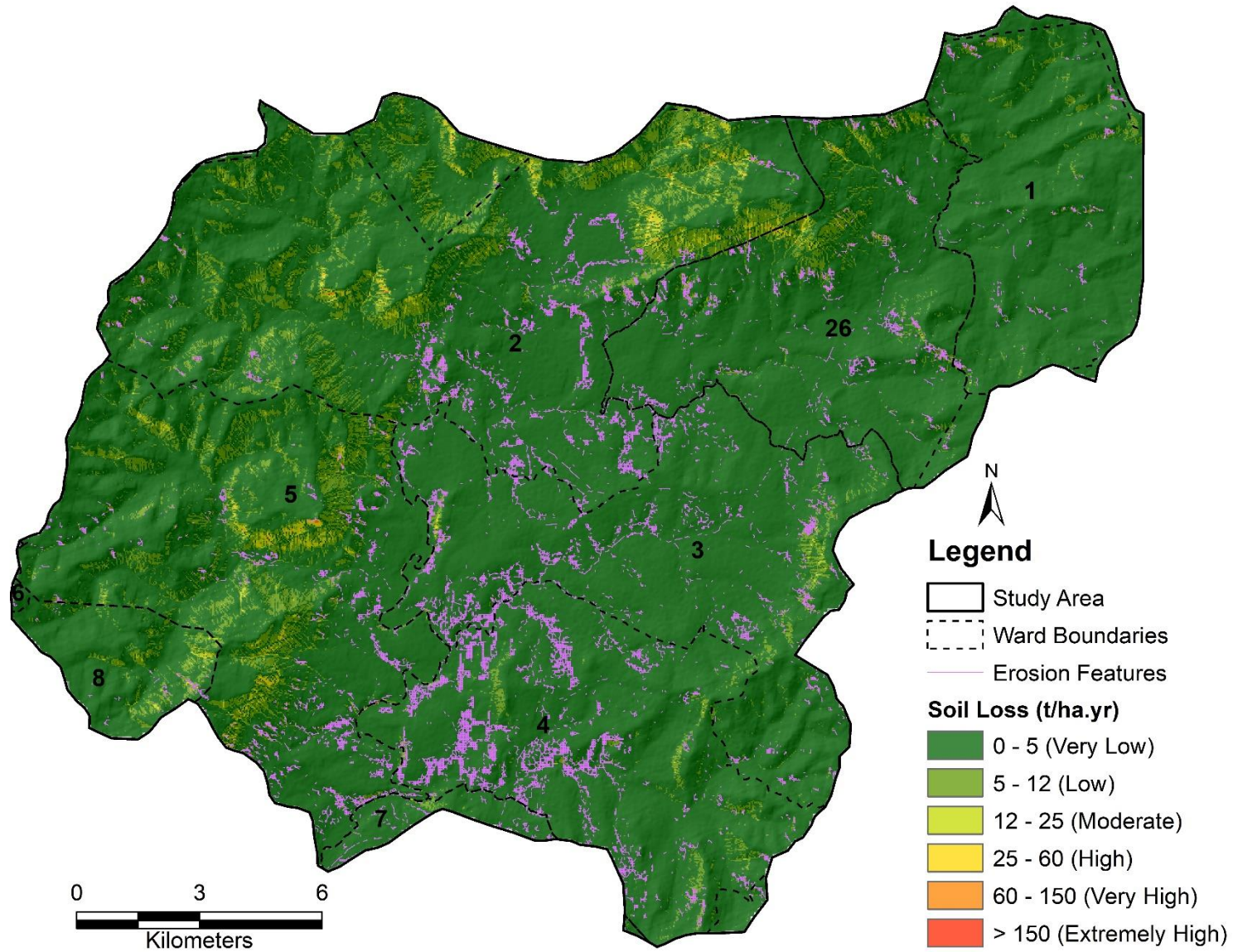


Figure 3.6 Soil erosion risk map for the study area. (Note: this map combines both NDVI-derived soil erosion and RUSLE-estimated soil loss).

3.6. Discussion

Results derived from the integrated use of RUSLE, remote sensing and GIS to determine water-borne soil erosion vulnerability and risk in the Umzintlava Catchment indicate that the catchment suffers from unprecedented rates of soil loss as high as $11\,752\text{ t ha}^{-1}\text{yr}^{-1}$, with some areas recording soil losses varying from 12 to $>150\text{ t ha}^{-1}\text{yr}^{-1}$, far beyond the soil loss tolerance rates proposed for South Africa (McPhee and Smithen, 1984), namely; $3\text{ t ha}^{-1}\text{yr}^{-1}$ for shallow soils and $10\text{ t ha}^{-1}\text{yr}^{-1}$ for deep alluvial soils. Such areas exceeding soil loss tolerances are generally located on steep slopes. This observation is consistent with findings from previous studies including Kamaludin et al. (2013), Gashaw et al. (2016), and Gelagay and Minale (2016) amongst other studies.

Different factors contribute to soil erosion in the Umzintlava Catchment. The LS-factor which represents the overall effect of topography on soil erosion, appears to be the most important soil erosion factor. This is attested by the significant positive correlation ($p < 0.001$, $r^2 = 0.954$, and $r^2\text{ cubic} = 0.928$) between soil loss and the LS-factor (Table 3.9 and Figure 3.7). The P-factor which represents the impact of soil management practices on erosion through the control of runoff also showed a significant correlation ($p < 0.001$ and $r^2 = 0.951$ and $r^2\text{ cubic} = 0.920$) to soil loss, indicating that there are either weak or no erosion control measures in those areas associated with high soil loss rates. These areas include communally held grazing lands and some abandoned agricultural lands. The only erosion control measure widely used in the study area is contouring, commonly practiced in agricultural fields. A statistically significant ($p < 0.001$) relationship was observed between the C- factor and soil loss, however, the correlation coefficient ($r^2 = 0.533$ and $r^2\text{ cubic} = 0.459$) revealed a rather weak relationship between the two. Statistically, there was no significant relationship between soil loss and other RUSLE parameters like the K-factor ($p = 0.903$) and R-factor ($p = 0.230$). These parameters, respectively recorded negative correlation coefficients of $r^2 -0.019$ and $r^2 = -0.182$ (Table 3.9), suggesting that they are not causative factors to soil erosion in the study area.

One objective of this study was to assess soil erosion risk and vulnerability of the Umzintlava Catchment. The rates of soil loss reported in this study certainly highlight the need for prioritisation of the affected areas in the catchment. However, prior to using the RUSLE model as a guide for identifying priority areas, the RUSLE-estimated soil loss results ought to be interpreted with extreme care. In the present study, RUSLE appears to have only

Table 3.9 Pearson's correlations for spatial autocorrelation between RUSLE parameters and soil loss

Variable	Pearson's correlations	Soil loss	C-factor	K-factor	LS-factor	P-factor	R-factor
Soil loss	Correlation coefficient	1	0.533	-0.019	0.954	0.951	-0.182
	<i>p</i> -value		0.001	0.903	0.001	0.001	0.230
C-factor	Correlation coefficient		1	0.256	0.320	0.336	-0.106
	<i>p</i> -value			0.090	0.032	0.024	0.489
K-factor	Correlation coefficient			1	-0.153	-0.114	-0.509
	<i>p</i> -value				0.316	0.455	0.001
LS-factor	Correlation coefficient				1	0.917	-0.145
	<i>p</i> -value					0.001	0.343
P-factor	Correlation coefficient					1	-0.170
	<i>p</i> -value						0.266
R-factor	Correlation coefficient						1

N = 45

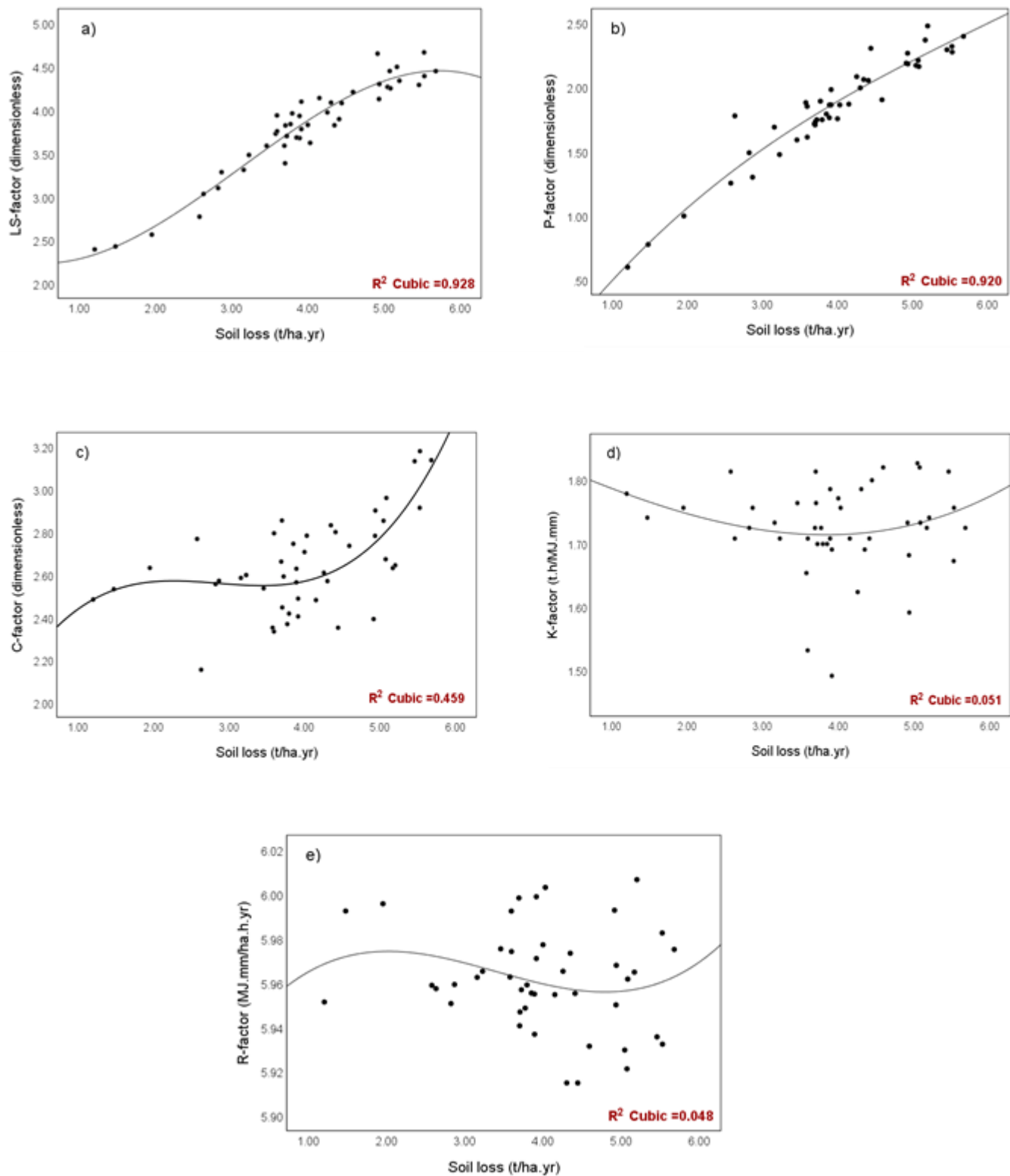


Figure 3.7 Relationship between soil loss and RUSLE parameters: (a) LS-factor, (b) P-factor, (c) C-factor, (d) K-factor, and (e) R-factor.

considered hillslope erosion, giving the impression that erosion-prone areas are restricted to steep gradients. However, field observation together with qualitative assessment of the spatial distribution of soil erosion features (Figure 3.6), indicate that areas located on low gradients also suffer considerable soil erosion in the form of gully. Most of these areas are dominated by shallow soils such as Mispah and Glenrosa soil forms with mean and maximum soil erodibility of 0.054 and 0.071 t h MJ⁻¹mm⁻¹, respectively. These potentially erodible soils (Weaver, 1991), combined with poor or no vegetation cover are possibly the main contributing factors to erosion, particularly in communal settlements.

In their study conducted in a different catchment in Eastern Cape, Mhangara et al. (2012) also observed that communal settlements were predisposed to considerable levels of soil erosion due to overgrazing and wood harvesting. However, since slope steepness proved to be the overriding factor of soil loss in this study, it is apparent that the RUSLE model underestimated soil loss in certain parts of the catchment where for example soil erosion, particularly rill and interrill erosion occur over flat and gentle sloping areas. Such underestimations of soil loss may also be related to the fact, whereas RUSLE considers soil loss related to top soil properties (Hartmann et al., 1989), gully erosion which to a considerable extent is influenced by unstable subsoil, is a dominant erosion form in the Umzintlava Catchment (Phinzi and Ngetar, 2017). It is probably for this reason that the K-factor values obtained in this study poorly correlated ($p = 0.903$ and $r^2 = -0.019$) to soil loss values.

It must also be acknowledged however that, the weak relationship ($p = 0.230$ and $r^2 = -0.182$) exhibited between the R-factor and soil loss in this study was least expected given the predominant view that soil erosion increases with rainfall erosivity (Stocking and Elwell, 1976; Garland, 1995; Morgan, 2005; Angulo-Martínez and Beguería, 2009). Apparently, this view does not hold in the present study. Although higher rainfall amounts may lead to higher rainfall erosivity (Laker, 2004), there is also a positive aspect about high rainfall which should also be considered in the analysis of rainfall erosivity-soil loss relationship. This relates to the fact that higher rainfall can also lead to more vegetative cover, thus leading to less soil loss (Laker, 1990; Laker, 2004). This conceptual and practical though probably explains the paradoxically weak relationship between the R-factor and soil loss in this study, which suggests that higher rainfall in the study area may have contributed to healthy vegetation and soil stability.

Clearly, as this discussion reveals, RUSLE alone cannot be used for soil erosion risk assessment at least in the case of Umzintlava Catchment and Eastern Cape in general where gully erosion is a major contributor to soil loss. It is for this reason that in the present study, RUSLE-derived soil loss estimates and soil erosion features extracted from NDVI (Figure 3.2b) were used to assess soil erosion risk in the Umzintlava Catchment. Despite the debatable results obtained from this study, the spatial overlay of RUSLE-derived soil loss results and remote sensing-classified soil erosion results represent a more accurate method to assess soil erosion in the catchment. Based on this approach (Figure 3.6), the areas requiring urgent intervention in the catchment are ward 2, 5, 4, 3, 26, 8, 1, and 6, respectively. It must be borne in mind that the rates of soil loss derived from the RUSLE model are mere estimates as opposed to absolute values of soil loss (Le Roux et al., 2008), hence must be treated with considerable caution. Overall, the approach employed in the present study was sufficient for identifying the spatial distribution of erosion prone areas in the study area.

3.7. Conclusion

The objectives of this study were (1) to assess soil erosion vulnerability of the Umzintlava Catchment, and (2) to explore the relationship, if any, between soil loss and different erosion factors *viz.* RUSLE parameters. Though not without challenges, the study successfully delineated soil erosion-prone areas in the Umzintlava Catchment. Approximately 11 752 t ha⁻¹yr⁻¹ average annual soil loss has been estimated for the entire catchment. Based on the visual interpretation of the soil loss results which are corroborated by results of statistical analysis, topography (LS-factor) is the most responsible factor for soil erosion and soil loss in the study area. This is also true with the P-factor which also exhibited a very strong correlation to soil loss due to inadequate or non-existence of soil erosion protection measures. Other RUSLE parameters including the C-factor, R-factor, and K-factor weakly correlated to soil loss, suggesting that they do not significantly contribute to soil loss in the study area. However, despite the statistical poor correlation of these factors to soil loss, field observation supports the conclusion that the K-factor is also an important contributor to soil loss in the study area due to the existence of gullies and numerous erosion pipes, providing evidence of erodible subsoil horizons.

Overall, this study demonstrated that the application of the empirical RUSLE model combined with remote sensing-derived soil erosion results adequately identify areas suffering from soil loss or prone to erosion. These in turn can guide the application of appropriate soil conservation and erosion control practices. The methodology proposed in this study could be

adopted by future studies integrating the RUSLE model, remote sensing and GIS in the assessment of soil erosion in catchments with similar conditions. Additionally, the methodology is both cost-effective and time-efficient and therefore useful in countries where there are financial resource constraints. This study also provides a simple framework that can easily be implemented in data-poor locations in South Africa and elsewhere in the world, particularly in rural areas where there is much reliance on subsistence agriculture, limited financial resources and are vulnerable to soil erosion.

CHAPTER 4

LAND USE/LAND COVER CHANGE AND SOIL EROSION

This chapter is based on:

Phinzi, K. and Ngetar, N.S. (In Review). The impact of land use/land cover change on soil erosion in the Umzintlava Catchment (T32E), Eastern Cape, South Africa. *Geoderma Regional*.

Abstract

Land use/land cover (LULC) change is often recognized as one of the most sensitive indicators of the interaction between human and natural environment contributing to soil erosion. Assessing the impact of LULC change on soil erosion is imperative for soil conservation planning. The main objective of this paper was to assess the impact of LULC change on soil erosion in the Umzintlava Catchment from the period 1989-2017 (28 years). To achieve this objective, multi-temporal Landsat data together with the Revised Universal Soil Loss Equation (RUSLE) model were used. Six LULC classes including water bodies, badlands, bare soil and built-up area, agriculture, grassland, and forest were derived for the years 1989, 2001, and 2017. A post-classification change detection analysis showed that water bodies, agriculture, and grassland decreased by 0.04%, 1.80%, and 13.42%, respectively, whereas the areas covered by forest, badlands, and bare soil and built-up area increased by 3.73%, 1.78%, and 9.74% respectively, during the study period. The mean annual soil loss in the study area declined from 1027.36 t ha⁻¹yr⁻¹ in 1989 to 769.62 t ha⁻¹yr⁻¹ in 2001 and then further to 138.71 t ha⁻¹yr⁻¹ in 2017. Despite this consistent decline in mean annual soil loss, the analysis of soil loss results by different LULC classes revealed that all LULC classes, except badlands, experienced an increase in mean annual soil loss rates during the last 28 years. Overall, this study provided relevant knowledge on the relationship between LULC change and soil erosion, highlighting the necessity and importance of integrating remote sensing and soil loss models in spatio-temporal soil erosion assessment at the catchment level.

Keywords: Land use/land cover (LULC) change; Soil erosion; Revised Universal Soil Loss Equation (RUSLE); Multi-temporal remote sensing; Umzintlava Catchment

4.1. Introduction

Water-borne erosion is an important factor causing land degradation (Flanagan, 2002), and is increasingly becoming a serious threat to the sustainability of non-renewable natural resources including soil around the world (Wang et al., 2016). Due to this apparent threat, soil erosion by water has attracted considerable attention in the past few years (Singer and Shainberg, 2004; Jin et al., 2008; Phinzi and Ngetar, 2017). Various factors affect soil erosion and can be broadly grouped into natural factors (rainfall, vegetation, soil type, and topography) and anthropogenic activities (livestock rearing, deforestation, agriculture, and impervious surfaces, etc.). These natural and anthropogenic factors vary both spatially and temporally, making soil erosion a complex and dynamic phenomenon, hence difficult to

assess. Despite the existence of this complexity, many models have been developed to assess water-borne erosion, one of which is the Revised Universal Soil Loss Equation – RUSLE (Renard et al., 1991; Renard et al., 1997). This model is the most widely applied worldwide (Alexekis *et al.*, 2013; Xiao *et al.*, 2015) because of its simplicity and compatibility with geospatial technologies like geographic information system (GIS) and remote sensing.

RUSLE quantifies soil loss as a direct product of five erosion factors including rainfall erosivity (R-factor), soil erodibility (K-factor), slope length and steepness (LS-factor), vegetation cover and management (C-factor), and support practice (P-factor) (Renard et al., 1997). Land use/land cover (LULC) change is recognised as one of the most sensitive indicators of the interactions between human and natural environment (Alkharabsheh et al., 2013). It directly and indirectly impacts on each of the above RUSLE parameters. Amongst these parameters, the C-factor is by far the most important parameter which can easily be influenced by LULC change as it measures the combined effect of all interrelated cover and management variables (Benkobi et al., 1994; Toy et al., 1999) through human intervention.

Holding other RUSLE parameters constant, an increase or decrease in C-factor due to LULC change can result in an increase or decrease in soil erosion, respectively. Hence, assessing the response of soil erosion to LULC change is imperative for soil conservation planning (Xiao et al., 2015). Due to its dynamic nature, remotely sensed data combined with RUSLE is increasingly recognized as one of the most rapid, credible, and effective methods (Yin et al., 2007; Sylla et al., 2012; Yang, 2014) for assessing the LULC-soil erosion nexus in space and time. Many studies have used the RUSLE model in conjunction with remote sensing to assess the impact of LULC change on soil erosion in different catchments around the world (Geberesamual et al., 2010; Paiboonvorachat and Oyana, 2011; Alkharabsheh et al., 2013; Mallick et al., 2014; Wang et al., 2016; Kavian et al., 2017; Tadesse et al., 2017). However, in other parts of the world like South Africa, the impacts of LULC dynamics on soil erosion have been given little attention. Yet, like any other developing country, South Africa has undergone serious land cover modifications over the last few decades. The main purpose of this study is to assess the impact of LULC change on soil erosion in the Umzintlava Catchment in Eastern Cape, South Africa from the period 1989-2017, using multi-temporal remotely sensed data together with the RUSLE model.

4.2. Materials and methods

4.2.1. Study area

The study was conducted in the Umzintlava Catchment (T32E) which occupies a surface area of about 382km², in the Eastern Cape, one of the most severely eroded provinces in South Africa. The catchment is situated between latitudes 30°36'55" S and 30°49'28" S and longitudes 29°32'34" E and 29°14'26" E. The elevation of the catchment varies approximately from 890m – 2015m above sea level. The climate is semi-arid with warm and rainy summer months (November to January) as well as dry and cold winter months (May to July). The average minimum temperatures for the catchment lie in the range of 7 °C – 10 °C in winter and 18 °C – 30 °C in summer with an average annual rainfall of about 671mm. The catchment is characterised by three major vegetation types, namely: Highland Sourveld and Dohne Sourveld, Southern Tall Grassveld, as well as Valley Bushveld. The Highland and Dohne Sourveld type typically occupies the elevated areas while other vegetation types are commonly found in areas of low elevation. Like in most rural catchments in the country, the majority of inhabitants in the Umzintlava Catchment are involved in subsistence agriculture.

4.2.2. Datasets

To achieve the aim of the study, multi-source datasets including satellite images, climate data, digital elevation model (DEM), and soil data were obtained from various sources. Remote sensing data included three Landsat images from 1989 to 2017 (Table 4.1), downloaded from the United States Geological Survey (USGS) website (<https://earthexplorer.usgs.gov/>). Landsat images are particularly preferred in this study because of their free availability in addition to providing the oldest archive of images, permitting the analysis of historical LULC changes and their impact on soil erosion. A 1-arc second (approximately 30m) Shuttle Radar Topography Mission (SRTM) Void Filled DEM was also downloaded from the USGS website. Like Landsat data, the SRTM DEM was also chosen because of its free availability. Both the DEM and satellite images were obtained already projected to the Universal Transverse Mercator (UTM), zone 35 South (S), and referenced to the World Geodetic System 1984 (WGS84) datum. Monthly rainfall data spanning a period of 46 years (1970-2016) was obtained from the South African Weather Services (SAWS) and was used for computing the erosivity index. To compute the soil erodibility index, twenty four soil samples were collected from the top soil layer (between 0 - 30cm). The sampling points were selected in Google Earth so as to represent the spatial heterogeneity of major soil types and land use in the catchment.

Table 4.1 Landsat images and their characteristics

Sensor Name*	Acquisition Date	Scene ID	Path, Row	Spatial Resolution (m)	Number of MS bands*	Cloud Cover (%)
Landsat 5 TM	1989/03/09	ETP169R81_5T19890309	169, 081	30	6	5
Landsat 7 ETM+	2001/03/02	ELP169R081_7T20010302	169, 081	30	6	0
Landsat 8 OLI	2017/03/22	LC81690812017081LGN00	169, 081	30	8	0

*TM = Thematic Mapper, ETM+ = Enhanced Thematic Mapper plus, OLI = Operational Land Imager, MS = Multispectral.

4.2.3. Image pre-processing

Traditionally, an important step prior to any further analysis of remotely sensed imagery is image pre-processing. Image pre-processing relates to operations that precede the actual image analysis (Campbell and Wynne, 2011). Such operations improve the interpretability of the image while ensuring that the image is close to the true radiant energy and spatial characteristics at the time of its acquisition (Taruvunga, 2008). In this study, each Landsat scene was subjected to absolute atmospheric correction where their digital numbers (DNs) were converted to surface reflectance (Song et al., 2001). This was achieved by means of the ‘Apparent Reflectance’ function located in the Image Analysis module in ArcMap 10.4. All Landsat scenes were acquired already projected to the desired coordinate system, namely, WGS84 UTM 35 S, necessitating no further geometric corrections.

4.2.4. Classification and accuracy assessment

An important step in determining the impact of LULC change on soil erosion is LULC classification. A semi-automatic image classification method was employed using different Normalised Difference Vegetation Index (NDVI) thresholds (Table 4.2) to derive different LULC classes in the study. Firstly, the ‘Band Arithmetic Function’ tool available in ArcMap, was used to compute the NDVI for 1989, 2001, and 2017, after which suitable NDVI classification thresholds were determined for individual LULC classes (Table 4.2).

Table 4.2 LULC classes and their respective NDVI classification thresholds

LULC class	Description	NDVI threshold
Water Bodies	Rivers, dams, and lakes	$0 \leq$
Badlands	Severely eroded areas with no agricultural potential.	$0 - 0.40$
Bare soil and Built-up area	Areas with no vegetation cover such as bare soil, exposed rocks and sand. Residential areas including roads, and other impervious surface features	$0.40 - 0.52$
Agriculture	Uncultivated agricultural areas with minimal or sparse vegetation cover.	$0.52 - 0.60$
Grassland	Grassland areas including shrub lands.	$0.60 - 0.70$
Forest	Photosynthetic, and dense vegetation cover such as trees.	> 0.70

To assess changes in LULC during the period of study, image post-classification comparison was used. One advantage of this approach is that the classification, rather than the original band-by-band DN values, is used for comparison, thus minimizing atmospheric, sensor, and environmental differences between the images (Peneva-Reed, 2014). This was followed by accuracy assessment. The simplest and widely accepted way of assessing the accuracy is to compare the classified image to reference data using the confusion matrix (Story and Congalton, 1986; Lillesand and Kiefer, 2000). A total of 180 random points were generated and each LULC class was assigned 30 points. Confusion matrices for different years (1989, 2001, and 2017) were computed in the ArcMap environment.

4.2.5. Calculation of *RUSLE* parameters

The determination of soil loss using the *RUSLE* model was imperative for the LULC change versus soil erosion comparison. *RUSLE* quantifies soil loss as a function of five parameters and can be computed by Equation [4.1] (Wischmeier and Smith, 1978; Renard *et al.*, 1997). Table 4.3 shows different empirical equations that were used in this study to derive individual *RUSLE* parameters. To determine the annual soil loss for different years, namely 1989, 2001, and 2017, all *RUSLE* parameters were held constant except the C-factor. The C-factor is the most important *RUSLE* parameter that influence soil erosion, following the LS-factor.

$$A = R \times K \times LS \times C \times P \quad [4.1]$$

Where:

A = mean annual soil loss ($\text{t ha}^{-1}\text{yr}^{-1}$)⁶.

R = rainfall erosivity ($\text{MJ mm. ha}^{-1}\text{h}^{-1}\text{yr}^{-1}$)⁶. This factor relates to the potential ability of the rainfall and runoff to cause soil erosion (Morgan, 2005). The monthly rainfall data (1972-2016) of three meteorological stations, *viz.* Hillendale, Fort Donald, and Insizwa stations located around the study area, were used to derive R values. To compute the erosivity index, the derived R values were interpolated using the Inverse Distance Weighted (IDW) technique located in the Spatial Analyst extension of ArcMap 10.4.

K = soil erodibility ($\text{t J}^{-1}\text{mm}^{-1}$)⁶. Whether or not a particular soil is susceptible to erosion, depends on a range of soil properties. *RUSLE* considers physical properties such as the soil organic matter, particle size, soil structure, and soil permeability as key factors affecting the

⁶ Note: These abbreviations have been described in Chapter 2, Section 2.2.

Table 4.3 Empirical equations used to derive RUSLE parameters in this study

RUSLE parameter	Formula	Reference
<i>R</i>	$R = \sum_{i=1}^{12} 1.735 \times 10^{(1.5 \log \frac{p_i^2}{p} - 0.8188)}$ <p>Where p_i represents the total monthly precipitation (mm), and p is the mean annual precipitation (mm).</p>	Wischmeier and Smith (1978)
<i>K</i>	$K = 2.77 \times 10^{-7}(12 - OM)M^{1.14} + 4.28 \times 10^{-3}(s - 2) + 3.29 \times 10^{-3}(p - 3)$ $M = [(Sil + vFSa) \times (100 - Cla)]$ <p>Where K is the soil erodibility factor ($\text{t h MJ}^{-1}\text{mm}^{-1}$), OM is the soil organic matter content (%), Sil is the silt fraction (%), $vFSa$ is the very fine sand fraction (%), $Cl a$ is the clay fraction (%), S is a soil structure code, P is a permeability class.</p>	Rosewell (1993)
<i>LS</i>	$LS = \left(\frac{A}{22.13}\right)^m \times \left(\frac{\sin\beta}{0.0896}\right)^n A = (\text{Flow accumulation} \times \text{Cell value})$ <p>Where LS is the slope length and slope steepness (dimensionless), A is the upslope contributing area per unit cell (m), m (0.4) is a variable slope length exponent, n (1.3) is a slope steepness exponent.</p>	Moore and Burch (1986)
<i>C</i>	$C = \exp\left(-a \frac{NDVI}{(\beta - NDVI)}\right)$ <p>Where C represents the cover and management factor (dimensionless), a and β are the parameters that determine the shape of the NDVI curve.</p>	Van der Knijff et al., 1999, 2000
<i>P</i>	$P = 0.2 + 0.03 \times S$ <p>Where P is the support practice factor (dimensionless), and S is the slope (%).</p>	Wener's (1981)

erodibility of a particular soil. In this study, these soil properties were determined in a laboratory following standard laboratory procedures (Rowell, 1994), after which K values were calculated (Rosewell, 1993) and interpolated using the IDW interpolation to create the erodibility index.

LS = slope length and slope steepness factor (dimensionless). This parameter represents the overall contribution of topography to soil erosion. Prior to deriving the LS-factor and related parameters such as slope, flow direction, and flow accumulation, the SRTM DEM was hydrologically corrected using the 'Sink' tool found in the hydrology toolset of ArcMap 10.4 environment. Thereafter, the LS-factor was computed from the corrected DEM using the method proposed by Moore and Burch (1986).

C = cover and management factor (dimensionless). The C-factor which indicates the effect of cropping and other management practices on soil erosion (Uddin et al., 2016), was empirically derived from the NDVI map using the equation of Van der Knijff et al. (1999, 2000).

P = support practice factor (dimensionless). The P-factor relates to the impact of management practices like contouring and strip cropping which alters and reduce the pattern, direction, and speed of runoff (Renard and Foster, 1983; Renard et al., 2011). The information on this factor was derived from the slope map based on the empirical relation of Wener (1981).

4.3. Results

4.3.1. LULC classification

Figure 4.1 shows the spatial distribution of six LULC classes (water bodies, badlands, bare soil and built-up area, agriculture, grassland, and forest) for the three time periods, (a) 1989, (b) 2001, and (c) 2017. During all the years, badlands occurred in the central parts whereas forests occurred in the northwestern, northern and northeastern parts of the study area. A considerable part of the catchment surface area is occupied by bare soil and built-up area, and agricultural land. These LULC classes, i.e. bare soil and built-up area, and agricultural land, combined contributed about 61.19% in 1989, 58.55% in 2001, and 61.18% in 2017 of the total surface area (382 km²) of the Umzintlava Catchment (Figure 4.2). Forest and water bodies occupied a comparatively small proportion of the catchment. Specifically, water bodies covered a surface area of approximately 0.04% in 1989, 0.01% in 2001, and 0.001%

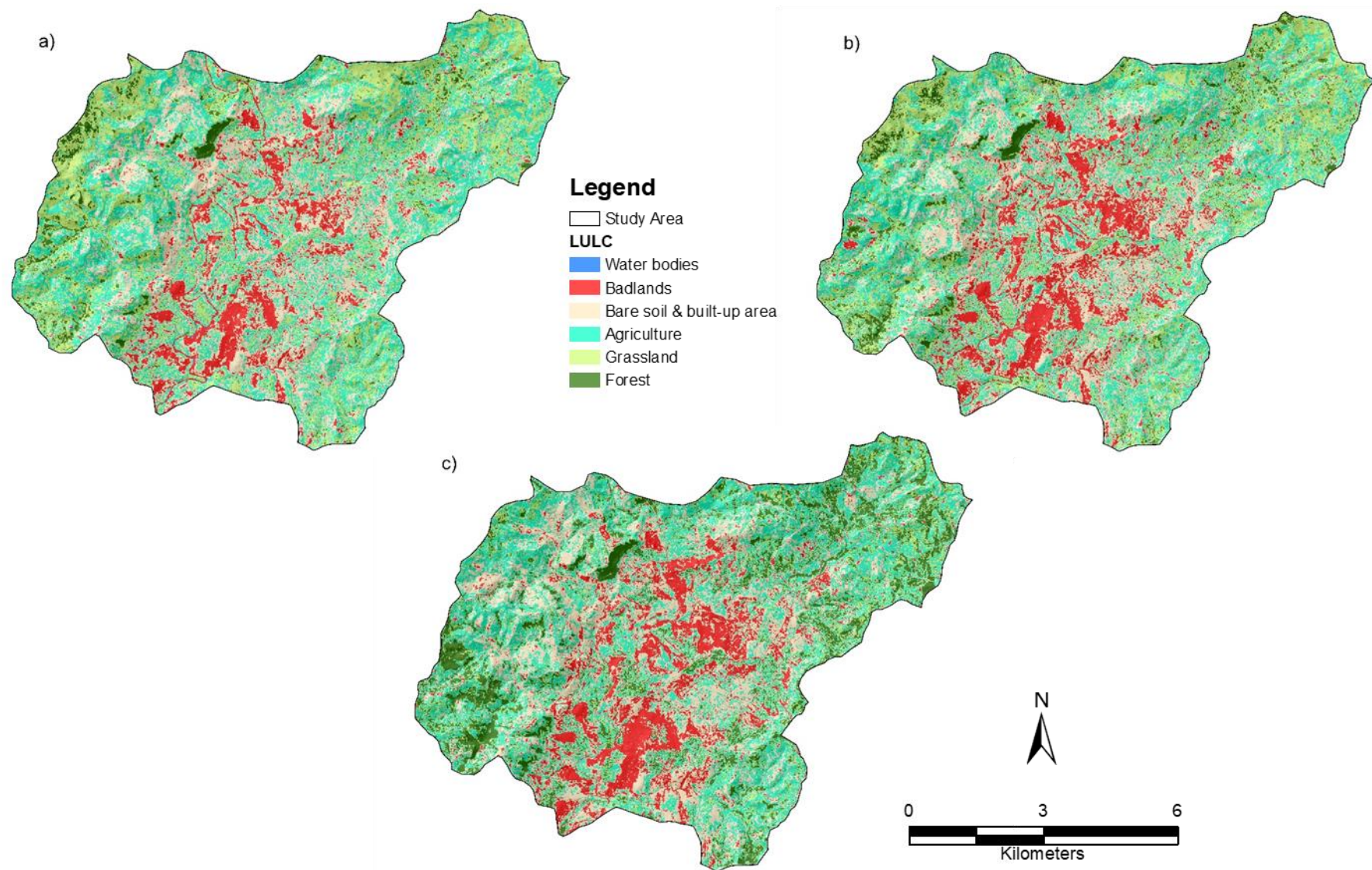


Figure 4.1 LULC for different years: (a) 1989, (b) 2001, and (c) 2017.

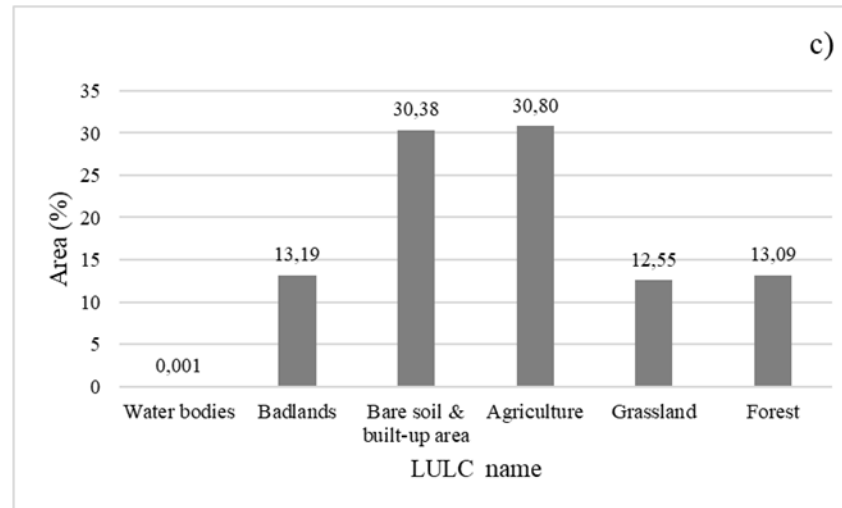
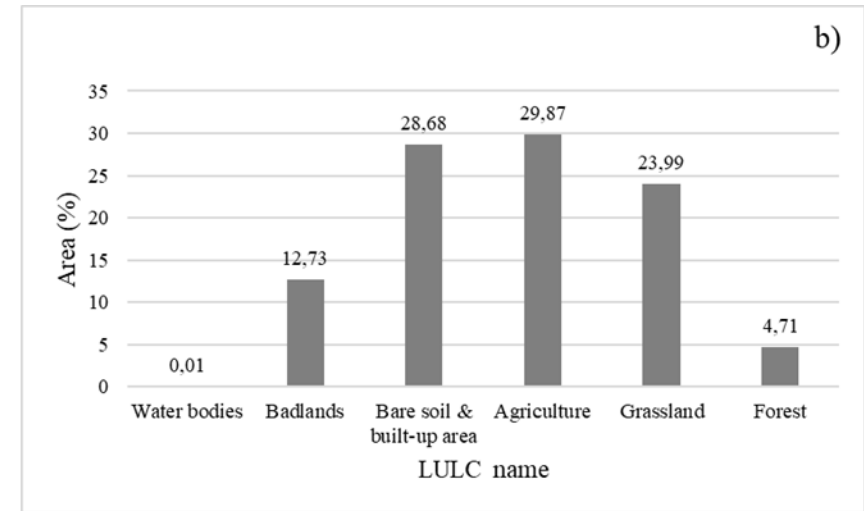
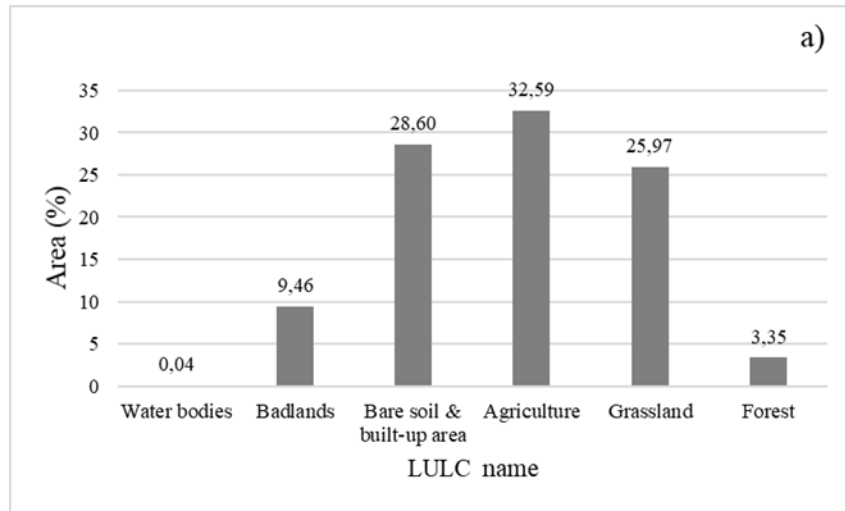


Figure 4.2 LULC surface area: (a) 1989, (b) 2001, and (c) 2017.

in 2017 whereas forest occupied 3.35% in 1989, 4.71% in 2001, and 13.09% in 2017 (Figure 4.2). Over the years covering the study period, there was a consistent increase in the surface area covered by badlands, bare soil and built-up area, and forest (Figure 4.2). On the contrary, the surface area covered by water bodies, and grassland declined whereas agricultural land fluctuated over the years (Figure 4.2).

4.3.2. Accuracy assessment

Tables 4.4, 4.5, and 4.6 respectively present the classification accuracies for the years 1989, 2001, and 2017. While various accuracy indices are presented in these tables including producer's accuracy (PA), user's accuracy (UA), overall accuracy (OA), and kappa coefficient (Story and Congalton, 1986), the foci of the analysis in this section is on OA and kappa coefficient. The 1989 LULC (Table 4.4) and 2001 LULC (Table 4.5) classifications recorded the same accuracies in relation to the OA (0.79) and kappa coefficient (0.75). On the contrary, the 2017 LULC classification results yielded a comparatively low OA of 0.74 and 0.69 kappa coefficient (Table 4.6). These results show relative accuracies of individual years but not the accuracy of the change detection itself. To obtain the accuracy of change detection for a specific period (1989-2001, 2001-2017, 1989-2017), the OAs of the two classifications were multiplied (Singh, 1989). The periods 1989-2001 and 2001-2017 recorded the same change detection accuracy of 0.58 ($0.79 * 0.74$) whereas the entire period (1989-2017) achieved an accuracy of 0.62 ($0.79 * 0.79$).

4.3.3. Temporal trends of soil loss and rainfall

The integration of RUSLE results and GIS (Figure 4.3) show that the mean annual soil loss decreased during the study period from $1027.36 \text{ t ha}^{-1}\text{yr}^{-1}$ in 1989, $769.62 \text{ t ha}^{-1}\text{yr}^{-1}$ in 2001, to $138.71 \text{ t ha}^{-1}\text{yr}^{-1}$ in 2017. Between 1989 and 2001, soil loss decreased by approximately $257.74 \text{ t ha}^{-1}\text{yr}^{-1}$ (14.34%) while the period 2001-2017 experienced an even higher decrease of about $630.91 \text{ t ha}^{-1}\text{yr}^{-1}$ (69.46%). Such consistent decline in mean annual soil loss could partly be due to temporal trends in the mean annual rainfall during the study period. The mean annual rainfall fluctuated over the years with the year 2000 recording the highest (>300 mm) and 2015 recording the least (<150 mm) rainfall (Figure 4.4). The years 1989, 1997, 1998, 2006, and 2012 recorded a mean annual rainfall of >250 mm whereas the remaining other years recorded below 250 mm. The trend line (red) shows that the catchment experienced a decrease in mean annual rainfall during the study period (Figure

4.4), which probably explains the continuous decrease in the mean annual soil loss over the years.

Although there was a consistent decrease in the mean annual soil loss during the study period (from 1027.36 t ha⁻¹yr⁻¹ in 1989 to 138.71 t ha⁻¹yr⁻¹ in 2017), some areas experienced increased rates of soil loss. For example, the proportion of the study area experiencing moderate to extremely high rates of soil loss consistently increased during the same period (Table 4.7). This observation can also be confirmed by a visual assessment which shows consistency in erosion intensity or severity (areas in orange and red colours), commonly occurring in elevated areas over the years (Figure 4.3). The results show that highlands with steep slopes are increasingly subjected to alarming rates of soil loss than areas with gentle slopes (Table 4.7). Such findings are comparable to other RUSLE-related studies conducted elsewhere around the world. For example, in Saudi Arabia, Mallick et al. (2014) found that the erosion risk was low in areas with flat or almost flat slopes but increased with increasing gradient. Similar findings were reported by Khosrokhani and Pradhan (2014) in Malaysia, among other studies.

In 1989, an estimated 99.968% (99.542 + 0.426) of the study area experienced ‘Very low (0 – 5 t ha⁻¹yr⁻¹)’ to ‘Low (5 – 12 t ha⁻¹yr⁻¹)’ levels of soil loss (Table 4.7). The area slightly decreased to 99.923% (99.149 + 0.774) in 2001 and 97.387% (77.430 + 19.957) in 2017. Conversely, the areas experiencing ‘Moderate (12 – 25 t ha⁻¹yr⁻¹)’ rates of soil loss increased from 0.026% in 1989, to 0.068% in 2001, and 2.252% in 2017. Similarly, the area with ‘High (25 – 60 t ha⁻¹yr⁻¹)’ to ‘Extremely high (>150 t ha⁻¹yr⁻¹)’ soil losses increased consistently over the years, from 0.006% (0.004 + 0.001 + 0.001) in 1989 to 0.010% (0.006 + 0.003 + 0.001) in 2001, and 0.362% (0.330 + 0.030 + 0.002) in 2017 (Table 4.7).

Table 4.4 Confusion matrix for 1989 LULC

LULC*	C1	C2	C3	C4	C5	C6	Total	UA	OA	Kappa
C1	24	5	0	1	0	0	30	80%	-	-
C2	0	24	6	0	0	0	30	80%	-	-
C3	0	2	21	6	1	0	30	70%	-	-
C4	0	0	2	23	5	0	30	77%	-	-
C5	0	0	0	2	24	4	30	80%	-	-
C6	0	0	1	0	3	26	30	87%	-	-
Total	24	31	30	32	33	30	180	-	-	-
PA	100%	77%	70%	72%	73%	87%	-	-	-	-
OA	-	-	-	-	-	-	-	-	79%	-
Kappa	-	-	-	-	-	-	-	-	-	0.75

*C1 = Water Bodies, C2 = Built-up Areas, C3 = Barren Land, C4 = Agricultural Land, C5 = Rangeland, C6 = Forest, UA = User's Accuracy, PA = Producer's Accuracy, and OA = Overall Accuracy.

Table 4.5 Confusion matrix for 2001 LULC

LULC*	C1	C2	C3	C4	C5	C6	Total	UA	OA	Kappa
C1	19	7	4	0	0	0	30	63%	-	-
C2	0	20	9	1	0	0	30	67%	-	-
C3	0	4	24	2	0	0	30	80%	-	-
C4	0	0	2	24	4	0	30	80%	-	-
C5	0	0	0	7	22	1	30	73%	-	-
C6	0	0	0	0	6	24	30	80%	-	-
Total	19	31	39	34	32	25	180	-	-	-
PA	100%	65%	62%	71%	69%	96%	-	-	-	-
OA	-	-	-	-	-	-	-	-	74%	-
Kappa	-	-	-	-	-	-	-	-	-	0.69

*C1 = Water Bodies, C2 = Built-up Areas, C3 = Barren Land, C4 = Agricultural Land, C5 = Rangeland, C6 = Forest, UA = User's Accuracy, PA = Producer's Accuracy, and OA = Overall Accuracy.

Table 4.6 Confusion matrix for 2017 LULC

LULC*	C1	C2	C3	C4	C5	C6	Total	UA	OA	Kappa
C1	22	3	5	0	0	0	30	73%	-	-
C2	0	27	2	1	0	0	30	90%	-	-
C3	0	2	23	1	1	3	30	77%	-	-
C4	0	3	3	24	0	0	30	80%	-	-
C5	0	5	3	0	20	2	30	67%	-	-
C6	0	0	0	2	2	26	30	87%	-	-
Total	22	40	36	28	23	31	180	-	-	-
PA	100%	68%	64%	86%	87%	84%	-	-	-	-
OA	-	-	-	-	-	-	-	-	79%	-
Kappa	-	-	-	-	-	-	-	-	-	0.75

*C1 = Water Bodies, C2 = Built-up Areas, C3 = Barren Land, C4 = Agricultural Land, C5 = Rangeland, C6 = Forest, UA = User's Accuracy, PA = Producer's Accuracy, and OA = Overall Accuracy.

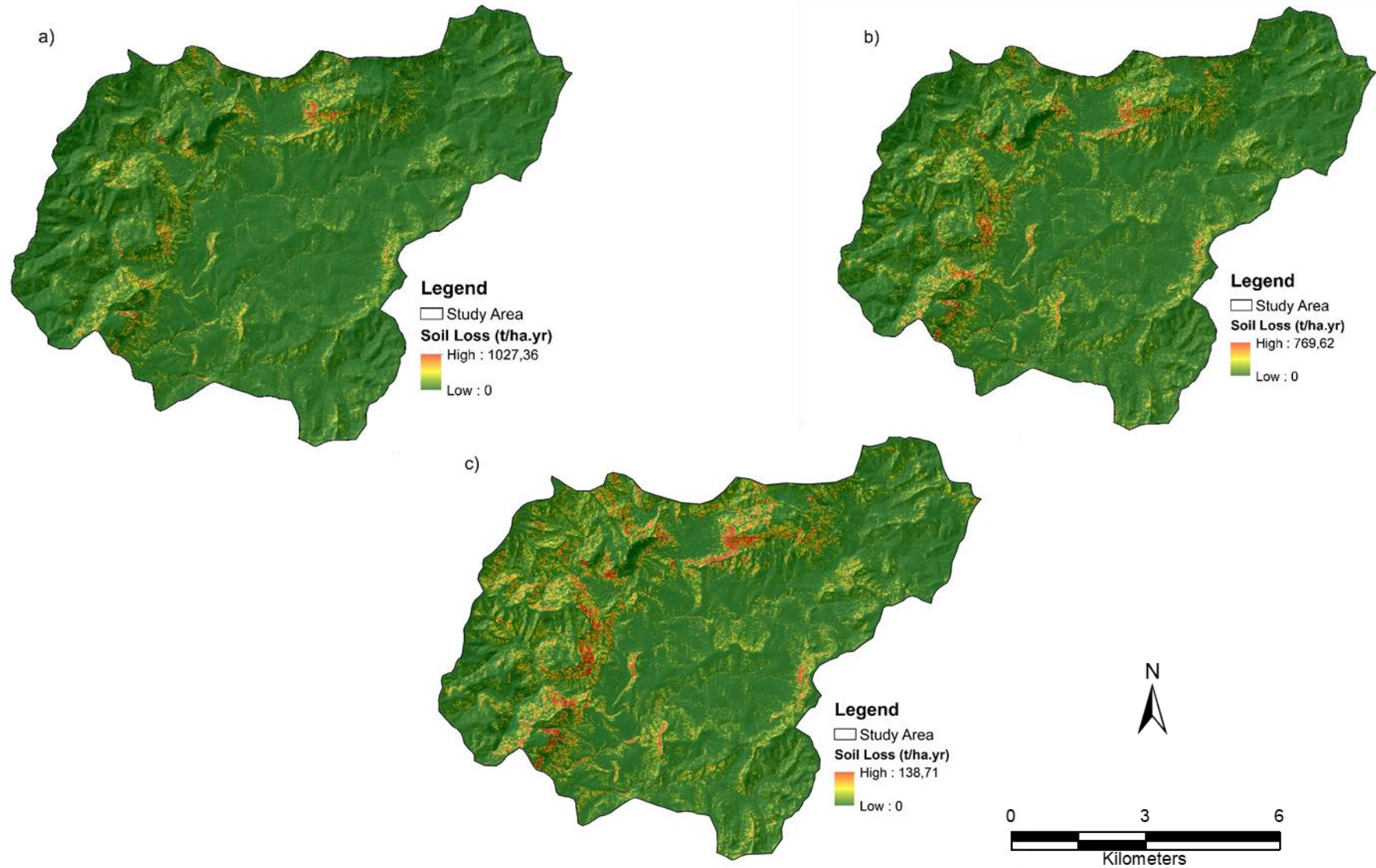


Figure 4.3 Mean annual soil loss: (a) 1989, (b) 2001, and (c) 2017.

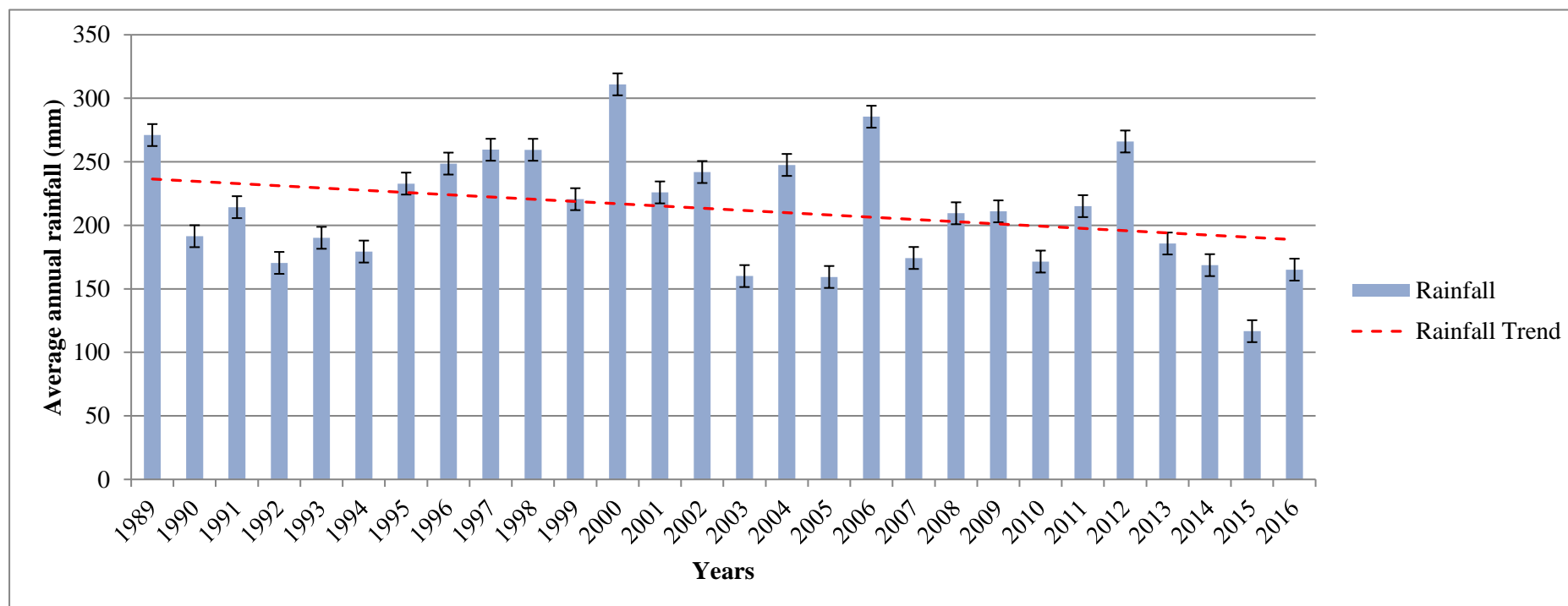


Figure 4.4 Mean annual rainfall (1989 – 2016) from three meteorological stations adjacent to Umzintlava Catchment with a $\pm 5\%$ standard error indicated by the sign (I) for each year.

Table 4.7 Annual soil loss rates with corresponding severity classes and area covered in each year

Mean soil loss ($\text{t ha}^{-1}\text{yr}^{-1}$)	Severity class	Area 1989 (%)	Area 2001 (%)	Area 2017 (%)
0 – 5	Very low	99,542	99,149	77,430
5 – 12	Low	0,426	0,774	19,957
12 – 25	Moderate	0,026	0,068	2,252
25 – 60	High	0,004	0,006	0,330
60 – 150	Very high	0,001	0,003	0,030
>150	Extremely high	0,001	0,001	0,002

4.3.4. LULC change, cover management, and soil loss trends

Figure 4.5 illustrates the overall LULC change with corresponding mean annual soil loss over the last 28 years (1989-2017) of study period. During this period, water bodies, agriculture, and grassland areas declined by 0.04%, 1.80%, and 13.42%, respectively (Figure 4.5). On the contrary, badlands, bare soil and built-up area, and forest increased. In terms of soil loss over the past 28 years, it can be observed from Figure 4.5 that all LULC classes, with the exception of badlands, experienced an increase. With a soil loss of $0.054 \text{ t ha}^{-1}\text{yr}^{-1}$, the bare soil and built-up area recorded the highest soil loss, followed by agriculture, forest with $0.036 \text{ t ha}^{-1}\text{yr}^{-1}$ and grassland with $0.031 \text{ t ha}^{-1}\text{yr}^{-1}$. Bare soil and built-up area recorded the least LULC increase (1.78%), but the highest soil loss ($0.054 \text{ t ha}^{-1}\text{yr}^{-1}$). Conversely, grassland recorded the highest LULC decrease of 13.42% but the least soil loss of $0.031 \text{ t ha}^{-1}\text{yr}^{-1}$.

Field-based evidence of LULC and soil erosion relations in the Umzintlava Catchment is shown in Figure 4.6. Human and animal pathways contribute to the development of rill erosion (Figure 4.6a) through the removal of vegetative cover. Overgrazing also contributes to the susceptibility of some parts of the study area to erosion. Built-up areas such as dirty/gravel roads with poorly constructed drainage systems facilitate gully erosion (Figure 4.6b) which in turn threatens agricultural activities like maize cultivation (Figure 4.6c).

Table 4.8 presents the mean C values together with the mean annual soil loss by LULC class over different years. In general, C values vary from 0 to 1 (Wischmeier and Smith, 1978; Wang et al., 2016). The LULC class that completely prevents soil erosion has a C value of 0, whereas the one that do not act as a protection against erosion has a C value of 1, and for the rest of the conditions the C value is lower than 1 (Tanyaş et al., 2015). Over the years, the mean annual soil loss in grassland areas increased consistently from $0.141 \text{ t ha}^{-1}\text{yr}^{-1}$ in 1989 to $0.142 \text{ t ha}^{-1}\text{yr}^{-1}$ in 2001, and $0.172 \text{ t ha}^{-1}\text{yr}^{-1}$ in 2017. These soil loss increases are corroborated by increases in C values from 0.030 in 1989 and 2001 to 0.039 in 2017 (Table 4.8).

In forested areas, soil loss slightly decreased between 1989 and 2001 from $0.033 \text{ t ha}^{-1}\text{yr}^{-1}$ to $0.032 \text{ t ha}^{-1}\text{yr}^{-1}$ as C values remained constant at 0.005 during this period, but increased between 2001 and 2017 from 0.005 in 2001 to 0.016 in 2017, resulting in a corresponding increase in soil loss from $0.032 \text{ t ha}^{-1}\text{yr}^{-1}$ to $0.070 \text{ t ha}^{-1}\text{yr}^{-1}$. Badlands recorded a C value of 0.386 in 1989,

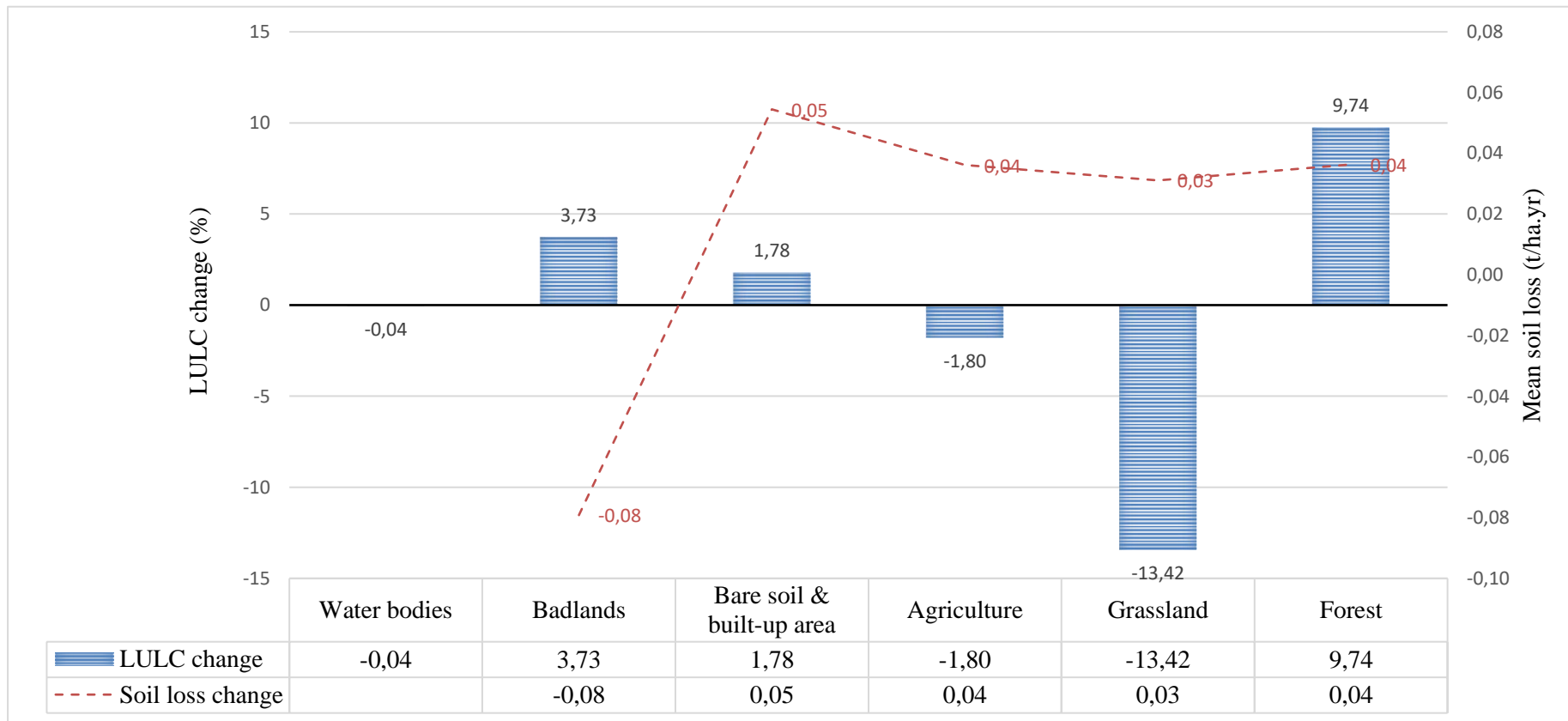


Figure 4.5 Overall LULC change with corresponding change in the mean annual soil loss from 1989 – 2017.

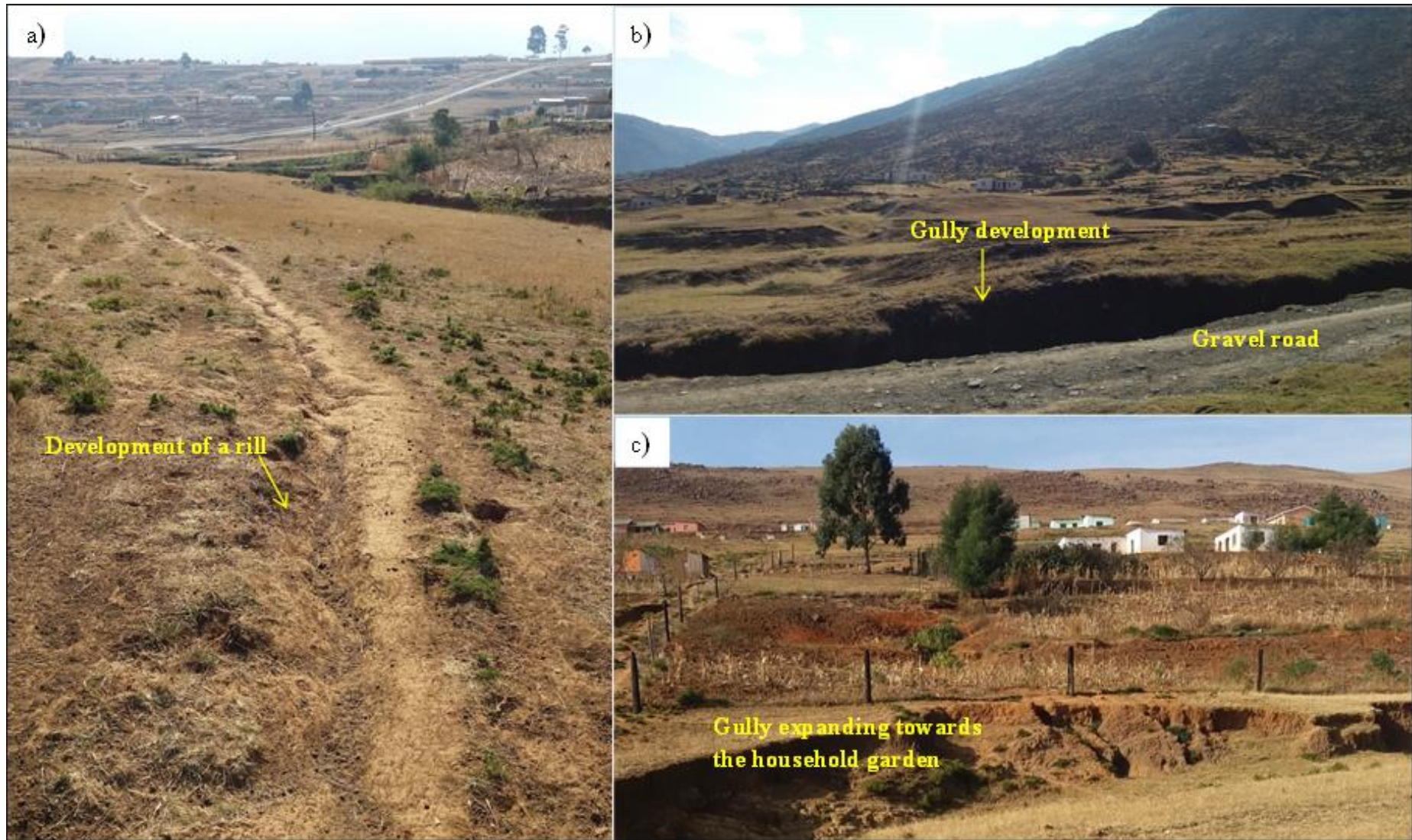


Figure 4.6 Field photos of soil erosion observed in the study area: (a) initiation of rill erosion, (b) gully erosion next to the road, and (c) classical gully system.

Table 4.8 Mean C values and average annual soil loss ($\text{t ha}^{-1}\text{yr}^{-1}$) by LULC class for different years

LULC	1989			2001			2017		
	Area (%)	C value	Soil loss	Area (%)	C value	Soil loss	Area (%)	C value	Soil loss
Water bodies	0,04	-	-	0,01	-	-	0,001	-	-
Badlands	9,46	0,386	1,089	12,73	0,400	0,899	13,19	0,402	1,010
Bare soil and built-up area	28,60	0,170	0,645	28,68	0,173	0,610	30,38	0,171	0,699
Agriculture	32,59	0,079	0,339	29,87	0,079	0,371	30,80	0,080	0,376
Grassland	25,97	0,030	0,141	23,99	0,030	0,142	12,55	0,039	0,172
Forest	3,35	0,005	0,033	4,71	0,005	0,032	13,09	0,016	0,070

0.400 in 2001, and 0.402 in 2017, whereas soil loss decreased from 1.089 t ha⁻¹yr⁻¹ in 1989 to 0.099 t ha⁻¹yr⁻¹ in 2001 and increased again to 1,010 t ha⁻¹yr⁻¹ in 2017. For the bare soil and built-up area category, the C values were 0.170 in 1989 and increased to 0.173 in 2001 and decreased to 0.171 in 2017. The mean annual soil loss also followed exactly the same trend exhibited by the C values for this LULC category. During the years 1989 and 2001, the C values remained constant at 0.079 for agriculture with a slight increase to 0.080 in 2017 whereas soil loss increased continuously in all the years.

4.4. Discussion

The results of this study indicate that the catchment has experienced a sharp decline in soil loss from 1027.36 t ha⁻¹yr⁻¹ in 1989 to 769.62 t ha⁻¹yr⁻¹ in 2001, and then further to 138.71 t ha⁻¹yr⁻¹ in 2017 (Figure 4.3). Such consistent decrease in soil loss in the study area could be attributed to two possible factors, including (a) rainfall and (b) cover management. Although there were variations in the temporal distribution of mean annual rainfall between different years, the overall rainfall trend (as indicated by a red dotted trend line) during the study period (1989 – 2017) shows a consistent decline in rainfall (Figure 4.4). The ability of rainfall to cause erosion, also referred to as rainfall erosivity (Morgan, 2005), depends largely on the amount of rainfall among other factors. For this reason, it could be reasonably presumed that the general decrease in rainfall might have contributed, to some extent, to the decline in soil loss in the study area.

Another possible factor responsible for the decrease of soil loss during the study period could be the improvement in cover and management in terms of forest plantation. Between 1989 and 2017, the proportion of the study area covered by forest increased by 9.74% (Figure 4.5). The majority of the forests within the study area occur naturally. Like all plants, trees strongly depend on the availability of water for growth (Toledo et al., 2011). Accordingly, tree growth increases with increasing rainfall (Dauber et al., 2005) and decreases with drought (Nath et al., 2006). In this study however, the area covered by forest increased irrespective of the continuous decline in mean annual rainfall. This means that such decline in rainfall was not significant enough to influence temporal variations of forest distribution. Perhaps, the increase in forest area may be due to other factors like the presence of soil nutrients which are independent of rainfall (Malhi et al., 2004). Additionally, although most forests occur naturally in the study area, the possibility exists that the increased forested area may have resulted from forest plantations during the 28 years study period. An example is the

plantation of exotic species resistant to low rainfall like *eucalyptus* trees, grown predominantly for timber (Spatial Development Framework – SDF, 2011). In addition to their resistance to low rainfall, *eucalypts* are particularly preferred for afforestation due to their fast-growing rates (7 – 10 years) and because none of the indigenous tree species which yield useful timber grow at rates considered profitable (Albaugh et al., 2013).

Although the mean annual soil loss decreased on an overall basis, close examination of soil loss results in different LULC classes revealed that all LULC classes, except badlands, experienced an increase in mean annual soil loss rates (Figure 4.5). The bare soil and built-up area class recorded the least change (1.78%) but the highest soil loss of about 0.054 t ha⁻¹yr⁻¹. Soil erosion occurring within this LULC category in the study area is a direct consequence of the removal or lack of vegetative cover. For instance, the construction of dirty or gravel roads often results in the removal of vegetation cover, leaving the area exposed to soil erosion (Figure 4.6b). In some cases, poorly constructed road drainage networks further compounds the problem of soil erosion (Addisu, 2009; Seutloali et al., 2016).

Forest recorded the lowest C values throughout the study period (Table 4.8), making it the most effective LULC category in providing protection against soil erosion in the study area. However, an improvement of 9.74% in forest cover resulted to an increase of 0.04 t ha⁻¹yr⁻¹ in soil loss (Figure 4.5). The occurrence of soil erosion in forested areas makes sense considering that most of the forests in the study area occur naturally and are generally distributed in elevated areas with steep slopes. The topography therefore may be the strongest driver of soil erosion in natural forests, especially when not well protected. This interpretation is supported by previous studies (Lufafa et al., 2003; Pimentel, 2006). Karamage et al. (2016) reported soil loss rates of 11 t ha⁻¹yr⁻¹ in moderate natural forest and 10.6 t ha⁻¹yr⁻¹ in dense natural forest located in highland areas with steep topography. Harvesting of trees for fuel wood and as building materials may be another possible cause of soil erosion in forested areas in the study area.

Similar to forest area, the area under agriculture experienced an increase of 0.04 t ha⁻¹yr⁻¹ of soil loss following a decline of 1.80% in aerial cover. The decline in agricultural land accompanied by increasing rates of soil loss is becoming an issue of serious concern given that most households derive their livelihoods from agriculture at a subsistence level in the study area and Umzimvubu Municipality at large (Phinzi and Ngetar, 2017). Further to this

concern of soil erosion in agricultural land, is the decline in both the quality and quantity of water resources. The results of this study indicate that the surface area covered by water bodies in the Umzintlava Catchment has declined by 0.04% between 1989 and 2017 (Figure 4.5) and this could be either due to soil erosion or climate, namely, decreased rainfall (Figure 4.4). Within the agriculture category, cropland is generally the most susceptible land to soil erosion due to poor farming and lack of effective erosion control and support practices (Pimentel et al., 1995).

Between 1989 and 2017, grassland decreased by 13.42%, resulting in a soil loss change of $0.031 \text{ t ha}^{-1}\text{yr}^{-1}$. The decline in grassland is a direct consequence of increase in human population (Karamage et al., 2016), putting a severe strain on these natural ecosystems which in turn results in the conversion of such ecosystems to other LULC types. An increase of 1.78% and 9.74% in bare soil and built-up area, and forests (Figure 4.5), respectively, attest to this observation. Soil loss rates in the natural grassland areas are due to livestock overgrazing (Maetens et al., 2012). This was especially evident in this study (Figure 4.6a), particularly in communally-held grazing land where there are no clear policies governing access or use of grassland ecosystems for grazing of livestock (Mhangara, 2011).

In order to determine whether the rates of soil loss experienced in each LULC presents a potential risk for soil productivity loss or land degradation, soil loss tolerance rates ought to be considered (Alewell et al., 2015). In South Africa, the proposed soil loss tolerance values (McPhee and Smithen 1984) lie between $3 \text{ t ha}^{-1}\text{yr}^{-1}$ for shallow soils and $10 \text{ t ha}^{-1}\text{yr}^{-1}$ for deep alluvial soils. Although the aforementioned LULC classes (forest, bare soil and built-up area, agriculture, and grassland) experienced increased soil loss rates during the study period (Figure 4.5), such soil loss rates are within acceptable or tolerable levels of soil loss as per MCPhee and Smithen's (1984) proposed soil loss rates. Contrary to Chapter 3 (Section 3.6) which presents soil loss above tolerable limits, the estimated soil loss rates in this chapter are within tolerable limits. The discrepancy in these results could be explained by the differences in the spatial resolution of SPOT ($5\text{m} * 5\text{m}$) and Landsat ($30\text{m} * 30\text{m}$) images used in chapters 3 and 4 respectively (discussed further in Chapter 5, Section 5.5). Despite these low rates of soil loss, it is still necessary and important to avoid practices that increase soil erosion. According to Pimentel (2006), even low rates of erosion sustained over billions of years, result in the displacement of enormous quantities of top soil whilst adversely impacting on soil fertility.

Unexpected however, is the decrease in soil loss ($0.079 \text{ t ha}^{-1}\text{yr}^{-1}$) occurring on badlands given that this LULC class has a relatively poor protective cover, namely a C value of 0.400. Such underestimates of soil loss by RUSLE could partly be due to the fact that badlands are characterized by extensively rilled and gullied areas occurring on less steep sloping lands (Boardman et al., 2003). It must be borne in mind that RUSLE was originally developed for assessing sheet and rill erosion but not gully erosion (Wischmeier and Smith, 1978; Renard et al., 1997). Apart from this limitation, another possible cause for underestimates of soil loss in badlands in this study relates to the coarser spatial resolution ($30\text{m} \times 30\text{m}$) of the SRTM DEM used to derive topographic parameters (LS-factor). High spatial resolution DEMs such as those from stereo SPOT images are expensive and not readily available, hence the SRTM DEM was used instead. Considering the sensitivity of topography particularly slope steepness to soil loss (Renard et al., 2011), it is evident from the results that the coarser spatial resolution of the SRTM DEM has had a strong bearing on the overall estimates and distribution of soil loss in the study area. This interpretation is supported by Renard et al. (2011) who maintain that low spatial resolution can lead to the erroneous exclusion of small concentrated flow channels commonly found at the bottom of a RUSLE hillslope where substantial deposition takes place.

Another aspect of this study worth discussing relates to LULC classification method since it affects the quality and reliability of LULC change detection results. The success of any post-image classification change detection depends on the method of image classification employed (Singh, 1989; Lu and Wang, 2007). In turn, whether or not the image classification method was successful depends upon many considerations including data availability, the purpose and scale of the study, among other things (Lu et al., 2004). One objective way to assess the success of an image classification method is the accuracy of the derived LULC results. Such accuracy is based on the level (statistics) of agreement between classification results and reference data summarized in the form of kappa coefficient (Congalton and Mead, 1983; Foody, 2002). Kappa coefficient ranges from 0 to 1, with values >0.80 representing strong agreement, $0.40\text{-}0.80$ representing moderate agreement, and values <0.40 representing poor agreement (Lands and Koch, 1977).

In this study, the kappa coefficients for all the years fell within the moderate agreement category ($0.40\text{-}0.80$), suggesting a successful image classification (Phinzi and Ngetar, 2017). For instance, LULC maps classified from the 1989 and 2017 images recorded the same kappa coefficient (0.75) whereas the 2001 LULC classification results produced a kappa coefficient

of 0.74. The overall change detection (1989-2017) however, recorded comparatively low accuracy of 0.62 though this still fell within the moderate agreement category. Overall, such findings show that the NDVI-image classification method, used in this study was successful although there were some complications including the difficulty to spectrally discriminate between the bare soil and built-up area. Due to this limitation, the pixels belonging to these two LULC classes were grouped together based on their spectral homogeneity to form one class called 'bare soil and built-up area'.

4.5. Conclusion

This study assessed the impact of LULC change on soil erosion in the Umzintlava Catchment over a 28 year period (1989 – 2017), using multi-temporal Landsat data and RUSLE. A post-classification change detection comparison showed that water bodies, agriculture, and grassland areas have decreased, whereas the area covered by forests, badlands, and bare soil and built-up area increased during the study period. The results indicated that the catchment experienced a consistent decline in the mean annual soil loss, from 1027.36 t ha⁻¹yr⁻¹ in 1989, to 769.62 t ha⁻¹yr⁻¹ in 2001, and then further to 138.71 t ha⁻¹yr⁻¹ in 2017. Despite the decreasing trend of soil loss rates on an overall catchment basis, further analysis of soil loss in different LULC classes suggested that most LULC classes experienced increased rates of soil loss. The bare soil and built-up area, followed by agriculture and forest categories, recorded the highest rates of soil loss whereas grasslands experienced the least rates of soil loss. Contrary to other LULC categories, badlands experienced decreased rates of soil loss contributing to the overall reduction in erosion, an error not captured through the formation of gullies.

From a theoretical and methodological point of view, the NDVI-based image classification technique combined with RUSLE modeling resulted in a semi-objective approach with reasonable accuracy and can be adopted in future studies related to LULC changes versus soil erosion. Such a semi-objective approach simplifies the complexity and dynamic relationship between LULC change and soil erosion and at a practical level will facilitate efforts towards LULC planning and soil conservation in the Umzintlava Catchment and the Eastern Cape at large.

Admittedly, however, the approach suffered a couple of setbacks arising mainly from the lack of data with sufficient spatial resolution for the scale of the study, *viz.* catchment scale. Taking this and the accuracy achieved in this study into consideration, it is apparent that there

is still a room for improvement, for example using SPOT imagery, which have reasonable spatial resolution.

CHAPTER 5

SYNTHESIS AND RECOMMENDATIONS

5.1. Introduction

Soil erosion by water is no doubt a worst form of land degradation with serious environmental and socio-economic ramifications (Chapter 1 and Chapter 2). In response to this, many empirical erosion models have been developed in different parts of the world for soil erosion assessment. Because of its simplicity and more importantly its consideration for many important erosion factors, the RUSLE model is presently the most widely used model with great successes worldwide. Despite these successes, an important limitation with RUSLE is that it is inherently restricted to plot scale or small catchments and does not consider gully erosion.

Despite these setbacks however, the advent of geospatial technologies like GIS and remote sensing, is now making it possible to circumvent these RUSLE limitations and still achieve reasonable accuracies in cost-effective and time-efficient way. As a result, interest in the assessment of soil erosion using the RUSLE model coupled with these geospatial technologies is growing. However, in other parts of the world like South Africa, little attention has been paid to the spatial and temporal patterns of soil erosion and its relation to constantly changing LULC. As a developing country, South Africa has undergone tremendous LULC changes. Remote sensing, and in particular, readily available imageries from optical sensors such as Landsat and SPOT, permits rapid assessment of not only LULC changes but also soil erosion on a spatial and temporal basis with reasonable accuracies. Thus, the objectives of this study were:

- 1) To review recent developments on the use of GIS and remote sensing technologies in assessing and deriving soil erosion factors as represented by RUSLE parameters.
- 2) To assess soil erosion vulnerability of the Umzintlava Catchment using geospatial driven RUSLE model.
- 3) To assess the impact of LULC change on soil erosion in the Umzintlava Catchment during the period 1989 – 2017.

5.2. Objective 1: Recent developments in the integrated use of GIS and remote sensing for assessing and deriving RUSLE parameters

Soil erosion results from the complex interactions between natural and anthropogenic factors which vary over space and time. The RUSLE model provides a simple and yet comprehensive framework for soil erosion assessment. Specifically, RUSLE calculates soil loss as a function of six soil erosion factors or parameters including rainfall (R), topography

(LS), soil erodibility (K), cover management (C), and support practice (P). Increasingly, advances in GIS and remote sensing technologies play an integral role in deriving RUSLE parameters. The main objective of this chapter (Chapter 2) was to provide an overview of recent developments in the integrated use of GIS and remote sensing in deriving individual RUSLE parameters, placing an emphasis on related successes and challenges. The literature revealed that GIS is mainly used for computation of individual RUSLE parameters while satellite remote sensing forms an important data source for deriving RUSLE parameters.

Successes have been achieved in estimating the rainfall erosivity (R-factor) from satellite-borne precipitation products like the TRMM-TMPA data (Section 2.3.1). The use of other space-based precipitation products like CFSR, CMAP, HydroEstimator, MPE, NRL-blended, and PERSIANN in deriving the R-factor has not yet been reported in the literature. An important challenge however with such satellite-borne precipitation products is the quantitative determination of rainfall which often requires complex algorithms.

Physical soil properties such as the primary particle size distribution, soil organic matter content, soil structure, and permeability contribute to soil erodibility (K-factor). The combination of GIS, remote sensing and statistical models has proven helpful in determining some of these soil properties (Section 2.3.2). The literature showed that multiple regression, geostatistics, and spectral mixture are the most commonly used approaches for extracting soil attributes information from remotely sensed data. Though successes have been achieved in relating soil properties to remote sensing spectra, it still remains a challenge to satisfactorily quantify each soil property from remotely sensed data for input in the RUSLE erodibility equation.

In terms of deriving topographical attributes (LS-factor), detailed literature survey indicated that the ASTER and SRTM DEMs have been the most widely applied products worldwide probably because they provide near-global coverage, in addition to their free availability to the research community (Section 2.3.3). Most RUSLE studies use these DEM products as a given parameter without first pre-processing them and assessing their suitability for terrain modelling at the desired scale of study. Yet, these DEMs are subject to errors such as voids, residual cloud patterns and strip effects.

Remote sensing classified LULC maps and spectral indices are increasingly preferred over conventional techniques due to their objectivity, low costs, and relative accurate data analysis. The literature showed that regression equations and statistical analysis are used to

relate the C values to spectral indices mostly derived from Landsat data (Section 2.3.4). NDVI was the most widely used vegetation index for deriving the C-factor information (Section 2.3.4). Similar to C-factor, the most commonly used approach to obtain the P-factor information is through field observation and visual image interpretation in which case high resolution aerial photographs are used. An increasing number of studies assign the P-factor values obtained from literature to satellite derived-LULC maps whereas some studies derive the P-factor values from the slope map (%). The unavailability of satellite data (e.g. images and DEM) presents an important challenge to the determination of both C-factor and P-factor information from satellite data.

Despite the challenges associated with deriving individual RUSLE parameters from the integrated use of GIS and remote sensing, this chapter (Chapter 2) has shown that GIS and remote sensing technologies are still far more beneficial compared to traditional methods which are relatively costly and time-consuming. This is reflected by the continuous increase of studies that use these technologies in RUSLE erosion modelling.

5.3. Objective 2: Soil erosion vulnerability assessment

A necessary step towards designing and implementing relevant soil and water conservation measures at catchment level is the assessment of erosion distribution and erosion prone areas in a geographic context with adequate accuracy. In order to achieve this, the study employed the RUSLE model in combination with GIS and remotely sensed data, namely SPOT data (Chapter 3). More specifically, the objectives were (1) to assess soil erosion risk in the Umzintlava Catchment, and (2) to explore the relationship, if any, between soil loss and different erosion factors as represented by RUSLE parameters including R-factor, K-factor, LS-factor, C-factor, and P-factor.

The study showed that the Umzintlava Catchment experiences an average annual soil loss of $11\,752\text{ t ha}^{-1}\text{yr}^{-1}$, with approximately 90.19% of the catchment experiencing very low soil loss rates *viz.* $0 - 5\text{ t ha}^{-1}\text{yr}^{-1}$ (Chapter 3). About 8.86% and 0.79% of the study area catchment are subject to low ($5 - 12\text{ t ha}^{-1}\text{yr}^{-1}$) and moderate ($12 - 25\text{ t ha}^{-1}\text{yr}^{-1}$) soil erosion rates respectively, whereas the remainder of the catchment, namely, 0.95% experiences, high ($25 - 60\text{ t ha}^{-1}\text{yr}^{-1}$), very high ($60 - 150\text{ t ha}^{-1}\text{yr}^{-1}$), and extremely high ($> 150\text{ t ha}^{-1}\text{yr}^{-1}$) rates of soil loss. The study further revealed that highland areas with steep slopes and poor vegetation cover are more prone to high rates of soil loss than areas with gentle slopes, while areas with gentle or flat slopes are also susceptible to soil erosion in

form of gullies. This is evident in low-lying areas, especially the central parts of the catchment. The spatial integration of RUSLE-derived soil loss and remote sensing-classified soil erosion indicated that the entire catchment is at risk of soil erosion. Different factors including rainfall (R), soil erodibility (K), topography (LS), cover management (C), and support practice (P) are responsible for soil erosion in the Umzintlava Catchment.

Statistically, the LS-factor representing topographic attributes and P-factor representing support practice, appeared to be overriding factors influencing soil erosion in the Umzintlava Catchment, with the P-factor indicating the existence of either weak or no erosion control measures in those areas associated with high soil loss rates (Chapter 3, Section 3.6). This was further compounded by poor vegetative cover as represented by high C-factor values. Both the climate and soil erodibility as represented by the R-factor and K-factor, poorly correlated to soil loss. The study revealed that such poor correlation between the R-factor and soil loss was due to higher rainfall leading to more stable soils and vegetation cover which in turn overshadowed the effects of rainfall erosivity. Statistically, the K-factor weakly correlated to soil loss. However, qualitative analysis of remote sensing-derived erosion results combined with field observations revealed a strong relationship between the two especially in gully-affected areas. The results from this chapter highlight the need and importance of spatial integration RUSLE and remote sensing-derived soil erosion information.

5.4. Objective 3: LULC change and soil erosion

In order to proactively conserve soil and water resources, it is often appropriate to understand the dynamics of soil erosion as related to LULC changes. Freely available optical sensors like Landsat are capable of providing information on historical LULC changes on a time-efficient basis. In Chapter 4 of this study, the use of Landsat multi-temporal data together with the RUSLE model assisted in assessing the impact of LULC changes on soil erosion in the Umzintlava Catchment from 1989-2017 period.

The results indicated that the catchment has undergone significant changes in LULC over the past 28 years (1989-2017). Water bodies, agriculture, and grassland areas declined by 0.04%, 1.80%, and 13.42%, respectively whereas the aerial coverage of forest increased by 3.73%, badlands by 1.78%, and bare soil and built-up area by 9.74% (Chapter 4). The catchment recorded about 1027.36 t ha⁻¹yr⁻¹ of soil loss in 1989, declining to 769.62 t ha⁻¹yr⁻¹ in 2001, and 138.71 t ha⁻¹yr⁻¹ in 2017. Notwithstanding the overall decline of soil loss, close examination of soil loss in different LULC classes suggested that all LULC classes have

experienced increased rates of soil loss during the observed period, with the exception of badlands (Chapter 4, Section 4.3.4), which are characterized by gullies.

The bare soil and built-up area class recorded the least change (1.78%) but the highest soil loss of about $0.054 \text{ t ha}^{-1}\text{yr}^{-1}$. Forest increased by 9.74% resulting in an increase of $0.036 \text{ t ha}^{-1}\text{yr}^{-1}$ in soil loss. Similarly, the area under agriculture experienced an increase of $0.036 \text{ t ha}^{-1}\text{yr}^{-1}$ in soil loss following a decline of 1.80% in aerial cover. Grassland areas decreased by 13.42%, resulting in soil loss increase of $0.031 \text{ t ha}^{-1}\text{yr}^{-1}$. These results show that changes in different LULC classes impact on soil erosion rates, with some LULC classes resulting to more soil loss than others. The information on LULC changes and soil erosion provide in Chapter 4 is important to both LULC planning and soil conservation at catchment level.

5.5. Limitations

Although successful, this study suffered from a few setbacks arising mainly from the lack of data with sufficient spatial resolution for the scale of the study, *viz.* catchment. The unavailability of SPOT image scenes for 1989 and 2001 periods for instance influenced the decision to use Landsat imagery (a coarser spatial resolution sensor) for these periods, and even for 2017 period. As a result, LULC classes derived from a 2016 SPOT imagery (Chapter 3) differ from those classified from Landsat images (Chapter 4). With a spatial resolution of $5\text{m} * 5\text{m}$, SPOT permitted classification of six LULC classes (including water bodies, built-up areas, barren land, agricultural land, rangeland, and forest) in the study area. On the contrary, only five LULC classes were classified from Landsat at a spatial resolution of $30\text{m} * 30\text{m}$. With this spatial resolution, it was difficult to spectrally discriminate between bare soil and built-up area; hence a decision was made to merge these two classes into one class called 'Bare soil and built-up area'.

Image spatial resolution did not only affect LULC classification but also impacted on soil loss estimates. The mean annual soil loss was estimated at approximately $11\,752 \text{ t ha}^{-1}\text{yr}^{-1}$ using a $5\text{m} * 5\text{m}$ SPOT image grid-based approach (Chapter 3), whereas soil loss estimates at $30\text{m} * 30\text{m}$ spatial resolution ranged from $1027.36 \text{ t ha}^{-1}\text{yr}^{-1}$ - $138.71 \text{ t ha}^{-1}\text{yr}^{-1}$ (Chapter 4). Further to the issue of spatial resolution and soil loss discussed in Chapter 3 (Section 3.6), the estimated soil loss rates in different Wards exceed the proposed (McPhee and Smithen, 1984) tolerable rates of soil loss. This is likely because the SPOT images used with a spatial resolution of $5\text{m} * 5\text{m}$ were able to pick-up more areas with soil losses. On the contrary, in

Chapter 4 (Section 4.3.4), Landsat-based estimated soil loss rates in different LULC class are below tolerable levels possible due to coarser Landsat spatial resolution (30m * 30m). Although the estimated soil loss rates in Chapter 4 are within tolerable levels, such soil loss rates continuously increased during the study period and may pose a greater threat to both soil quantity and quality in the long-run (Chapter 4, Section 4.4). This discrepancy reveal that the use of high spatial resolution satellite images and DEMs (which were not available for the present study) could have improved the results of this study.

5.6. Conclusions

The main aim of this study was to assess the spatial and temporal patterns of water-borne erosion in the Umzintlava Catchment, Eastern Cape, using the RUSLE model in conjunction with geospatial technologies related to GIS and remote sensing. Based on research findings reported in this thesis (Chapter 3 and 4), the following major conclusions can be drawn:

- 1) The Umzintlava Catchment is subject to considerable levels of soil erosion, pointing to the need for counter measures, especially in locations where soil is continuously lost at rates far exceeding tolerable rates proposed for South Africa.
- 2) The topography as represented by RUSLE LS-factor is the main driving force behind hillslope erosion including rill and sheet erosion. In gully-dominated areas however, the topography has little influence, but soil types as represented by K-factor is the overriding factor.
- 3) The impact of LULC change on soil erosion is a cause for concern in the Umzintlava Catchment and Eastern Cape at large. Natural grasslands in particular are increasingly converted to built-environment in addition to being used for animal grazing, leading to increased susceptibility of an area to erosion by water.
- 4) Throughout the observed period (1989-2017), soil loss by different LULC classes consistently increased and may continue if proactive measures are not taken to control or manage soil erosion in the catchment.

Overall, from a theoretical and methodological point of view, the integration of the RUSLE model with GIS and remote sensing has proven not only reasonably accurate and time-efficient in identifying erosion prone areas in both spatial and temporal terms, but also cost-effective alternative to traditional field-based methods. Taking the setbacks or limitations (Section 5.4) encountered into consideration and research gaps identified in this study

(Chapters 2, 3, and 4), it is apparent that there is still some room for improvements, hence the following recommendations and directions for future research are provided.

5.7. Recommendations and directions for future research

5.7.1. Recommendations

- 1) Due to poor spatial resolution provided by Landsat imagery, it is recommended that future studies use SPOT imagery in LULC change detection given its high spatial resolution and its free availability in South Africa.
- 2) The use of high spatial resolution commercial sensors like QuickBird, WorldView, IKONOS, and GeoEye is also recommended although these may be costly.
- 3) Given that there are currently no policies governing access to or use of communal land for livestock grazing (SDF, 2011), local authorities including municipal government and traditional leaders must enact policies on the use of communally-held lands for livestock grazing.
- 4) In order to bridge the gap between theory and practice, there must be on-going soil erosion workshops among various stakeholders including communities actively involved in agriculture, policy-makers, land development, and soil erosion experts. These workshops should disseminate information on soil erosion causes, processes, management and soil conservation practices.
- 5) More vegetation cover must be planted in areas of concern such as elevated areas with steep slopes and poor vegetative cover. In addition to this, the existing natural or indigenous forests must be well-protected, as these in turn provide best protection (e.g. low C values) of soil against erosion.

5.7.2. Directions for future research

- 1) Further research should investigate the impact of spatial resolution on RUSLE-estimated soil loss. This includes comparing free multispectral sensors like SPOT, Sentinel, and Landsat, amongst others.
- 2) More research, especially in the South African context, is required to determine the most important factors influencing soil erosion, taking into account variations in local environmental conditions.
- 3) More research is needed on the impacts of soil erosion on agriculture, livestock farming and food security.

- 4) Research on policies relating to the use of communal land for grazing livestock is needed. The use of fire in communal grazing land should be investigated.
- 5) Future research should also focus on developing innovative and/or improving existing soil erosion control measures.

REFERENCES

- Acocks, J. P. H. (1988). Veld types of South Africa. *Memoirs of the Botanical Survey of South Africa*, 57, 1-146.
- Addisu, S. (2009). *Assessment of the impact of road construction on physical land degradation in central highlands of Ethiopia: the case of two selected projects* (Master's Thesis, Addis Ababa University).
- Adger, W. N., Benjaminsen, T. A., Brown, K., and Svarstad, H. (2001). Advancing a political ecology of global environmental discourses. *Development and Change*, 32(4), 681-715.
- Adler, R. F., Huffman, G. J., Bolvin, D. T., Curtis, S., and Nelkin, E. J. (2000). Tropical rainfall distributions determined using TRMM combined with other satellite and rain gauge information. *Journal of Applied Meteorology*, 39(12), 2007-2023.
- Adler, R. F., Huffman, G. J., Chang G. J., Ferraro, R., Xie, P. P., Janowiak, J., Rudolf, B., Schneider, U., Curtis, S., Bolvin, D., Gruber, A., Susskind, J., Arkin, P., and Nelkin, E. (2003). The version-2 global precipitation climatology project (GPCP) monthly precipitation analysis (1979-present). *Journal of Hydrometeorology*, 4, 1147-1167.
- AghaKouchak, A., and Nakhjiri, N. (2012). A near-real satellite-based global climate data record. *Environmental Research Letters*, 7(4), 1-8.
- AghaKouchak, A., Behrangi, A., Sorooshian, S., Hsu, K., and Amitai, E. (2011). Evaluation of satellite-retrieved extreme precipitation rates across the central United States. *Journal of Geophysical Research*, 116, 1-11.
- Agricultural Research Council – Institute for Soil, Climate, and Water, ARC-ISCW., (2006). Soil type.
- Aiello, A., Adamou, M., and Canoga, F. (2015). Remote sensing and GIS to assess soil erosion with RUSLED and USPED at river basin scale in southern Italy. *Catena*, 131, 174-185.
- Albaugh, J. M., Dye, P. J., and King, J. S. (2013). Eucalyptus and water use in South Africa. *International Journal of Forestry Research*, 2013, 1-11.
- Alewell, C., Egli, M., and Meusburger, K. (2015). An attempt to estimate tolerable soil erosion rates by matching soil formation with denudation in Alpine grasslands. *Journal of Soils and Sediments*, 15(6), 1383-1399.
- Alexakis, D. D., Hadjimitsis, D. G., and Agapiou, A. (2013). Integrated use of remote sensing, GIS and precipitation data for the assessment of soil erosion rate in the catchment area of “Yialias” in Cyprus. *Atmospheric Research*, 131, 108-124.
- Alkharabsheh, M. M., Alexandridis, T. K., Bilas, G., Misopolinos, N., and Silleos, N. (2013). Impact of land cover change on soil erosion hazard in northern Jordan using remote sensing and GIS. *Procedia Environmental Sciences*, 19, 912-921.
- Angulo-Martínez, M., and Beguería, S. (2009). Estimating rainfall erosivity from daily precipitation records: A comparison among methods using data from the Ebro Basin (NE Spain). *Journal of Hydrology*, 379(1-2), 111-121.

- Arnoldus, H. M. J. (1977). Methodology used to determine the maximum potential average annual soil loss due to sheet and rill erosion in Morocco. In *Assessing soil degradation*. FAO Soil Bulletins, 34, Rome.
- Arnoldus, H. M. J. (1980). An approximation of the rainfall factor in the Universal Soil Loss Equation. In M. De Boodt and D. Gabriels(Eds.), *Assessment of erosion* (pp. 127-132). Chichister: John Wiley and Sons.
- Aronoff, S. (1989). *Geographic Information Systems: a management perspective*. Ottawa: WDL Publications.
- Ashiagbor, G., Forkuo, E. K., Laari, P., and Aabeyir, R. (2013). Modeling soil erosion using RUSLE and GIS tools. *International Journal of Remote Sensing and Geoscience*, 2(4), 1-17.
- Asner, G. P., and Heidebrecht, K. B. (2002). Spectral unmixing of vegetation, soil and dry carbon cover in arid regions: comparing multispectral and hyperspectral observations. *International Journal of Remote Sensing*, 23(19), 3939-3958.
- Athmania, D., and Achour, H. (2014). External validation of the ASTER GDEM2, GMTED2010 and CGIAR-CSI-SRTM v4.1 free access Digital Elevation Model (DEMs) in Tunisia and Algeria. *Remote Sensing*, 6, 4600-4620.
- Bahrawi, J. A., Elhag, M., Aldhebiani, A. Y., Galal, A. K. H., and Alghailani, E. (2016). Soil erosion estimation using remote sensing techniques in Wadi Yalamlam Basin, Saudi Arabia. *Advances in Materials Science and Engineering*, 2016, 1-8.
- Baskan, O., Cebel, H., Akgul, S., and Erpul, G. (2009). Conditional simulation of USLE/RUSLE soil erodibility factor by geostatistics in a Mediterranean catchment, Turkey. *Environmental Earth Sciences*, 60(6), 1179-1187.
- Beasley, D. B., Huggins, L. F., and Monke, E. J. (1980). ANSWERS – a model for watershed planning. *Transactions of American Society of Agricultural Engineers*, 23, 938-944.
- Beckedahl, H. R., and De Villiers, A. B. (2000). Accelerated erosion by piping in the Eastern Cape Province, South Africa. *South African Geographical Journal*, 82(3), 157-162.
- Benkobi, L., Trlica, M. J., and Smith, J. L. (1994). Evaluation of a refined surface cover subfactor for use in RUSLE. *Journal of Range Management*, 74-78.
- Bhandari, A. K., Kumar, A., and Singh, G. K. (2012). Feature extraction using Normalized Difference Vegetation Index (NDVI): A case study of Jabalpur city. *Procedia technology*, 6, 612-621.
- Bhat, S. A., Hamid, I., Dar, M. U. D., Rasool, D., Pandit, B. A., and Khan, S. (2017). Soil erosion modeling using RUSLE and GIS on micro watershed of JandK. *Journal of Pharmacognosy and Phytochemistry*, 6(5), 838-842.
- Bhattarai, R., and Dutta, D. (2007). Estimation of soil erosion and sediment yield using GIS at catchment scale'. *Water Resources Management*, 21(10), 1635-1647.
- Bingfang, W., Miaomiao, L., Changzhen, Y., Weifeng, Z., and Changzhen, Y. (2004). Developing method of vegetation fraction estimation by remote sensing for soil loss

- equation: a case in the upper basin of Miyun Reservoir. *IEEE International Geoscience and Remote Sensing Symposium*, 20-24 September 2004.
- Bizuwerk, A., Tadesse, G., and Getahun, Y. (2008). *Application of GIS for modelling soil loss rate in Awash Basin, Ethiopia*. Addis Ababa: International Livestock Research Institute (ILRI),.
- Boardman, J. (2006). Soil erosion science: reflections on the limitations of current approaches. *Catena*, 68, 73-86.
- Boardman, J., Dearing, J. A., and Foster, I. D. L. (1990). Soil erosion studies; some assessments. In *Soil erosion on agricultural land. Proceedings of a workshop sponsored by the British Geomorphological Research Group, Coventry, UK, January 1989*. (pp. 659-672). John Wiley and Sons Ltd..
- Boardman, J., Parsons, A. J., Holland, R., Holmes, P. J., and Washington, R. (2003). Development of badlands and gullies in the Sneeuberg, Great Karoo, South Africa. *Catena*, 50(2-4), 165-184.
- Bols, P. (1978). *The iso-erodent map of Java and Madura*. Belgian Technical Assistance Project ATA 105, Soil Research Institute, Bogor, Indonesia.
- Bonilla, C. A., and Vidal, K. L. (2011). Rainfall erosivity in central Chile. *Journal of Hydrology*, 410(1-2), 126-133.
- Breetzke, G. D., Koomen, E., and Critchley, W. R. S. (2013). GIS-assisted modelling of soil erosion in a South African catchment: evaluating the USLE and SLEMSA approach. *Water Resources Planning, Development and Management*. Retrieved from <http://www.intechopen.com/books/water-resources-planningdevelopment-and-management>.
- Breul, P., and Gourves, R. (2006). In field soil characterization: approach based on texture image analysis. *Journal of Geotechnical and Geoenvironmental Engineering*, 132(1), 102-107.
- Bu, Z. (1993). Preliminary study on algorithm formula of vegetative factor for undisturbed areas in remote sensing monitoring soil loss. *Remote Sensing Technology and Application*, 8(4), 16-22.
- Campbell, J. B., and Wynne, R. H. (2011). *Introduction to remote sensing*. Guilford Press, New York.
- Carter, L. J. (1977). Soil erosion: the problem persists despite the billions spent on it. *American Association for the Advancement of Science*, 196(4288), pp. 409-411.
- Collison, B., Collison, W., and Tucci, C. E. M. (2008). Daily hydrological modelling in the Amazon basin using TRMM rainfall estimates. *Journal of Hydrology*, 360, 207-216.
- Congalton, R. G., and Mead, R. A. (1983). A quantitative method to test for consistency and correctness in photointerpretation. *Photogrammetric Engineering and Remote Sensing*, 49(1), 69-74.

- Council for Geoscience. (2012). Geological, geohydrological and development potential zonation influence; environmental management framework for uMkhanyakude District, KwaZulu-Natal. Viewed on 18 April 2018 <http://www.kzndae.gov.za>.
- Cracknell, A. P. (1998). Synergy in remote sensing-what's in a pixel? *International Journal of Remote Sensing*, 19, 2025-2047.
- Cruse, R. M., Berghoefter, B. E., Mize, C. W., and Ghaffarzadeh, M. (2000). Water drop impact angle and soybean protein amendment effects on soil detachment. *Soil Science Society of America Journal*, 64(4), 1474-1478.
- Curcio, D., Ciraolo, G., Asaro, F.D., and Minacapilli, M. (2013), Prediction of soil texture distributions using VNIR-SWIR reflectance spectroscopy. *Procedia Environmental Sciences*, 19, 494-503.
- Da Silva, A. M. (2004). Rainfall erosivity map for Brazil. *Catena*, 57(3), 251-259.
- Da Silva, C. C., De Carvalho, W., Bhering, S. B., and Filho, B. C. (2016). Spatial prediction of soil surface texture in a semiarid region using random forest and multiple linear regressions. *Catena*, 139, 232-240.
- Datta, P. S., and Schack-Kirchner, H. (2010). Erosion relevant topographical parameters derived from different DEMs – a comparative study from the Indian Lesser Himalayas. *Remote Sensing*, 2, 1941-1961.
- Dauber, E., Fredericksen, T. S., and Pena, M. (2005). Sustainability of timber harvesting in Bolivian tropical forests. *Forest Ecology and Management*, 214(1-3), 294-304.
- De Asis, A., and Omasa, K. (2007). Estimation of vegetation parameter for modelling soil erosion using linear spectral mixture analysis of Landsat ETM data. *ISPRS Journal of Photogrammetry and Remote Sensing*, 62, 309-324.
- De Carvalho, D. F., Durigon, V. L., Antunes, M. A. H., de Almeida, W. S., and de Oliveira, P. T. S. (2014). Predicting soil erosion using RUSLE and NDVI time series from TM Landsat 5. *Pesquisa Agropecuaria*, 49(3), 215-224.
- De Jong, S. M. (1994). *Applications of reflective remote sensing for land degradation studies in a Mediterranean environment* (Doctoral dissertation). Universiteit Utrecht, Nederland.
- De Vente, J., and Poesen, J. (2005). Predicting soil erosion and sediment yield at the basin scale: scale issues and semi-quantitative models. *Earth-Science Reviews*, 71, 95-125.
- De Vente, J., Poesen, J., Govers, G., and Boix-Fayos, C. (2009). The implications of data selection for regional erosion and sediment yield modelling. *Earth Surface Processes and Landforms*, 34, 1994-2007.
- De Villiers, M. C., Nell, J. P., Barnard, R. O., and Henning, A. (2003). Salt-affected soils: South Africa. *Food agricultural organization contract No. PR*, 26897.
- Demattê, J. A. M., Galdos, M. V., Guimaraes, R. V., Genu, A. M., Nanni, M. R., and Zullo, J. R. (2007). Quantification of tropical soil attributes from ETN+/Landsat-7 data. *International Journal of Remote Sensing*, 28(17), 3813-3829.

- Department of Agriculture, DoA. (2007). *Chapter 2 Sectoral Overview and Performance*. Viewed 22 May 2018 <http://www.nda.agric.za/docs/StratPlan07/07sectoral.pdf>.
- Desmet, P. J. J., and Govers, G. (1996). A GIS procedure for automatically calculating the USLE LS factor on topographically complex landscape units. *Journal of Soil and Water Conservation*, 51(5), 427-433.
- Devatha, C. P., Deshpande, V., and Renukaprasad, M. S. (2015). Estimation of soil loss using USLE model for Kulham Watershed, Chattisgarh – A case study. *Aquatic Procedia*, 4, 1429-1436.
- Dickinson, A., and Collins, R. (1998). Predicting erosion and sediment yield at the catchment scale. *Soil erosion at multiple scales. CAB Int*, 317-342.
- Diodato, N., and Bellocchi, G. (2010). MedREM, a rainfall erosivity model for the Mediterranean region. *Journal of Hydrology*, 387, 119-127.
- Duraes, MF, de Mello, CR, and Beskow, S. (2016). Sediment yield in Paraopeba River Basin-MG, Brazil. *International Journal of River Basin Management*, 14 (4), 367-377.
- Durigon, V. L., Carvalho, D. F., Antunes, M. A. H., Oliveira, P. T. S., and Fernandes, M. M. (2014). NDVI time series for monitoring RUSLE cover management factor in a tropical watershed. *International Journal of Remote Sensing*, 35, 441-453.
- Dutta, S. (2016). Soil erosion, sediment yield and sedimentation of reservoir: a review. *Modelling Earth Systems and Environment*, 2(123), 1-18.
- Eisazadeh, L., Sokouti, R., Homaei, M., and Pazira, E. (2012). Comparison of empirical models to estimate soil erosion and sediment yield in macro catchments. *Eurasian Journal of Soil Science*, 1, 28-33.
- Elwell, H. A. (1977). *Soil loss estimation for southern Africa*. Harare: Zimbabwe Department of Conservation and Extension, Research Bulletin 22.
- Farhan, Y., Zregat, D., and Farhan, I. (2013). Spatial estimation of soil erosion risk using RUSLE approach, RS, and GIS techniques: A case study of Kufranja Watershed, Northern Jordan. *Journal of Water Resource and Protection*, 5, 1247-1261.
- Fathizad, H., Karimi, H., and Alibakhshi, S. M. (2014). The estimation of erosion and sediment by using the RUSLE model, RS and GIS techniques (Case study: arid and semi-arid regions of Dovoraj, Ilam province, Iran). *International Journal of Agriculture and Crop Sciences*, 7(6), 304-314.
- Ferro, V., and Porto, P. (2000). Sediment delivery distributed (SEDD) model. *Journal of hydrologic engineering*, 5(4), 411-422.
- Fisher, P. F., and Tate, N. J. (2006). Causes and consequences of error in digital elevation models. *Progress in Physical Geography*, 30(4), 467-489.
- Flanagan, D.C. (2002). *Erosion*. Encyclopedia of Soil Sciences. Marcel Dekker Publishers, New York, 395-398.
- Foody, G. M. (2002). Status of land cover classification accuracy assessment. *Remote Sensing of Environment*, 80(1), 185-201.

- Forkuor, G., Hounkpatin, O. K. L., Welp, G., and Thiel, M. (2017). High resolution mapping of soil properties using remote sensing variables in south western Burkina Faso: a comparison of machine learning and multiple linear regression models. *PLoS ONE*, 12(1), 1-21.
- Foster, G. R., McCool, D. K., Renard, K. G., and Moldenhauer, W. C. (1981). Conversion of the universal soil loss equation to SI metric units. *Journal of Soil and Water Conservation*, 36(6), 355-359.
- Foster, G. R., Yoder, D. G., Weesies, G. A., McCool, D. K., McGregor, K. C., and Bingner, R. L. (2003). *User's guide: Revised Universal Soil Loss Equation*. Washington DC: U.S. Department of Agriculture, Research Service.
- Fu, G., Chen, S., and McCool, D. K. (2006). Modelling the impact of no-till practice on soil erosion and sediment yield with RUSLE, SEDD, and ArcView GIS. *Soil and Tillage Research*, 85, 38-49.
- Gabriels, D., Ghekiere, G., Schiettecatte, W., and Rottiers, I. (2003). Assessment of USLE cover-management C-factor for 40 crop rotation system on arable farms in the Kemmelbeek watershed, Belgium. *Soil Tillage Research*, 74, 47-53.
- Ganasri, BP., and Ramesh, H. (2015). Assessment of soil erosion by RUSLE model using remote sensing and GIS – A case study of Nethravathi Basin. *Geoscience Frontiers*, 7(6), 953-961.
- Garland, G. G. (1995). *Soil erosion in South Africa: a technical review*. Report for the National Department of Agriculture. Department of Geography and Environmental Science, University of Natal, Durban, South Africa.
- Garland, G.G., Hoffman, M.T. and Todd, S. (2000). *Soil degradation. A National Review of Land Degradation in South Africa*. South African National Biodiversity Institute, Pretoria, South Africa, pp.69-107.
- Gashaw, T., Tulu, T., and Argaw, M. (2016). Erosion risk assessment for prioritization of conservation measures in Geleda watershed, Blue Nile basin, Ethiopia. *Environmental Systems Research*, 6(1), 1-14.
- Gebresamuel, G., Singh, B. R., and Dick, Ø. (2010). Land-use changes and their impacts on soil degradation and surface runoff of two catchments of Northern Ethiopia. *Acta Agriculturae Scandinavica Section B–Soil and Plant Science*, 60(3), 211-226.
- Gelagay, H. S., and Minale, A. S. (2016). Soil loss estimation using GIS and remote sensing techniques: a case of Koga watershed, northwestern Ethiopia. *International Soil and Water Conservation Research*, 4, 126-136.
- Gerber, F. A., and Harmse, V. M. (1987). Proposed procedure for identification of dispersive soils by chemical testing. *Civil Engineer in South Africa*, 29(10), 397-399.
- Gertner, G., Wang, G., Fang, S., and Anderson, A. B. (2002). Mapping and uncertainty of predictions based on multiple primary variables from joint co-simulation with Landsat TM image and polynomial regression. *Remote Sensing of Environment*, 83, 498-510.

- Getirana, A. C. V., Espinoza, J. C. V., Ronchail, J., and Filho, O. C. R. (2011). Assessment of different precipitation datasets and their impacts on the water balance of the Negro River basin. *Journal of Hydrology*, 404, 304-322.
- Ghadiri, H. (2004). Crater formation in soils by raindrop impact. *Earth Surface Processes and Landforms: The Journal of the British Geomorphological Research Group*, 29(1), 77-89.
- Gitas, I. Z., Douros, K., Minakou, C., Silleos, G. N., and Karydas, C. G. (2009). Multi-temporal soil erosion risk assessment in N. Chalkidiki using a modified USLE raster model. *EARSeL eProceedings*, 8(1), 40-52.
- Goovaerts, P. (1997). *Geostatistics for natural resources evaluation*. New York: Oxford University Press.
- Grimes, D. I. F., Pardo-Iguzquiza, E., and Bonifacio, R. (1999). Optimal areal rainfall estimation using rain gauges and satellite data. *Journal of Hydrology*, 222, 93-108.
- Grunwald, S., Vasques, G. M., and Rivero, R. G. (2015). Fusion of soil and remote sensing data to model soil properties. In D. L. Sparks(Eds.), *Advances in Agronomy* (pp. 1-344). Waltham, MA: Elsevier Inc.
- Gutman, G., and Ignatov, A. (1998). The derivation of the green vegetation fraction from NOAA/AVHRR data for use in numerical weather prediction models. *International Journal of Remote Sensing*, 19, 1533-1543.
- Gyamfi, C., Ndambuki, J. M., and Salim, R. W. (2016). Spatial variability modelling of soil erodibility index in relation to some soil properties at field scale. *Environment and Natural Resources Research*, 6(2), 16-27.
- Harris, A. T., and Asner, G. P. (2003). Grazing gradient detection with airborne imaging spectroscopy on a semi-arid rangeland. *Journal of Arid Environments*, 55, 391-404.
- Hartmann, M. O., McPhee, P. J., and Bode, M. L. (1989). The erodibility of some soil series in the pineapple-producing coastal area of the Eastern Cape. *South African Journal of Plant and Soil*, 6(4), 271-275.
- Heinemann, T., Latanzio, A., and Roveda, F. (2002). The Eumetsat multi-sensor precipitation estimate (MPE). *Proceedings of the 2nd International Precipitation Working Group (IPWG)*, Madrid, Spain.
- Heung, B., Bakker, L., Schmidt, M. G., and Dragičević, S. (2013). Modelling the dynamics of soil redistribution induced by sheet erosion using the Universal Soil Loss Equation and cellular automata. *Geoderma*, 202, 112-125.
- Hill, J., and Schutt, B. (2000). Mapping complex patterns of erosion and stability in dry Mediterranean ecosystems. *Remote Sensing of Environment*, 74, 557-569.
- Hirt, C., Filmer, M. S., and Featherstone, W. E. (2010). Comparison and validation of the recent freely available ASTER-GDEM ver1, SRTM ver4.1 and GEODATE DEM-9S ver3 digital elevation models over Australia. *Australian Journal of Earth Sciences*, 57, 337-347.

- Hoffman, T., and Ashwell, A. (2001). *Nature divided: land degradation in South Africa*. University of Cape Town Press.
- Hsu, K. I., Gao, X. G., Sorooshian, S., and Gupta, H. V. (1997). Precipitation estimation from remotely sensed information using artificial neural networks. *Journal of Applied Meteorology*, 36, 1176-1190.
- Huete, A. (2004). Remote sensing of soils and soil processes, Part 1. USFIN S. *Remote Sensing for Natural Resources Management and Environmental Monitoring: Manual of Remote Sensing*, 4.
- Huffman, G. J., Adler, R. F., Morrissey, M. M., Bolvin, D. T., Curtis, S., Joyce, R., McCavock, B., and Susskind, J. (2001). Global precipitation at one-degree daily resolution from multisatellite observations. *Journal of Hydrometeorology*, 2, 36-50.
- Huffman, GJ., Pendergrass, AG and National Centre for Atmospheric Research Staff (Eds.). (2017). The climate data guide: TRMM: Tropical Rainfall Measuring Mission. Retrieved from <https://climatedataguide.ucar.edu/climate-data/trmm-tropical-rainfall-measuring-mission>.
- Hutchinson, M. F., and Gallant, J. C. (2000). Digital elevation models and representation of terrain shape. In J. P. Wilson and J. C. Gallant(Eds.), *Terrain analysis: principles and applications* (pp. 29-50). New York: John Wiley and Sons.
- Integrated Development Plan, IDP., 2013. Umzimvubu Local Municipality Draft IDP 2013/2014. Viewed on 20 June 2018 http://www.umzimvubu.gov.za/Municipal_documents/idp/Documents/IDP%202013%20-2014.pdf.
- Iyer, H. S. (1974). Use of aerial photographs for soil erosion studies. *Journal of the Indian Society of Photo-Interpretation*, 2(2), 33-45.
- Jahun, B. G., Ibrahim, R., Dlamini, N. S., and Musa, S. M. (2015). Review of soil erosion assessment using RUSLE model and GIS. *Journal of Biology, Agriculture and Healthcare*, 5(9), 36-47.
- Jain, M. K., and Das, D. (2010). Estimation of sediment yield and areas of soil erosion and deposition for watershed prioritization using GIS and remote sensing. *Water Resources Management*, 24(10), 2091-2112.
- Jamshid, F., and Abbas, F. (2002). Remote sensing and modelling of topsoil properties: a clue for assessing land degradation. In *17th World congress of soil science CD-ROM proceedings: Confronting new realities in the 21st century: 14-21 August, Bangkok, Thailand*. <https://pdfs.semanticscholar.org/a147/c2ad2437201cc85318e6ee31e0d29a5de7d9.pdf>.
- Jamshidi, R., Dragovich, D., and Webb, A. A. (2014). Catchment scale geostatistical simulation and uncertainty of soil erodibility using sequential Gaussian simulation. *Environmental Earth Sciences*, 71(12), 4965-4976.
- Jayawardena, A. W., and Bhuiyan, R. R. (1999). Evaluation of an interrill soil erosion model using laboratory catchment data. *Hydrological Processes*, 13(1), 89-100.

- Jia, K., Li, Y., Liang, S, Wei, X., and Yao, Y. (2017). Combining estimation of green vegetation fraction in an arid region from Landsat 7 ETM+ data. *Remote Sensing*, 9(1121), 1-15.
- Jin, K., Cornelis, W. M., Gabriels, D., Schiettecatte, W., De Neve, S., Lu, J., ... and Harmann, R. (2008). Soil management effects on runoff and soil loss from field rainfall simulation. *Catena*, 75(2), 191-199.
- Johannsen, C. J., and Barney, T. W. (1981). Remote sensing applications for resource management. *Journal of Soil and Water Conservation*, 36(3), 128-134.
- Johanson, R. C., Imhoff, J. C., and Davis, H. H. (1980). *User's manual for the hydrologic simulation program – Fortran (HSPF) version No. 5.0, EPA-600/9-80-105*. Athens, GA: U.S. EPA Environmental Research Laboratory.
- Johnson, B., Tateishi, R., and Kobayashi, T. (2012). Remote sensing of fractional green vegetation cover using spatially-interpolated endmembers. *Remote Sensing*, 4, 2619-2634.
- Jones, C., Lowe, J., Liddicoat, S., and Betts, R. (2009). Committed terrestrial ecosystem changes due to climate change. *Nature Geoscience*, 2, 484-487.
- Joyce, R. J., Janowiak, J. E., Arkin, P. A., and Xie, P. P. (2004). CMORPH: A method that produces global precipitation estimates from passive microwave and infrared data at high spatial and temporal resolution. *Journal of Hydrometeorology*, 5, 487-503.
- Kamaludin, H., Lihan, T., Rahman, Z. A., Mustapha, M. A., Idris, W. M. R., and Rahim, S. A. (2013). Integration of remote sensing, RUSLE and GIS to model potential soil loss and sediment yield (SY). *Hydrology and Earth System Sciences*, 10, 4567-4596.
- Kavian, A., Hoseinpoor Sabet, S., Solaimani, K., and Jafari, B. (2017). Simulating the effects of land use changes on soil erosion using RUSLE model. *Geocarto International*, 32(1), 97-111.
- Karamage, F., Zhang, C., Liu, T., Maganda, A., and Isabwe, A. (2017). Soil Erosion Risk Assessment in Uganda. *Forests*, 8(2), 52.
- Karydas, C. G., Sekuloska, T., and Silleos, G. N. (2009). Quantification and site-specification of the support practice factor when mapping soil erosion risk associated with olive plantations in the Mediterranean island of Crete. *Environmental Monitoring and Assessment*, 149(1-4), 19-28.
- Khosrokhani, M., and Pradhan, B. (2014). Spatio-temporal assessment of soil erosion at Kuala Lumpur metropolitan city using remote sensing data and GIS. *Geomatics, Natural Hazards and Risk*, 5(3), 252-270.
- Kidd, C., and Huffman, G. (2011). Global precipitation measurement. *Meteorological Applications*, 18, 334-353.
- Kidd, C., Bauer, P., Turk, J., Huffman, G. J., Joyce, R., Hsu, K. L., and Braithwaite, D. (2012). Intercomparison of high-resolution precipitation products over northwest Europe. *Journal of Hydrometeorology*, 13, 67-83.
- Kinnell, P. I. A. (2005). Why the universal soil loss equation and the revised version of it do not predict event erosion well. *Hydrological Processes*, 19, 851-854.

- Kinnell, P. I. A. (2010). Event soil loss, runoff and the Universal Soil Loss Equation family of models: A review. *Journal of Hydrology*, 385(1-4), 384-397.
- Kouli, M., Soupios, P., and Vallianatos, F. (2009). Soil erosion prediction using the revised universal soil loss equation (RUSLE) in a GIS framework, Chania, Northwestern Crete, Greece. *Environmental Geology*, 57(3), 483-497.
- Kubota, T., Shige, S., Hashizume, H., Aonashi, K., Takahashi, N., Seto, S., Hirose, M., Takayabu, YN., Ushio, T., Nakagawa, K., Wanami, K., Kachi, M., and Okamoto, K. (2007). Global precipitation map using satellite-borne microwave radiometers by the GSMaP project: production and validation. *IEEE Transactions on Geoscience and Remote Sensing*, 45, 2259-2275.
- Kumar, S., and Kushwaha, S. P. S. (2013). Modelling soil erosion risk based on RUSLE-3D using GIS in a Shivalik sub-watershed. *Journal of Earth System Sciences*, 122(2), 389-398.
- Laflen, J. M., Lane, L. J., and Foster, G. R. (1991). A generation of erosion prediction technology'. *Journal of Soil and Water Conservation*, 46, 34-38.
- Laker, M. C. (1990). The conservation status of agricultural resources in the developing areas of South Africa. In *Proceedings of the National Veld Trust Conference on the Conservation Status of Agricultural Resources in RSA*, Pretoria, South Africa.
- Laker, M. C. (2004). Advances in soil erosion, soil conservation, land suitability evaluation and land use planning research in South Africa, 1978–2003. *South African Journal of Plant and Soil*, 21(5), 345-368.
- Lakshmi, V. S., James, J., Soundariya, S., Vishalini, T., and Pandian, K. P. (2015). A comparison of soil texture distribution and soil moisture mapping of Chennai Coast using Landsat ETM+ and IKONOS data. *Aquatic Procedia*, 4, 1452-1460.
- Lal, R. (1994). Water management in various crop production systems related to soil tillage. *Soil and Tillage Research*, 30(2-4), 169-185.
- Lal, R. (1995). Global soil erosion by water and carbon dynamics. *Soils and Global Change*, 131-142.
- Lal, R. (2001). Soil degradation by erosion. *Land Degradation and Development*, 12(6), 519-539.
- Lal, R. (2003). Soil erosion and the global carbon budget. *Environment International*, 29(4), 437-450.
- Lal, R. and Stewart, B.A. (1990). *Soil degradation*, Springer-Verlag, New York.
- Landis, J. R., and Koch, G. G. (1977). The measurement of observer agreement for categorical data. *Biometrics*, 159-174.
- Lane, L. J., Kidwell, M. R., and Weltz, M. A. (2000). Watershed sediment yield and rangeland health. *International Journal of Sediment Research*, 15(1), 51-59.
- Lazzari, M., Gioia, D., Piccarreta, M., Danese, M., and Lanorte, A. (2015). Sediment yield and erosion rate estimation in the mountain catchments of the Camastra artificial reservoir

- (Southern Italy): A comparison between different empirical methods. *Catena*, 127, 323-339.
- Le Roux, J. J., Morgenthal, T. L., Malherbe, J., Pretorius, D. J., and Sumner, P. D. (2008). Water erosion prediction at a national scale for South Africa. *Water SA*, 34(3), 305-314.
- Levizzani, V., Schmetz, J., Lutz, H. J., Kerkmann, J., Alberoni, P. P., and Cervino, M. (2001). Precipitation estimations from geostationary orbit and prospects for METEOSAT second generation. *Meteorological Applications*, 8, 23-41.
- Li, H., Chen, X., Kyoung, J., Cai, X., and Myung, S. (2010). Assessment of soil erosion and sediment yield in Liao Watershed, Jiangxi Province, China, using USLE, GIS, and RS. *Journal of Earth Science*, 21(6), 941-953.
- Li, J., Zhao, W., and Zhang, X. (2010). The application of remote sensing data to assess soil erosion. *IEEE International Conference on Multimedia Technology*, China. Retrieved from <http://ieeexplore.ieee.org/document/5629726/>.
- Li, X., Wu, B., Wang, H., and Zhang, J. (2011). Regional soil erosion risk assessment in Hai Basin. *Yaogan Xuebao- Journal of Remote Sensing*, 15(2), 372-387.
- Li, X. H., Zhang, Q., and Xu, C. Y. (2012). Suitability of the TRMM satellite rainfalls in driving a distributed hydrological model for water balance computations in Xinjiang catchment, Poyang lake basin. *Journal of Hydrology*, 426-427, 28-38.
- Li, X., Zhang, Q., and Ye, X. (2013). Capabilities of satellite-based precipitation to estimate the spatiotemporal variation of flood/drought class in Poyang Lake Basin. *Advances in Meteorology*, 2013, 1-9.
- Li, Y., Wang, H., and Li, X. B. (2015). Fractional vegetation cover estimation based on an improved selective endmember spectral mixture model. *PLoS ONE*, 10(4), 1-15.
- Li, Z. (1992). Variation of the accuracy of digital terrain models with sampling interval. *Photogrammetric Record*, 14(79), 113-128.
- Lillesand, T. M., and Kiefer, R. W. (2000). *Remote sensing and image interpretation*, 4th edition, John Wiley and Sons, New York.
- Lim, K. J., Choi, J. D., Kim, K. S., Sagong, M., and Engel, B. A. (2003). Development of sediment assessment tool for effective erosion control (SATEEC) in small scale watershed. *Journal of the Korean Society of Engineers*, 20, 74-85.
- Lim, K. J., Sagong, M., Engel, B. A., Tang, Z., Choi, J., and Kim, K. S. (2005). GIS-based sediment assessment tool. *Catena*, 64(1), 61-80.
- Lin, C. Y., Lin, W. T., and Chou, W. C. (2002). Soil erosion prediction and sediment yield estimation: the Taiwan experience. *Soil and Tillage Research*, 68, 143-152.
- Lin, D., Gao, Y., Wu, Y., Shi, P., Yang, H., and Wang, J. (2017). A comparison method to determine the regional vegetation cover factor from standard plots based on large sample theory and TM images: a case study in the eastern farming-pasture ecotone of northern China. *Remote Sensing*, 9, 1-20.

- Lord, T. M., and McLean, A. (1969). Aerial photo interpretation on British Columbia rangelands. *Journal of Range Management*, 22(1), 3-9.
- Loureiro, N. S., and Coutinho, M. A. (2001). A new procedure to estimate the RUSLE EI30 index, based on monthly rainfall data and applied to the Algarve region, Portugal. *Journal of Hydrology*, 250, 12-18.
- Lu, D., Mausel, P., Brondizio, E., and Moran, E. (2004). Change detection techniques. *International Journal of Remote Sensing*, 25(12), 2365-2401.
- Lu, D., and Weng, Q. (2007). A survey of image classification methods and techniques for improving classification performance. *International Journal of Remote Sensing*, 28(5), 823-870.
- Lu, D., Li, G., Valladares, G. S., and Batistella, M. (2004). Mapping soil erosion risk in Rondônia, Brazilian Amazonia: using RUSLE, remote sensing and GIS. *Land Degradation and Development*, 15, 499-512.
- Lufafa, A., Tenywa, M. M., Isabirye, M., Majaliwa, M. J. G., and Woomer, P. L. (2003). Prediction of soil erosion in a Lake Victoria basin catchment using a GIS-based Universal Soil Loss model. *Agricultural Systems*, 76(3), 883-894.
- Luffman, I. E., Nandi, A., and Spiegel, T. (2015). Gully morphology, hillslope erosion, and precipitation characteristics in the Appalachian Valley and Ridge province, southeastern USA. *Catena*, 133, 221-232.
- Ma, X., He, Y., Xu, J., Noordwijk, M., and Lu, X. (2014). Spatial and temporal variation in rainfall erosivity in a Himalayan watershed. *Catena*, 121, 248-259.
- Maetens, W., Poesen, J., and Vanmaercke, M. (2012). How effective are soil conservation techniques in reducing plot runoff and soil loss in Europe and the Mediterranean? *Earth-Science Reviews*, 115(1-2), 21-36.
- Malhi, Y., Baker, T. R., Phillips, O. L., Almeida, S., Alvarez, E., Arroyo, L., ... and Killeen, T. J. (2004). The above-ground coarse wood productivity of 104 Neotropical forest plots. *Global Change Biology*, 10(5), 563-591.
- Mallick, J., Alashker, Y., Mohammad, S. A., Ahmed, M., and Hasan, M. A. (2014). Risk assessment of soil erosion in semi-arid mountainous watershed in Saudi Arabia by RUSLE model coupled with remote sensing and GIS. *Geocarto International*, 29(8), 915-940.
- Mashimbye, Z. N., De Clercq, W. P., and Van Niekerk, A. (2014). An evaluation of digital elevation models (DEMs) for delineating land components. *Geoderma*, 213, 312-319.
- McCool, D. K., Foster, G. R., Mutchler, C. K., and Meyer, L. D. (1989). Revised slope length factor for the Universal Soil Loss Equation. *Transactions of the ASAE*, 32(5), 1571-1576.
- McCool, D. K., Foster, G. R., Renard, K. G., and Weesies, G. A. (1995). *The revised universal soil loss equation*. Proceedings of DOD Interagency Workshop on Technologies to Address Soil Erosion on DOD Lands, San Antonio, Department of Defence. Retrieved from <https://www.tucson.ars.ag.gov/unit/publications/PDFfiles/1132.pdf>
- McPhee, P. J., and Smithen, A. A. (1984). Application of the USLE in the Republic of South Africa. *Agricultural Engineering in South Africa*, 18(1), 5-13.

- Merritt, W. S., Letcher, R. A., and Jakeman, A. J. (2003). A review of erosion and sediment transport models, *Environmental Modelling and Software*, 18(8-9), 761-799.
- Merzoul, A. (1985). *Relative erodibility of nine selected Moroccan soils related to their physical and chemical and mineralogical properties* (Doctoral dissertation). University of Minnesota, USA.
- Meusburger, K., Bänninger, D., and Alewell, C. (2010). Estimating vegetation parameter for soil erosion assessment in an alpine catchment by means of QuickBird imagery. *International Journal of Applied Earth Observation and Geoinformation*, 12, 201-207.
- Meyer, L. D. (1975). Source of soil eroded by water from upland slopes. In *Proc. Od sediment yield workshop, USDA sedimentation laboratory, Oxford, misc* (pp. 190-207).
- Meyer, L. D., and Wischmeier, W. H. (1969). Mathematical simulation of the process of soil erosion by water. *Transactions of the ASAE*, 12(6), 754-0758.
- Mhangara, P. (2011). *Land use/cover change modelling and land degradation assessment in the Keiskamma catchment using remote sensing and GIS* (Doctoral dissertation, Nelson Mandela Metropolitan University).
- Mhangara, P., Kakembo, V., and Lim, K. J. (2012). Soil erosion risk assessment of the Keiskamma catchment, South Africa using GIS and remote sensing. *Environmental Earth Sciences*, 65(7), 2087-2102.
- Millward, A. A., and Mersey, J. E. (1999). Adapting the RUSLE to model soil erosion potential in a mountainous tropical watershed. *Catena*, 38, 109-129.
- Minasny, B., and McBratney, A. B. (2007). Spatial prediction of soil properties using EBLUP with the Matérn covariance function. *Geoderma*, 140, 324-336.
- Mitasova, H., Barton, M., Ullah, I., Hofierka, J., and Harmon, R. S. (2013). GIS-based soil erosion modelling. In J. F. Shroder and M. P. Bishop(Eds.), *Treatise on Geomorphology* (pp. 228-258). San Diego: Academic Press.
- Mitasova, H., Hofierka, J., Zlocha, M., and Iverson, L. R. (1996). Modelling topographic potential for erosion and deposition using GIS. *International Journal of Geographical Information System*, 10(5), 629-641.
- Moore, I. D., and Burch, G. J. (1986). Physical basis of the length slope factor in the universal soil loss equation. *Soil Science Society of America*, 50, 1294-1298.
- Moore, I. D., and Wilson, J. P. (1992). Length-slope factors for the Revised Universal Soil Loss Equation: Simplified method of estimation. *Journal of Soil and Water Conservation*, 47(5), 423-428.
- Morgan, J. L., Gergel, S. E., and Coops, N. C. (2010). Aerial photography: a rapidly evolving tool for ecological management. *BioScience*, 60(1), 47-59.
- Morgan, R. P. C. (2009). *Soil erosion and conservation*. Blackwell Publishing, Malden.
- Morgan, R. P. C. (2005). *Soil erosion and conservation*. Blackwell Publishing, Oxford.

- Moses, A. N. (2017). GIS-RUSLE interphase modelling of soil erosion hazard and estimation of sediment yield for river Nzoia basin in Kenya. *Journal of Remote Sensing and GIS*, 6(3), 1-13.
- Moura-Bueno, J. M., Dalmolin, R. S. D., ten Caten, A., Ruiz, L. F. C., Ramos, P. V., and Dotto, A. C. (2016). Assessment of digital elevation model for digital soil mapping in a watershed with gently undulating topography. *Revista Brasileira de Ciência do Solo*, 40, 1-13.
- Nanni, M. R., and Demattê, J. A. M. (2006). Spectral reflectance methodology in comparison to traditional soil analysis. *Soil Science Society of America Journal*, 70, 393-407.
- Napieralski, J., Barr, I., Kamp, U., and Kervyn, M. (2013). Remote sensing and GIScience in geomorphological mapping. In J. F. Shroder and M. P. Bishop(Eds.), *Treatise on Geomorphology* (pp. 187-227). San Diego: Academic Press.
- Napoli, M., Cecchi, S., Orlandini, S., Muganai, G., and Zanchi, C. A. (2017). Simulation of field-measured soil loss in Mediterranean hilly areas (Chianti, Italy) with RUSLE. *Catena*, 145, 246-256.
- Nath, C. D., Dattaraja, H. S., Suresh, H. S., Joshi, N. V., and Sukumar, R. (2006). Patterns of tree growth in relation to environmental variability in the tropical dry deciduous forest at Mudumalai, southern India. *Journal of Biosciences*, 31(5), 651-669.
- New Partnership for Africa's Development, NEPAD., 2013. *Agriculture in Africa – transformation and outlook*. Viewed 03 June 2018 <http://www.un.org/en/africa/osaa/pdf/pubs/2013africanagricultures.pdf>
- Nil, D., Schwertmann, U., Sabel-Koschella, U., Bernard, M., and Breuer, J. (1996). *Soil erosion by water in Africa. Principles, prediction and protection* (No. 631.45 S683s). GTZ, Eschborn (Alemania).
- Noori, H., Siadatmousavi, S. M., and Mojaradi, B. (2016). Assessment of sediment yield using RS and GIS at two sub-basins of Dez Watershed, Iran. *International Soil and Water Conservation Research*, 4, 199-206.
- Okorafor, O. O., Akinbile, C. O., and Adeyemo, A. J. (2017). Determination of cover-crop management factor (C) for selected sites in Imo State using remote sensing technique and GIS. *Environment and Sustainability*, 1(4), 110-116.
- Oldeman, L. R., Hakkeling, R. T. A., and Sombroek, W. G. (1991). *World map of the status of human induced soil degradation: an explanatory note*. ISRIC, Wageningen.
- Onyando, J. O., Kisoyan, P., and Chemelil, M. C. (2004). Estimation of potential soil erosion for river Perkerra catchment in Kenya. *Water Resources Management*, 19, 33-143.
- Ostovari, Y., Ghorbani-Dashtaki, S., Bahrami, H., Naderi, M., and Damatte, J. A. M. (2017). Soil loss estimation using RUSLE model, GIS and remote sensing techniques: a case study from the Dembecha watershed, northwestern Ethiopia. *Geoderma Regional*, 11, 28-36.
- Paiboonvorachat, C., and Oyana, T. J. (2011). Land-cover changes and potential impacts on soil erosion in the Nan watershed, Thailand. *International Journal of Remote Sensing*, 32(21), 6587-6609.

- Panagopoulos, T., and Antunes, M. D. C. (2008). Integrating Geostatistics and GIS for assessment of erosion risk on low density quercus suber woodlands of South Portugal. *Arid Land Research and Management*, 22, 159-177.
- Panagos, P., Borrelli, P., Meusburger, K., Alewell, C., Lugato, E., and Montanarella, L. (2015). Estimating the soil erosion cover-management factor at the European scale. *Land Use Policy*, 48, 38-50.
- Panagos, P., Karydas, C. G., Ballabio, C., and Gitas, I. Z. (2014). Seasonal monitoring of soil erosion at regional scale: an application of the G2 model in Crete focusing on agricultural land uses. *International Journal of Applied Earth Observation and Geoinformation*, 27, 147-155.
- Parlak, M., and Parlak, A. Ö. (2010). Measurement of splash erosion in different cover crops. *Turkish Journal of Field Crops*, 15(2), 169-173.
- Parveen, R., and Kumar, U. (2012). Integrated approach of universal soil loss equation (USLE) and geographical Information System (GIS) for soil loss risk assessment in upper south Koel basin, Jharkand. *Journal of Geographic Information System*, 4, 588-596.
- Parwada, C., and Van Tol, J. (2017). Soil properties influencing erodibility of soils in the Ntabelanga area, Eastern Cape Province, South Africa. *Acta Agriculturae Scandinavica, Section B—Soil and Plant Science*, 67(1), 67-76.
- Parysow, P., Wang, G., Gertner, G. Z., and Anderson, A. B. (2003). Spatial uncertainty analysis for mapping soil erodibility based on joint sequential simulation. *Catena*, 53, 65-78.
- Patil, R. J., and Sharma, S. K. (2013). *Remote sensing and GIS based modelling of crop/cover management factor (C) of USLE in Shakker river watershed*. International Conference on Chemical, Agricultural and Medical Sciences, Malaysia. Retrieved from <http://iicbe.org/upload/3309C1213023.pdf>.
- Pendgrass, A., and National Centre for Atmospheric Research Staff. (2016). The climate data guide: GPCP (Monthly): Global Precipitation Climatology Project. Retrieved from <https://climatedataguide.ucar.edu/climate-data/gpcp-monthly-global-precipitation-climatology-project>.
- Peneva-Reed, E. (2014). Understanding land-cover change dynamics of a mangrove ecosystem at the village level in Krabi Province, Thailand, using Landsat data. *GIScience and remote sensing*, 51(4), 403-426.
- Peng, W., Wheeler, D. B., Bell, J. C., & Krusemark, M. G. (2003). Delineating patterns of soil drainage class on bare soils using remote sensing analyses. *Geoderma*, 115(3-4), 261-279.
- Phinzi, K., and Ngetar, N. S. (2017). Mapping soil erosion in a quaternary catchment in Eastern Cape using geographic information system and remotes sensing. *South African Journal of Geomatics*, 6(1), 11-29.
- Pimentel, D. (1993). *World soil erosion and conservation*. Cambridge University Press, Cambridge.

- Pimentel, D. (2006). Soil erosion: a food and environmental threat. *Environment, Development and Sustainability*, 8(1), 119-137.
- Pimentel, D., and Kounang, N. (1998). Ecology of soil erosion in ecosystems. *Ecosystems*, 1(5), 416-426.
- Pimentel, D., Harvey, C., Resosudarmo, P., Sinclair, K., Kurz, D., McNair, M., and Blair, R. (1995). Environmental and economic costs of soil erosion and conservation benefits. *Science*, 267(5201), 1117-1123.
- Poesen, J., Nachtergaele, J., Verstraeten, G., and Valentin, C. (2003). Gully erosion and environmental change: importance and research needs. *Catena*, 50(2-4), 91-133.
- Polidori, L., Hage, M., and Valeriano, M. D. (2014). Digital elevation model validation with no ground control: applications to the topodata DEM in Brazil. *Boletim de Ciências Geodésicas*, 20(2), 467-479.
- Prasannakumar, V., Vijith, H., Abinod, S., and Geetha, N. (2012). Estimation of soil erosion risk within mountainous sub-watershed in Kerala, India, using Revised Universal Soil Loss Equation (RUSLE) and geo-information technology. *Geoscience Frontiers*, 3(2), 209-215.
- Prevent, C. (2010). Precipitation retrieval from space: an overview. *Geoscience*, 342, 380-389.
- Puente, C., Olague, G., Smith, S. V., Bullock, S. H., Hinojosa-Corona, A., and González-Botello, M. A. (2011). A genetic programming approach to estimate vegetation cover in the context of soil erosion assessment. *Photogrammetric Engineering and Remote Sensing*, 77(4), 363-376.
- Qi, J., Chehbouni, A., Huete, A. R., and Kerr, Y. H. (1994). Modified soil adjusted vegetation index (MSAVI). *Remote Sensing of Environment*, 48, 119-126.
- Qin, Y., Chen, Z., Shen, Y., Zhang, S., and Shi, R. (2014). Evaluation of satellite rainfall estimates over the Chinese Mainland. *Remote Sensing*, 6, 11649-11672.
- Rahaman, S. A., Aruchamy, S., Jegankumar, R., and Ajeez, S. A. (2015). Estimation of annual average soil loss, based on RUSLE model in Kallar watershed, Bhavani basin, Tamil Nadu, India. *ISPRS Annals of the Photogrammetry, Remote Sensing and Spatial Information Sciences*, 2, 207-214. Retrieved from <https://www.isprs-ann-photogramm-remote-sens-spatial-inf-sci.net/II-2-W2/207/2015/isprsannals-II-2-W2-207-2015.pdf>
- Rahman, M. R., Shi, Z. H., and Chongf, C. (2009). Soil erosion hazard evaluation: an integrated use of remote sensing, GIS and statistical approaches with biophysical parameters towards management strategies. *Ecological Modelling*, 220, 1724-1734.
- Ran, Q., Su, D., Li, P., and He, Z. (2012). Experimental study of the impact of rainfall characteristics on runoff generation and soil erosion. *Journal of Hydrology*, 424, 99-111.
- Rankin, M. O., Semple, W. S., Murphy, B. W., and Koen, T. B. (2007). Is there a close association between 'soils' and 'vegetation'? A case study from central western New South Wales. *Cunninghamia*, 10(2), 199-214.

- Ray, S. S., Singh, J. P., Das, G., and Panigrahy, S. (2004). *Use of high resolution remote sensing data for generating site-specific soil management plan*. Retrieved from <https://pdfs.semanticscholar.org/c69a/f13fbfd1795dafb962619f1b7a673fdbb013.pdf>.
- Rienks, S. M., Botha, G. A., and Hughes, J. C. (2000). Some physical and chemical properties of sediments exposed in a gully (donga) in northern KwaZulu-Natal, South Africa and their relationship to the erodibility of the colluvial layers. *Catena*, 39(1), 11-31.
- Renard, K. G., and Foster, G. R. (1983). Soil conservation: principles of erosion by water. In H. E. Dregne and W. O. Willis(Eds.), *Dryland agriculture. Agronomy Monograph* (pp. 155-176), Madison: American Society of Agronomy.
- Renard, K. G., Foster, F. G., Weesies, G. A., McCool, D. K., and Yoder, D. C. (1997). *Predicting soil loss erosion by water: a guide to conservation planning with the revised Universal Soil Loss Equation (RUSLE)*. Washington, DC: U.S. Department of Agriculture.
- Renard, K. G., Foster, G. R., Weesies, G. A., and Porter, J. P. (1991). RUSLE: revised universal soil loss equation. *Journal of Soil and Water Conservation*, 46, 30-33.
- Renard, K. G., Foster, G. R., Weesies, G. A., McCool, D. K., and Yoder, D. C. (1997). *Predicting soil erosion by water: a guide to conservation planning with the Revised Universal Soil Loss Equation (RUSLE)* (Vol. 703). Washington, DC: United States Department of Agriculture.
- Renard, K. G., Foster, G. R., Yoder, D. C., and McCool, D. K. (1994). RUSLE revisited: status, questions, answers, and future. *Journal of Soil and Water Conservation*, 49(3), 213-220.
- Renard, K. G., Yoder, D. C., Lightle, D. T., and Dabney, S. M. (2011). Universal soil loss equation and revised universal soil loss equation. *Handbook of erosion modelling*, 8, 135-167.
- Reusing, M., Schneider, T., and Ammer, U. (2000). Modelling soil erosion rates in the Ethiopian highlands by integration of high resolution MOMS-02/D2-stereo-data in a GIS. *International Journal of Remote Sensing*, 21, 1885-1896.
- Risse, L. M., Nearing, M. A., Nicks, A., and Laflen, J. M. (1993). Error assessment in the universal soil loss equation. *Soil Science Society of American Journal*, 57, 825-833.
- Ritchie J. C. (2000). Soil erosion. In: Schultz G.A, Engman E.T (eds), *Remote Sensing in Hydrology and Water Management*. Springer: Berlin, 271.
- Röder, A., and Hill, J. (Eds.). (2009). *Recent advances in remote sensing and geoinformation processing for land degradation assessment*. Leiden: CRC Press.
- Rodriquez, J. L. G., and Suarez, M. C. G. (2012). Methodology for estimating the topographic factor LS of RUSLE3D and USPED using GIS. *Geomorphology*, 175-176, 98-106.
- Römken, M. J. M., Young, R. A., Poesen, J. W. A., McCool, D. K., El-Swaify, S. A., and Bradford, J. M. (1997). Soil erodibility factor. In K. G. Renard, G. R. Foster, G. A. Weesies, D. K. McCool and D. C. Yoder(Eds.), *Predicting soil erosion by water: a guide*

- to conservation planning with the Revised Soil Loss Equation (RUSLE). Washington, DC: U.S. Department of Agriculture.
- Rosewell, C. J. (1993). *SOILOSS: a program to assist in the selection of management practices to reduce erosion*. Technical handbook no. 11 (2nd ed.), Sydney: Conservation Services of New South Wales, Department of Conservation and Land Management.
- Rouse Jr, J., Haas, R. H., Schell, J. A., and Deering, D. W. (1974). *Monitoring vegetation systems in the Great Plains with ERTS*.
- Rowell, D. L. (1994). *Soil science: Methods and applications*. John Wiley and Sons, New York.
- Saha, S., Moorthi, S., Pan, H. L., Wu, X., Wang, J., Nadiga, S., ...and Goldberg, M. (2010). The NCEP climate forecast system reanalysis. *Bulletin of the American Meteorological Society*, 91(8), 1015-1057.
- Salako, F. K. (2010). Development of isoerodent maps for Nigeria from daily rainfall amount. *Geoderma*, 156(3-4), 372-378.
- Scherr, S.J., Yadav, S. (1997). Land degradation in the developing world: issues and policy options for 2020. International Food Policy Research Institute, 2020 Brief 44. Viewed on 20 June 2018 <http://ageconsearch.umn.edu/bitstream/16371/1/br44.pdf>.
- Schonbrodt, S., Saumer, P., Benrens, T., Seeber, C., and Scholten, T. (2010). Assessing the USLE crop and management factor C for soil erosion modelling in a large, mountainous watershed in central China. *Journal of Earth Science*, 21, 835-845.
- Schulze, R. E. (2007). Soils: Agrohydrological information needs, information sources and decision support. Schulze, RE (ed). *South African Atlas of Climatology and Agrohydrology*. Water Research Commission, Pretoria, South Africa, WRC Report 1489/1/06, Section 4.1.
- Sepal, T., Qi, J., Lawawirojwong, S., and Messina, J. P. (2016). Understanding spatio-temporal variation of vegetation phenology and seasonality in the monsoon Southeast Asia. *Environmental Research*, 147, 621-629.
- Sepuru, T. K., and Dube, T. (2017). An appraisal on the progress of remote sensing applications in soil erosion mapping and monitoring. *Remote Sensing Applications: Society and Environment*, 9, 1-9.
- Seutloali, K. E., Beckedahl, H. R., Dube, T., and Sibanda, M. (2016). An assessment of gully erosion along major armoured roads in south-eastern region of South Africa: a remote sensing and GIS approach. *Geocarto International*, 31(2), 225-239.
- Seutloali, K. E., Dube, T., and Sibanda, M. (2018), Developments in the remote sensing of soil erosion in the perspective of sub-Saharan Africa. Implications on future food security and biodiversity. *Remote Sensing Applications: Society and Environment*, 9, 100-106.
- Sharply, A. N., and Williams, J. R. (1990). *EPIC-erosion/productivity impact calculator I, Model documentation*. Beltsville, MD: U.S. Department of Agriculture Technical Bulletin, No.1768.

- Shen, Y., Xiong, A., Wang, Y., and Xie, P. (2010). Performance of high-resolution satellite precipitation products over China. *Journal of Geophysical Research*, 115, 1-17.
- Shi, Z. H., Cai, C. F., Ding, S. W., Wang, T. W., and Chow, T. L. (2004). Soil conservation planning at the small watershed level using RUSLE with GIS: a case study in the Three Gorge Area of China. *Catena*, 55(1), 33-48.
- Singer, M. J., and Shainberg, I. (2004). Mineral soil surface crusts and wind and water erosion. *Earth Surface Processes and Landforms: The Journal of the British Geomorphological Research Group*, 29(9), 1065-1075.
- Singer, M. J., and Warkentin, B. P. (1996). Soils in an environmental context: an American perspective. *Catena*, 27(3-4), 179-189.
- Singh, A. (1989). Review article digital change detection techniques using remotely-sensed data. *International Journal of Remote Sensing*, 10(6), 989-1003.
- Smith, H. J. (1999). Application of empirical soil loss models in southern Africa: a review'. *South African Journal of Plant and Soil*, 16(3), 158-163.
- Smith, S. V., Bullock, S. H., Hinojosa-Corona, A., Franco-Viscaíno, E., Escoto-Rodríguez, M., Kretzschmar, T. G., Farfan, L. M., and Salazar-Cesena, J. M. (2007). Soil erosion and significance for carbon fluxes in a mountainous Mediterranean-climate watershed. *Ecological Applications*, 17(5), 1379-1387.
- Song, C., Woodcock, C. E., Seto, K. C., Lenney, M. P., and Macomber, S. A. (2001). Classification and change detection using Landsat TM data: when and how to correct atmospheric effects?. *Remote sensing of Environment*, 75(2), 230-244.
- Spatial Development Framework, SDF., 2011. Umzimvubu Local Municipality: Spatial development framework. Viewed on 16 August 2018 http://www.umzimvubu.gov.za/Municipal_documents/SDF/Documents/UMZIMVUBU%20FINAL%20SDF.pdf.
- Stocking, M. A., and Elwell, H. A. (1976). Rainfall erosivity over Rhodesia. *Transactions of the Institute of British Geographers*, 1(2), 231-245.
- Story, M., and Congalton, R. G. (1986). Accuracy assessment: a user's perspective. *Photogrammetric Engineering and remote sensing*, 52(3), 397-399.
- Suepa, T., Qi, J., Lawawirojwong, S., & Messina, J. P. (2016). Understanding spatio-temporal variation of vegetation phenology and rainfall seasonality in the monsoon Southeast Asia. *Environmental Research*, 147, 621-629.
- Sylla, L., Xiong, D., Zhang, H. Y., and Bangoura, S. T. (2012). A GIS technology and method to assess environmental problems from land use/cover changes: Conakry, Coyah and Dubreka region case study. *The Egyptian Journal of Remote Sensing and Space Science*, 15(1), 31-38.
- Tadele, H., Mekuriaw, A., Selassie, Y. G., and Tsegaye, L. (2017). Land use/land cover factor values and accuracy assessment using a GIS and remote sensing in the case of the Quashay watershed in northwestern Ethiopia. *Journal of Natural Resources and Development*, 7, 38-44.

- Tadesse, L., Suryabhadgavan, K. V., Sridhar, G., and Legesse, G. (2017). Land use and land cover changes and soil erosion in Yezat watershed, north western Ethiopia. *International Soil and Water Conservation Research*, 5, 85-94.
- Tamene, L., Adimassu, Z., Aynekulu, E., and Yaekob, T. (2017). Estimating landscape susceptibility to soil erosion using GIS-based approach in Northern Ethiopia. *International Soil and Water Conservation Research*, 5, 221-230.
- Tanyaş, H., Kolat, Ç., and Süzen, M. L. (2015). A new approach to estimate cover-management factor of RUSLE and validation of RUSLE model in the watershed of Kartalkaya Dam. *Journal of Hydrology*, 528, 584-598.
- Taruvunga, K. (2009). *Gully mapping using remote sensing: Case study in KwaZulu-Natal, South Africa* (Master's thesis, University of Waterloo).
- Teng, H., Ma, Z., Chappell, A., Shi, Z., Liang, Z., and Yu, W. (2017). Improving rainfall erosivity
- Thomas, J., Joseph, S., and Thrivikramji, K. P. (2017). Assessment of soil erosion in a tropical mountain river basin of the southern Western Ghats, India using RUSLE and GIS. *Geoscience Frontiers*, 9(3), 893-906.
- Toledo, M., Poorter, L., Peña-Claros, M., Alarcón, A., Balcázar, J., Leño, C., ... and Bongers, F. (2011). Climate is a stronger driver of tree and forest growth rates than soil and disturbance. *Journal of Ecology*, 99(1), 254-264.
- Torri, D., Poesen, J., and Borselli, L. (1997). Predictability and uncertainty of the soil erodibility factor using global dataset. *Catena*, 31(1-2), 1-22.
- Toutin, T., and Gray, L. (2000). State-of-the-art of elevation extraction from satellite SAR data. *ISPRS Journal of Photogrammetry and Remote Sensing*, 55(1), 13-33.
- Toy, T. J., Foster, G. R., and Renard, K. G. (1999). RUSLE for mining, construction and reclamation lands. *Journal of Soil and Water Conservation*, 54(2), 462-467.
- Tran, L. T., Ridgley, M. A., Duckstein, L., and Sutherland, R. (2002). Application of fuzzy logic-based modelling to improve the performance of the Revised Universal Soil Loss Equation. *Catena*, 47, 203-226.
- Turk, F. J., and Miller, S. D. (2005). Toward improved characterization of remotely sensed precipitation regimes with MODIS/AMSR-E blended data techniques. *IEEE Transactions on Geoscience and Remote Sensing*, 43, 1059-1069.
- Tweddale, S. A., Echlschlaeger, C. R., and Seybold, W. F. (2000). *An improved method for spatial extrapolation of vegetative cover estimates (USLE/RUSLE C factor) using LCTA and remotely sensed imagery*. U.S. Army Corps of Engineers, Engineer Research and Development Centre (ERDC) Technical Report.
- U.S. Environmental Protection Agency-EPA. (2008). *Fate, Transport and Transformation Test Guidelines: OPPTS 835.1230 Adsorption/Deposition (Batch Equilibrium)*, viewed 07 March 2018, <https://nepis.epa.gov/Exe/ZyPDF.cgi/P1005IVR.PDF?Dockkey=P1005IVR.PDF> .

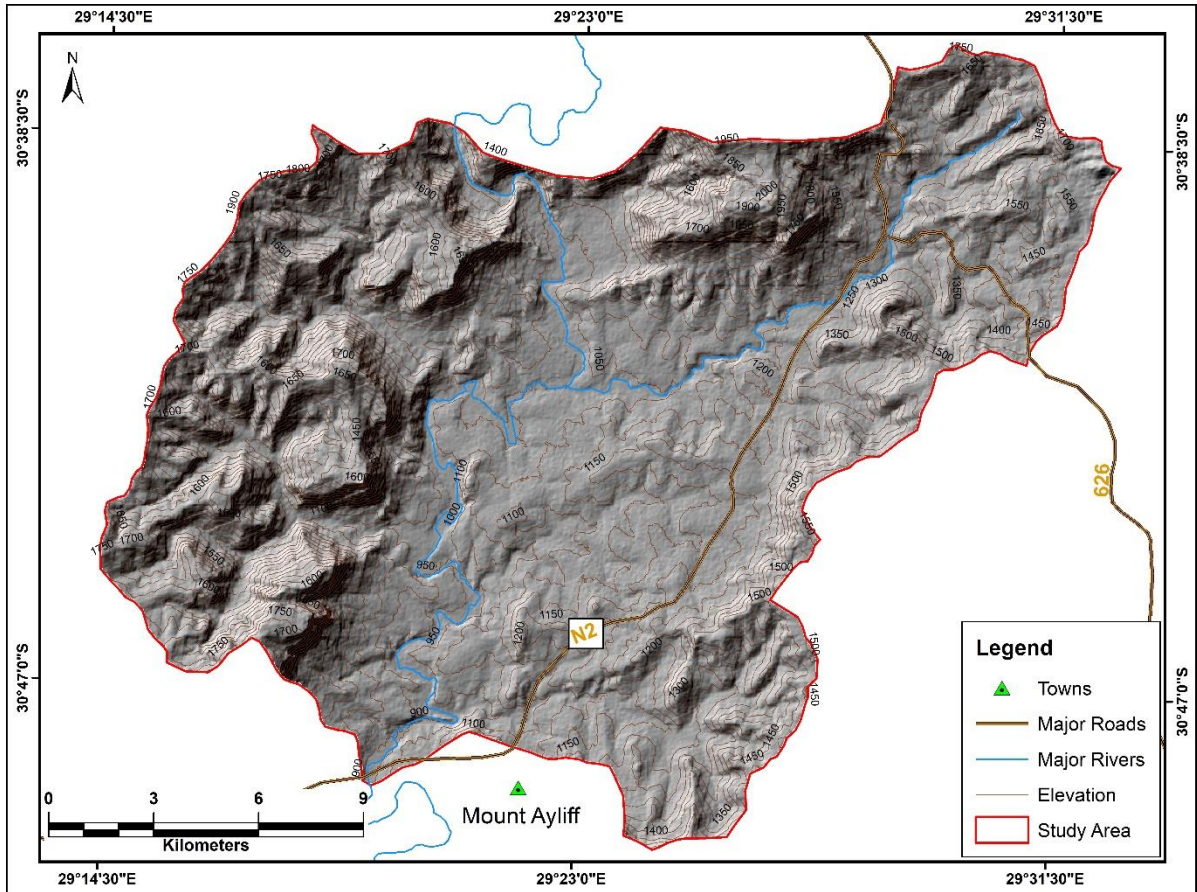
- Uddin, K., Murthy, M. S. R., Wahid, S. M., and Matin, M. A. (2016). Estimation of soil erosion dynamics in the Koshi basin using GIS and remote sensing to assess priority areas for conservation. *PLoS ONE*, *11*(13), 1-19.
- Valor, E., and Caselles, V. (1996). Mapping land surface emissivity from NDVI. Application to European, African and South American areas. *Remote Sensing of Environment*, *57*, 167-184.
- Van der Knijff, J. M. F., Jones, R. J. A., and Montanarella, L. (1999). *Soil erosion risk assessment in Italy*. European Soil Bureau, Joint Research Centre of the European Commission.
- Van der Knijff, J. M., Jones, R. J. A., and Montanarella, L. (2000). *Soil erosion risk assessment in Europe*. European Soil Bureau, Joint Research Centre of the European Commission.
- Van Niekerk, A. (2013). *Stellenbosch University Digital Elevation Model (SUDEM)*. Retrieved from http://www.innovus.co.za/media/documents/SUDEM_Product_Description_201404.pdf.
- Van Oost, K., Quine, T. A., Govers, G., De Gryze, S., Six, J., Harden, J. W., ... and Giraldez, J. V. (2007). The impact of agricultural soil erosion on the global carbon cycle. *Science*, *318*(5850), 626-629.
- Vidhya, L. S., Jijo, J., Soundariya, S., Vishalini, T., and Kasinatha, P. P. (2015). A comparison of soil texture distribution and soil moisture mapping of Chennai Coast using Landsat ETM+ and IKONOS data. *Aquatic Procedia*, *4*, 1452-1460.
- Vijith, H., Seling, L. W., and Dodge-Wan, D. (2017). Effect of cover management factor in quantification of soil loss: case study of Sungai Akah sub-watershed, Baram River basin Sarawak, Malaysia. *Geocarto International*, 1-17.
- Vincente, G. A., Scofield, R. A., and Menzel, W. P. (1998). The operational GEOS infrared rainfall estimation technique. *Bulletin of the American Meteorological Society*, *79*, 1883-1898.
- Viney, N. R., and Sivalapan, M. (1999). A conceptual model of sediment transport: application to the Avon River Basin in Western Australia. *Hydrological Processes*, *13*, 727-743.
- Vrieling, A. (2006). Satellite remote sensing for water erosion assessment: A review. *Catena*, *65*, 2-18.
- Vrieling, A., Sterk, G., and De Jong, S. M. (2010). Satellite-based estimation of rainfall erosivity for Africa. *Journal of Hydrology*, *395*, 235-241.
- Wang, G., Gertner, G., Fang, S., and Anderson, A. B. (2003). Mapping multiple variables for predicting soil loss by geostatistical methods with TM images and a slope map. *Photogrammetric Engineering and Remote Sensing*, *69*, 889-898.
- Wang, G., Gertner, G., Parysow, P., and Anderson, A. (2001). Spatial prediction and uncertainty assessment of topographic factor for revised universal soil loss equation using digital elevation models. *ISPRS Journal of Photogrammetry and Remote Sensing*, *56*, 65-80.

- Wang, G., Wente, S., Gertner, G. Z., and Anderson, A. (2002). Improvement in mapping vegetation cover factor for the universal soil loss equation by geostatistical methods with Landsat Thematic Mapper images. *International Journal of Remote Sensing*, 23(18), 3649-3667.
- Wang, G., Fang, Q., Teng, Y., and Yu, J. (2016). Determination of the factors governing soil erodibility using hyperspectral visible and near-infrared reflectance spectroscopy. *International Journal of Applied Earth Observation and Geoinformation*, 53, 48-63.
- Wang, R., Zhang, S., Yang, J., Pu, L., Yang, C., Yu, L., and Bu, K. (2016). Integrated use of GCM, RS, and GIS for the assessment of hillslope and gully erosion in the Mushi River Sub-Catchment, Northeast China. *Sustainability*, 8(4), 317.
- Wang, W., Lu, H., Zhao, T., Jiang, L., and Shi, J. (2017). Evaluation and comparison of daily rainfall from latest GPM and TRMM products over the Mekong River basin. *IEEE Journal of Selected Topics in Applied Earth Observations and Remote Sensing*, 10(6), 2540-2549.
- Wang, X., Zhao, X., Zhang, Z., Yi, L., Zuo, L., Wen, Q., ... and Liu, B. (2016). Assessment of soil erosion change and its relationships with land use/cover change in China from the end of the 1980s to 2010. *Catena*, 137, 256-268.
- Wasson, B., Banens, B., Davies, P., Maher, W., Robinson, S., Volker, R., and Watson-Brown, S. (1996). Inland waters. State of the Environment, Australia.
- Weaver, A. vB. (1991). The distribution of soil erosion as a function of slope aspect and parent material in Ciskei, Southern Africa. *GeoJournal*, 23(1), 29-34.
- Wei, H., Nearing, M. A., Stone, J. J., Guertin, D. P., Spaeth, K. E., Pierson, F. B., and Moffet, C. A. (2009). A new splash and sheet erosion equation for rangelands. *Soil Science Society of America Journal*, 73(4), 1386-1392.
- Wener, C. G. (1981). Soil Conservation In Kenya, Nairobi. *Ministry of Agriculture, Soil Conservation Extension Unit*.
- Williams, J. R., and Berndt, H. D. (1977). Sediment yield prediction based on watershed hydrology. *Transactions of American Society of Agricultural Engineers*, 20, 1100-1104.
- Wischmeier, W. H., and Smith, D. D. (1965). *Predicting rainfall erosion from cropland east of the Rocky Mountain: Guide for selection of practices for soil and water conservation*. U.S. Department of Agriculture Handbook, No. 282.
- Wischmeier, W. H., and Smith, D. D. (1978). *Predicting rainfall erosion losses: A guide to conservation planning*. U.S. Department of Agriculture Handbook, No. 537.
- Wischmeier, W. H., and Mannering, J. V. (1969). Relation of soil properties to its erodibility 1. *Soil Science Society of America Journal*, 33(1), 131-137.
- Wischmeier, W. H., Johnson, C. B., and Cross, B. V. (1971). A soil erodibility nomograph for farmland and construction sites. *Journal of Soil and Water Conservation*, 26(5), 189-193.

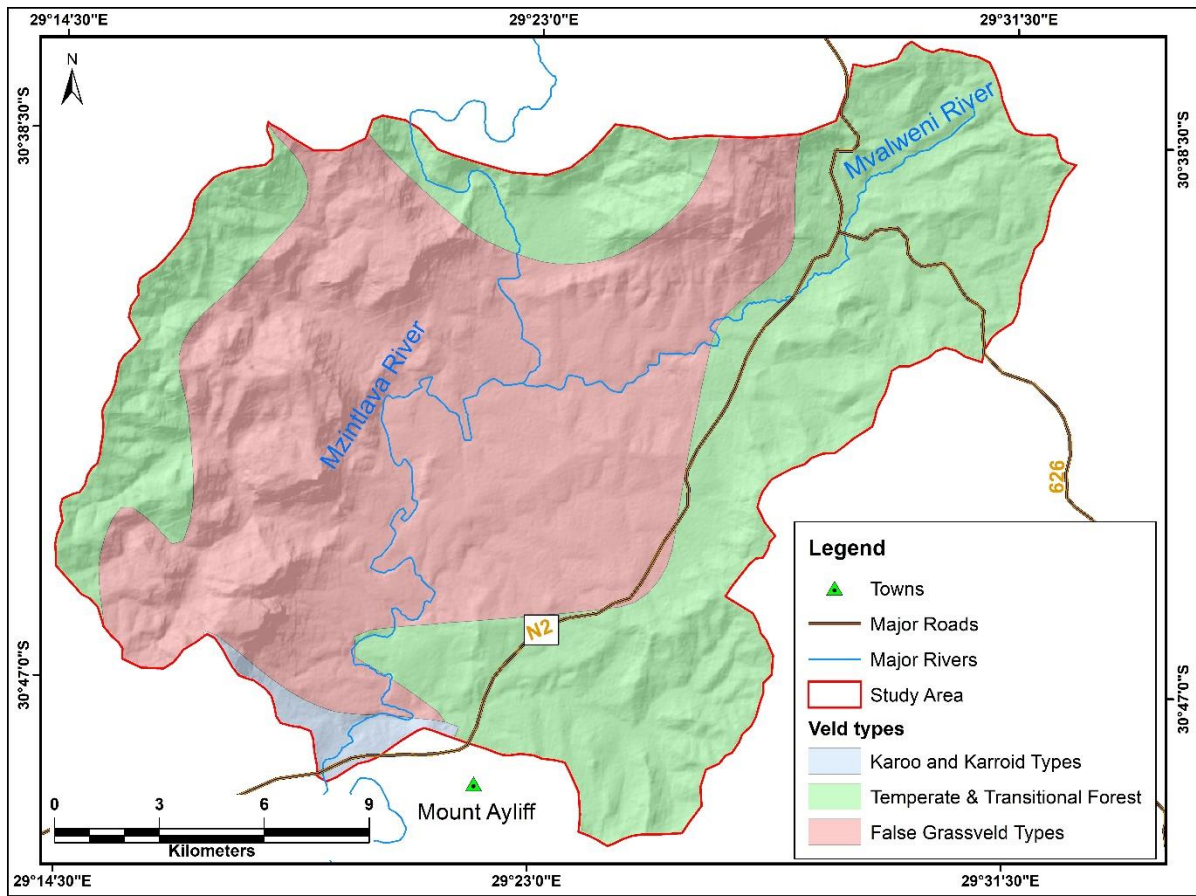
- Worqlul, A. W., Maathuis, B., Adem, A. A., Demissie, S. S., Langan, S., and Steenhuis, T. S. (2014). Comparison of rainfall estimations by TRMM 3B42, MPEG and CFSR with ground-observed data for the Lake Tana basin in Ethiopia. *Hydrology and Earth System Sciences*, 18, 4871-4881.
- Xiao, L., Yang, X., Chen, S., and Cai, H. (2015). An assessment of erosivity distribution and its influence on the effectiveness of land use conservation for reducing soil erosion in Jiangxi, China. *Catena*, 125, 50-60.
- Xie, P. P., and Arkin, P. A. (1997). Global precipitation: a 17-year monthly analysis based on gauge observations, satellite estimates, and numerical model outputs. *Bulletin of the American Meteorological Society*, 78, 2539-2558.
- Xie, P. P., Yarosh, Y., Love, T., Janwiak, J. E., and Arkin, P. A. (2002). *A real-time daily precipitation analysis over south Asia*. Retrieved from http://www.cpc.ncep.noaa.gov/products/fews/sasia_rfe.pdf.
- Yang, D., Kanae, S., Oki, T., Koike, T., and Musiak, K. (2003). Global potential soil erosion with reference to land use and climate changes. *Hydrological Processes*, 17(14), 2913-2928.
- Yang, X. (2014). Deriving RUSLE cover factor from time-series fractional vegetation cover for hillslope erosion modelling in New South Wales. *Soil Research*, 52(3), 253-261.
- Yang, X., Yong, B., Hong, Y., Chen, S., and Zhang, X. (2016). Error analysis of multi-satellite precipitation estimates with an independent rain gauge observation network over a medium-sized humid basin. *Hydrological Science Journal*, 61(10), 1813-1830.
- Yin, D., Chen, X., Yan, L., and Huang, Z. (2007). The research and realization of the land-use change forecasting model in development zones based on RS and GIS. In *Geoscience and Remote Sensing Symposium, 2007. IGARSS 2007. IEEE International* (pp. 3429-3432). IEEE.
- Yu, B., Rose, C. W., Cielsiolka, C. A. A., Coughlan, K. J., and Fentie, B. (1997). Towards a framework for runoff and soil loss prediction using GUEST technology. *Australian Journal of Soil Research*, 35, 1191-1212.
- Yufeng, G. E., Thomasson, J. A., and Sui, R. (2011). Remote sensing of soil properties in precision agriculture: a review. *Frontiers in Earth Science*, 5(3), 229-238.
- Zhongming, W., Lees, B. G., Feng, J., Wanning, I., and Haijing, S. (2010). Stratified vegetation cover index: a new way to assess vegetation impact on soil erosion. *Catena*, 83, 87-93.
- Zhu, Q., Chen, X. W., Fan, Q. X., Jin, H. P., and Li, J. R. (2011). A new procedure to estimate the rainfall erosivity factor based on Tropical Rainfall Measuring Mission (TRMM) data. *Science China: Technological Sciences*, 54, 2437-2445.

APPENDICES

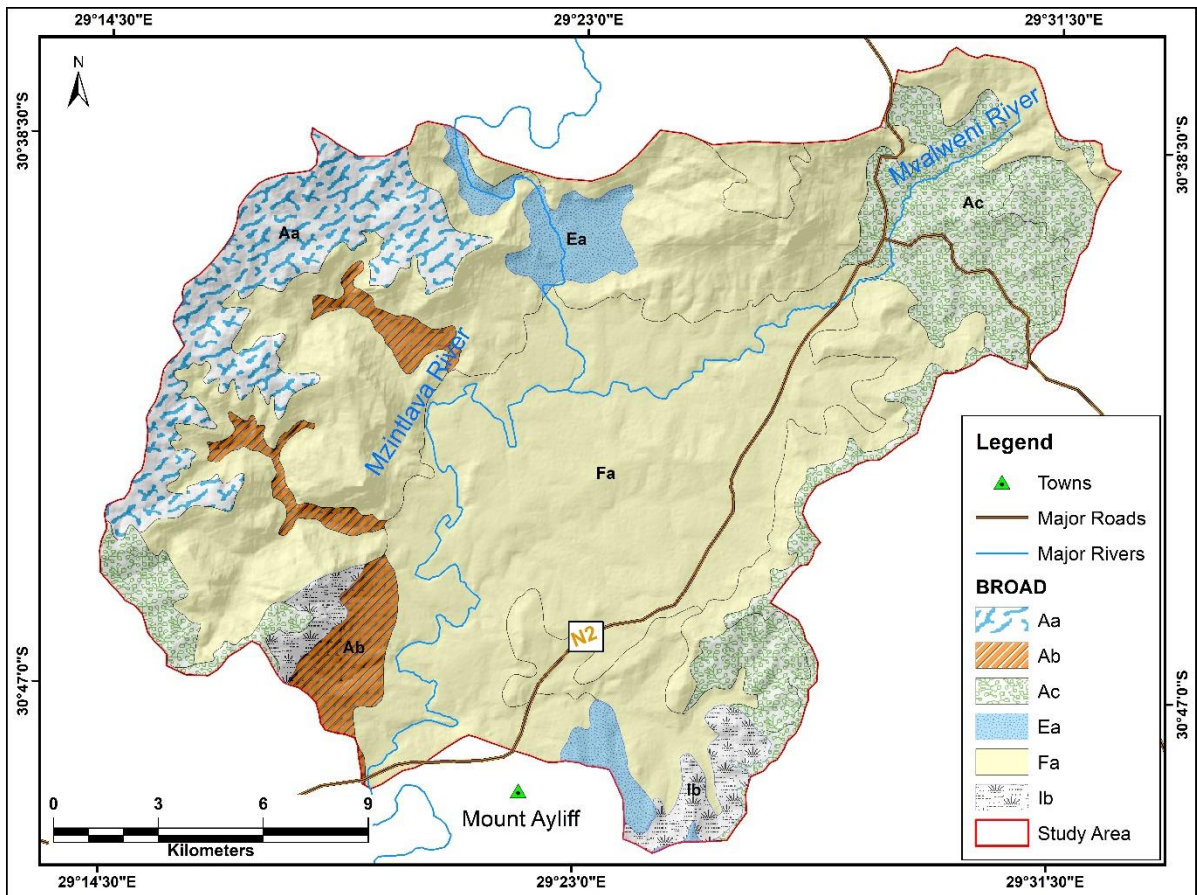
Appendix A: Elevation of the study area.



Appendix B: Major vegetation types in the Umzintlava Catchment.



Appendix C: Spatial distribution of six major soil types in the Umzintlava Catchment.



Appendix D: Physical properties of soil used to calculate soil erodibility.

Soil sample	Height (m)	Latitude	Longitude	vFSa (%)	Sil (%)	Cla (%)	OM (%)	S code	P class	K-factor
Aa	1655	-30.73653	29.27728	64.86	14.74	20.40	8.66	2	5	0.027
Ab1	1014	-30.76044	29.32833	86.93	5.94	7.13	6.36	2	5	0.054
Ab2	1011	-30.75922	29.32581	64.25	16.68	19.06	4.75	4	6	0.063
Ac1	1415	-30.77781	29.45381	83.21	7.84	8.96	6.48	2	4	0.048
Ac2	1364	-30.77781	29.45097	89.15	1.21	9.65	7.93	3	4	0.040
Ac3	1391	-30.77711	29.45236	84.73	4.17	11.11	8.54	2	5	0.033
Ac4	1445	-30.77433	29.45350	67.95	1.19	30.86	8.83	3	4	0.021
Ac5	1425	-30.77506	29.45256	91.50	3.64	4.86	7.28	3	2	0.043
Ea1	1241	-30.81289	29.40217	88.46	4.62	6.92	3.34	1	6	0.080
Ea3	1083	-30.65972	29.38178	95.40	2.30	2.30	6.90	4	6	0.067
Ea4	1123	-30.67342	29.39900	82.89	6.42	10.70	3.30	4	6	0.086
Fa1	1167	-30.70431	29.44333	58.15	19.76	22.09	3.34	1	2	0.042
Fa2	1167	-30.70464	29.44422	81.56	10.54	7.90	4.10	2	4	0.069
Fa3	1160	-30.70506	29.44428	82.14	10.99	6.87	3.41	1	3	0.069
Fa4	1177	-30.70508	29.44508	76.69	14.72	8.59	7.74	1	2	0.027
Fa5	1172	-30.70556	29.44450	78.16	7.28	14.56	6.13	1	2	0.034
Fa6	1233	-30.71250	29.45336	93.43	2.19	4.38	6.02	1	5	0.057
Fa7	1244	-30.71450	29.45422	89.02	1.57	9.41	7.28	1	4	0.037
Fa8	1248	-30.71517	29.45419	85.29	6.54	8.17	6.08	1	5	0.051

Appendix D: continued.

Soil sample	Height (m)	Latitude	Longitude	vFSa (%)	Sil (%)	Cla (%)	OM (%)	S code	P class	K-factor
Fa9	1352	-30.71622	29.46003	95.22	2.39	2.39	8.39	3	4	0.042
Fa10	1213	-30.72175	29.45219	88.80	3.20	8.00	5.90	4	5	0.066
Fa11	1204	-30.72153	29.45767	86.62	4.46	8.92	4.94	3	2	0.058
Fa12	1203	-30.72164	29.44000	65.83	9.20	24.97	1.92	4	6	0.071
Ib	1337	-30.81939	29.40581	70.20	12.42	17.39	7.74	2	3	0.028

Appendix E: Spatial distribution of random points that were used to extract values from soil loss map and individual RUSLE parameters for statistical analysis.

